Tomas Bata University in Zlín
Faculty of Technology

Doctoral Thesis

Preparation of Conductive and Semiconductive Patterns by Digital Printing of Nanodispersions for Sensing Devices of Organic Compound Vapours

Příprava vodivých a polovodivých vzorů digitálním tiskem nanodisperzí pro senzory par organických látek

Author: **Ing. Jan Mašlík**

Study programme: Chemistry and Materials Technology (P2808)

Study course: Technology of Macromolecular Compounds (2808V006)

Supervisor: Assoc. Prof. Ing. *et* Ing. Ivo Kuřitka, Ph.D. *et* Ph.D.

Consultant: Ing. Michal Machovský, Ph.D.

Zlín, April 2019

ACKNOWLEDGEMENT

TABLE OF CONTENTS

ABSTRACT

To simplify, accelerate, and facilitate production processes, ink-jet technology appears to be a very effective and inexpensive alternative to conventional deposition methods. Nowadays, it is rapidly developing in electronics, with the help of conductive polymers and various materials in the form of nanoparticles. The thesis deals with inkjet printing technology as a deposition technique of functional materials in the form of thin films and their applications. The literature review covers the current state and possibilities of inkjet technologies as well as the used materials, their compatibility with the printing equipment, the fabrication process, and the final application. First, it was necessary to optimize the fabrication of conductive interconnects from silver nanoparticles on flexible polymer foils. Then, ITO (indium tin oxide) nanoparticle ink was developed and characterized for application in sensing devices detecting vapours of the organic volatile compounds. As a side product of this work, a framework for ink and inkjet printing process optimization using dimensionless criteria was developed. The last part of presented results is devoted to a successful development of a ZnO nanowire forest hydrothermal deposition method and their utilization in preparation of the IDE designed printed sensor on a polymer substrate. Then, the same technique was applied for developing a novel low temperature operated miniature gas sensing device prepared directly on the top of the quartz window of a UV emitting LED using UV activation of the semiconducting ZnO sensing layer replacing high temperature activation.

ABSTRAKT

Pro zjednodušení, zrychlení a usnadnění výrobních procesů se jeví technologie inkjetového tisku jako velmi efektivní a nenákladná. Z tohoto důvodu se v současnosti rychle rozvíjejí především v oblasti elektroniky, s využitím nejrůznějších vodivých polymerů a materiálů ve formě nanočástic. Práce se zabývá technologií inkjetového tisku a jejího využití v depozici funkčních materiálů ve formě tenkých vrstev a jejich aplikací. Literární část obsahuje aktuální stav a možnosti inkjetových technologií stejně jako používané materiály a jejich kompatibilitu s tiskovým zařízením, výrobním procesem a výslednou aplikací. Nejprve bylo nutné optimalizovat přípravu vodivých cest ze stříbrných nanočástic na ohebných polymerních foliích. Poté byl vyvinut inkoust z ITO (indium cín oxid) nanočástic a charakterizován pro aplikaci v senzorech detekujících páry těkavých organických sloučenin. Jako další výsledek byla rozpracována metoda vývoje inkoustu a procesu tisku pomocí bezrozměrných kritérií. Poslední část prezentovaných výsledků je věnována úspěšnému vyvinutí hydrotermální metody depozice ZnO nanodrátkových polí a jejich využití v přípravě tištěného senzoru s designem interdigitálních elektrod na polymerním substrátu. Poté byla ta samá technika použita pro vývoj nového nízkoteplotně provozovaného miniaturního sensoru plynných látek připraveného přímo na křemenném okénku UV emitující LED a využívajícího tak UV aktivaci polovodičové ZnO senzorické vrstvy nahrazující aktivaci zvýšenou teplotou.

KEY WORDS/KLÍČOVÁ SLOVA

English

ink-jet printing, flexible electronics, printed conductors, nanoparticle ink, sensors

Czech

inkjetový tisk, flexibilní elektronika, tištěné vodiče, nanočásticový inkoust, senzory

SUMMARY OF THE THESIS

In the presented thesis, a literature review on the material deposition by ink-jet technologies is elaborated. Special attention is paid to nanodispersions and their formulation, important ink-jet process parameters and examples of selected materials and applications. According to the literature search, the aim and objectives of the dissertation work are defined. Used experimental methods are briefly described and explained and results of experimental research are discussed. The main area of interest is divided into three parts: (i) printing and characterization of thin conductive layers employed as interconnects and electrodes applicable in flexible electronics and conductive circuits, (ii) nanoparticles-based ink development and fabrication of thin semiconductor structures capable to detect volatile organic compounds (VOC) in gaseous phase.

Concerning the first topic, properties of ink-jet printed conductors of two silver nanoparticle-based inks allowing the printing on high-temperature-sensitive substrates are compared. For this purpose, polyethylene terephthalate and polyimide foils were chosen and commercially available inks used. The work focuses on development and optimization of the printing process and characterization of printed motifs.

The second topic includes the preparation and study of properties of ink-jet printed thin semiconductor films based on indium tin oxide nanoparticles. This required development of original ink based on nanodispersion. Fabrication of a room temperature sensor for toluene vapours is presented and its sensing properties are evaluated.

Last part of ongoing work aims on preparation of complex nanostructure for volatile organic compounds sensing devices. The precursor films consisting of ZnO nanoseeds were ink-jet deposited on pre-patterned electrode structures and nanowire networks were subsequently grown by a wet chemical deposition process. The influence of different growing bath conditions on their morphology and sensing properties were compared and the most appropriate structure was selected for further investigation. In addition, the sensing effect of the sensor was enhanced by UV irradiation, which replaces high operating temperatures of commercially available gas sensors. To the best of our knowledge, a novel approach of preparation a built-in UV-assisted sensor structure is described, and tested. Presented design facilitates the fabrication process and simplifies the operational setup applicable in flexible and hybrid printed electronics.

1. INTRODUCTION

Several well established general methods are known for preparing thin and thick metal oxide nanomaterial films which can be used in the fabrication of electronic devices. The most commonly used techniques can be divided into two main groups. The first is a plethora of gas phase fabrication techniques (PVD, CVD or thermal vapour transport methods). The second group of methods relies on liquid phase employing fabrication techniques such as sol-gel, spray pyrolysis, dip−coating, spin−coating and material printing methods. [1-4]

The above-mentioned conventional deposition techniques, gas phase and in-situ liquid phase growing mechanism techniques are strictly constrained by various physical and chemical parameters dictating the utilization of special equipment and the exposition of the substrate to reaction environment. The disadvantages of these techniques include, in most cases, the need to using vacuum technology, stencils and masks or subsequent separating, removing or etching processes. Such problems can be easily overcome by using material printing technology if the material can be prepared in form of a printable ink, paste, and powder or others in suitable formulation.

Material printing technologies (including screen-printing, roll-to-roll printing, gravure printing and ink-jet printing) are widely used especially in graphic and marking industry, however nowadays, the printing technology offers the possibility of applications in electronics (fabrication of conductive circuits and interconnects, solar cells, light-emitting and sensing devices, antennas, membranes etc.). Their advantageous application leads to accelerating and efficient production, reducing production costs and also the versatility of final products which can turn it into a commodity soon. [5]

These low-cost technologies are based on depositing functional materials onto a used substrate such as glass or transparent and flexible polymer foils, textile materials, ceramics or metal wafers. Unlike other printing methods, ink-jet printing does not require any master form, stencils or masks; therefore, it allows instantaneous and rapid designs and prototyping with no delay between digital motive generation and material deposition. The ink-jet printing is an interesting and versatile method to make controlled and localized deposition of functional materials with suitable geometry on various substrates at low processing temperatures. [4-7] The printed patterns are designed by common computer programs and can be saved as simple bitmap images for printing. It is possible to use a wide range of inorganic and organic materials, including inks based on metal

or metal oxide nanoparticles and polymer solutions. The size of used nanoparticles, their dispersion in a proper liquid medium and a suitable dispersion stabilization, viscosity and the surface tension of the ink composition for jetting are vitally important and challenging parameters to be developed for the required flow of the ink through the nozzles of a printing head yielding the proper generation and ejection of droplets, which is the limiting factor of this material deposition printing process. [4,8-10]

Mentioned advantages predict ink-jet printing a suitable technology for depositing both conductive interconnects using metal nanodispersions as well as active and passive elements from functional materials in the field of polymer electronics and sensors. Printing of inks based on silver nanoparticles (Ag NPs) enables low-cost deposition of precisely defined conductive tracks on a wide range of substrates. The ink-jet printing of Ag NPs inks can be performed at room temperature and without residual waste.

Together with conductive interconnects, it is also possible to print and form functional layers having semiconducting properties which jointly construct advanced devices such as various sensors and detectors. Especially, with regard to the environment, sensors monitoring air quality and detecting the threat of contamination of irritant, harmful fumes and gases are of particular interest. For this purpose, transparent conductive oxide (among them indium tin oxide— ITO being the most widely used) are indispensable materials in fabrication of optoelectronic devices and can be used as a semi-conductive material for gas detecting sensors based on the resistance variation due to its exposure to the target gas. Films made from ITO (In_2O_3:10 wt% SnO_2) have been extensively studied in recent years because they exhibit a relatively rare combination of high visible transmission and significant electrical conductivity, high substrate adherence, good hardness, and chemical inertness. [4,11]

The applicability of this degenerate n–type semiconductor as a thin film sensory device deposited by various techniques (such as the thermal evaporation technique, sputtering, screen–printing) has been widely reported with respect to sensing reducing and oxidizing gases and organic compounds (NH_3, CO, H_2, NO_2, toluene etc.). [4,12-16] Indium tin oxide reacts depending on ambient atmosphere composition by changing the electrical conductivity due to presence of oxygen vacancies and due to Sn doping. [13] Electrical conductivity is transferred as a signal of the electrical resistance variation of the deposited film upon the introduction of reducing or oxidizing gases. The signal is a function of partial pressure of target gas. [12-16]

Some applications of particulate ITO materials have been reported [15,22], although only rarely for sensing devices. It has already been demonstrated that the screen printing of organometallic precursor paste followed by annealing at high temperatures (600 °C) for a relatively long time (for 40 minutes at optimum for ITO crystallization) can be utilized for sensor fabrication [6]. The latest efforts demonstrated the suitability of screen printing for pastes directly composed from ITO nanocrystals and binders for sensor fabrication. [4,17,18]

Similarly, ZnO as a typical n-type semiconductor has found its applicability in many experimental fields especially due to a wide bandgap of 3.37 eV, high electron mobility, high transparency at visible wavelength, excellent chemical and thermal stability for which it is advantageously used in optoelectronic applications such as TFTs, LEDs etc. and due to its chemoresistive properties also as a sensing material. [11,19]

The vast majority of metal oxides are able to detect very low concentrations of analytes at elevated operating temperatures, e.g. ZnO (300-500) °C to overcome the activation energy barrier of a redox reaction and increase the reaction rate. Such a process is adverse for application on polymer foils and, prospectively, in portable or handheld devices. Moreover, it may be unadvisable in the presence of explosive gases. For this reason, advanced unique morphological sensing material based on ZnO nanostructures (nanotubes, nanorods, nanofibers, nanowires etc.) excellenting for high surface to volume ratio, density of defects such as oxygen vacancies and absorption of wavelengths in the ultraviolet region, which contribute to the room temperature gas sensing, has been studied. The material can be deposited either in form of a nanodispersion or in a form of precursor followed by in-situ formation of ZnO nanostructures. [20-23]

2. INK-JET MATERIAL PRINTING

Since its foundation in the 19th century until recently, the ink-jet printing has been used largely in publishing and graphic industry (printing news, magazines and photo images) and ink-jet printers spread widely into homes and offices during last few decades. For all mentioned reasons in the introductory part, ink-jet manufacturing technique has become to attract many industrial and experimental spheres. Thus several manufacturers such as Fujifilm-Dimatix, MicroFab Technologies and Meyer Burger have focused on the development and production of inkjet printers for deposition of versatile functional inks with regard to precise setting the process parameters.

Ink-jet printing involves several partial processes from the material deposition point of view. These include preparation and characterization of the printed fluid (allowing its compatibility with the substrate surface), layout and designing of the desired motifs, the printing process parameters setting and characterization of deposited structures. Material jetting consists in releasing fluid in the form of small droplets from the cartridge through the print head nozzles. The drops are deposited in precise location on the surface of the substrate. Each drop forms an equilibrial spherical cap after impact on its position. Thus, a single dot of material is formed after drying of the ink. Due to the overlap and coalescence of drops on the surface and appropriately set drop spacing, uniform films can be formed. Ink-jet printing is further divided according to the principle by which drops are formed and deposited. Dominant modes of drop generation are continuous ink-jet (CIJ) and drop-on-demand ink-jet (DOD) [6,24,25].
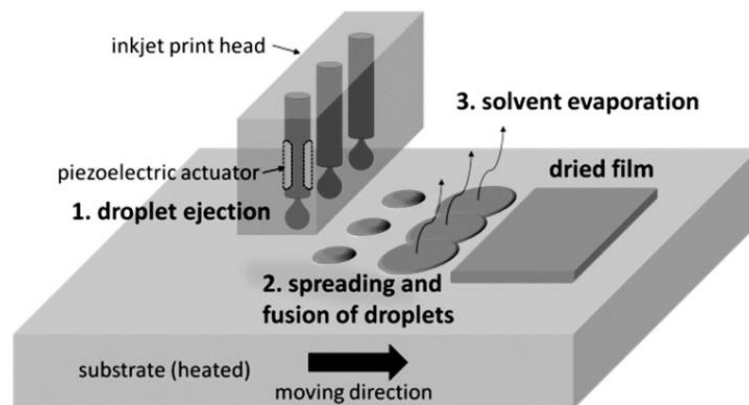
Figure 1 – Thin film formation using material ink-jet printer. Adopted from [26]

2.1 Continuous Ink-jet

Recently, different methods of continuous ink-jet (CIJ) printing have been developed and commercialized. In general, continuous ink-jet system jets energetically unstable stream of liquid from a high-pressurized ink reservoir. This free surface stream is subsequently break up into drops. Due to periodic stimulus applied by a vibrating piezoelectric transducer at the orifice of the printing nozzle it is possible to synchronize the breakup of each drop and to generate a steady stream of droplets having the same size, period (spacing between drops) and velocity [6,27-30]. Certain drops are subsequently charged and deflected from a continuous stream passing through a fixed high-voltage electrode plates to separate printing drops from nonprinting drops. Depending on the used technology, non- or deflected droplets land at the right place on a substrate to form the printing. The rest of unused drops is collected in a gutter and recirculated. [31-35]

However, fundamentally different approach known as *Stream Technology* (developed by the Eastman Kodak Company) is based on stimulating of a downstream of a liquid ink by thermal pulses applied by integrated ring-like micro heater elements into each nozzle. Thus, the temperature of the ink and its temperature-dependent properties such as surface tension, viscosity, and density are locally modified at the orifice of a nozzle. Modulated spatial gradient from lower to higher surface tension regions (from warmer to cooler regions) causes a deformation of the free surface and lead to instability and drop formation. [27,31-35] Due to varying of heating pulses it is possible to produce differently sized drops where the large drops are deposited while smaller sized drops are deflected by airflow and the ink is recycled.

Despite of many advantages of continuous ink-jet systems especially in large-scale manufacturing, CIJ is not versatile for printing of precise structures of sensitive nanoparticles-based inks or polymer solutions as the recirculation process may causes degradation after a long exposure to ambient conditions. [36] Therefore, drop-on-demand ink-jet system is an appersuitable alternative.

2.2 Drop-on-demand Ink-jet

Main characteristic feature of the drop-on-demand (DOD) ink-jet printing in comparison with CIJ printing is an activation of each micronozzle individually to produce pressure pulse inside the ejection chamber to generate well-defined volume and velocity of drops.

The comparison of the two CIJ technologies mentioned in the previous chapter with the DOD technology is schematically shown in Figure 2. Basically, the DOD technology can be divided into two distinct branches according to the principle of ink drop generation. The ink ejection and drop formation is most often driven by a piezoelectric transducer or by a thin-film resistive heater integrated into a wall of separated nozzle chambers and it is software-configurable as required.
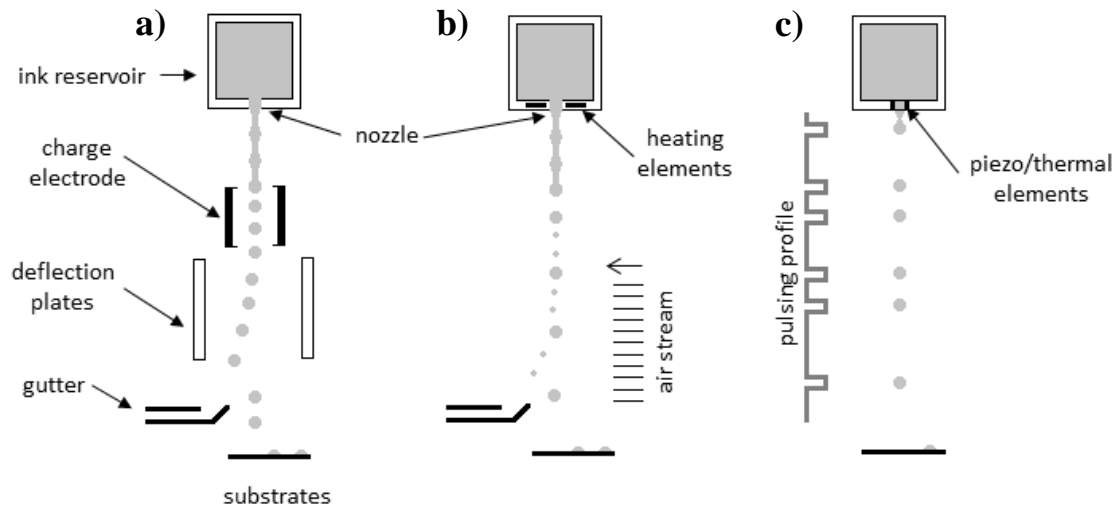
Figure 2 − *Schematic comparison of a) continuous ink-jet system, b) continuous Stream Technology ink-jet system and c) drop-on-demand ink-jet system*

2.2.1   Piezoelectric Drop-on-demand Ink-jet

Voltage-driven piezoelectric transducers (commonly based on lead zirconium titanate – PZT) converts applied voltage to mechanical deformation of separated ejection chambers of a printing head. Piezo element adjacent to / or placed inside of the ejection chamber, mechanically deforms its walls and generate pressure pulse inside. Generated pressure pulse in the fluid filled inside of ejection chamber feed a nozzle and force a fluid to be ejected. Depending on polarity of applied voltage the volume of the chamber contracts or expands and thus, raises or reduces the pressure inside. Applied voltage waveform tunes time-dependent pressure pulses inside the chamber optimizing well-defined volume and velocity of drop ejection and in the last step refills the chamber. A fluid inside the ejection chamber is contained at the orifice held by surface tension preventing spontaneous leaking. If the critical value of the surface tension is exceeded due to the applied pressure pulse, the liquid begins to separate through a neck forming as a droplet. The entire

10

process of drop generation is shown in Figure 3. At the beginning, the ejection chamber is filled by the ink and the piezo element in the standby position. Subsequently, voltage is applied to the piezo element adjacent to the ejection chamber causing its wall curvature. At this stage, the initial pressure is generated inside the chamber and disrupts the meniscus of the liquid. When the adjusted voltage is applied, the pressure pulse allows the liquid to eject in the form of broken-off droplet. By applying the opposite voltage, the walls of the chamber are straightened causing the ink to be refilled from the reservoir. [6,29,37-39]
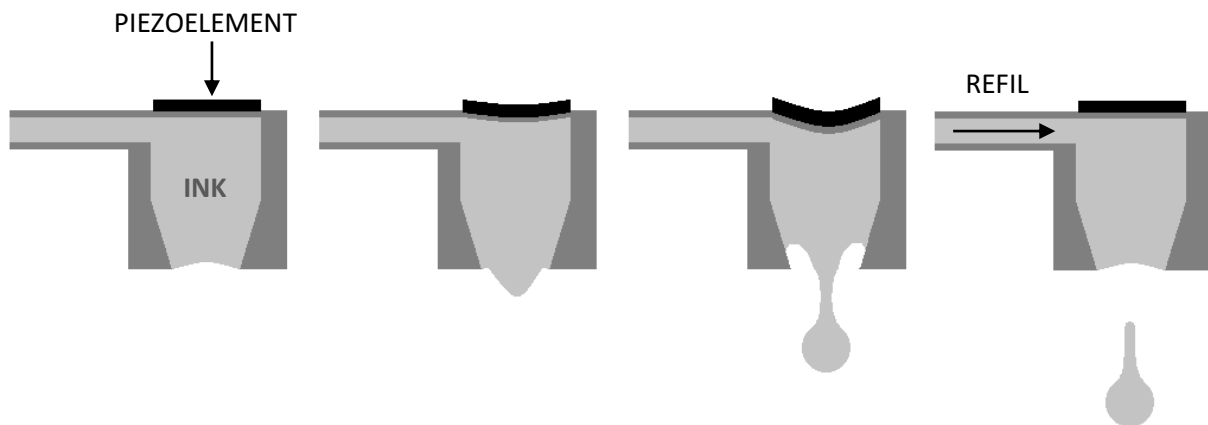
Figure 3 – Schematic representation of pressure pulse by piezo element, generation and droplet ejection of drop-on-demand ink-jet. Adopted from [24]

2.2.2 Thermal Drop-on-demand Ink-jet

A defined drop jetting is possible to control by thermal pulses applied inside of ejection chamber. Integrated thin-film resistive heater, activated by short-duration voltage pulses, raises the temperature of a thin layer of ink (up to 300 °C under atmospheric pressure) which evaporates explosively and produces a vapour bubble. Rapid expansion of the bubble inside of ejection chamber leads to ejection of the ink through the nozzle and forms a droplet of desired volume and velocity. Subsequently, the heat pulse is removed leading to collapse of the bubble and allows the ejection chamber to be refilled from an ink reservoir. [24,40,41]

3. INK FORMULATION

A crucial operation of the entire printing process is the preparation of a material being printed, which is required to be in a form liquid dispersion, i.e. an ink. The ink composition affects both the printing process and the properties of printed structures and hence a device. Parameters of the final printed layers are necessary to be considered while preparing the ink composition which has to meet all necessary chemical and physicochemical criteria to assure compatibility of the ink with the substrate, jetting performance and storage stability. It is a multidimensional parameter space that must be researched and where an optimum must be found between all and sometimes contradictory requirements imposed on the material and its processing with given equipment. The crucial fluid parameters enabling optimal printability are therefore ink density, viscosity, surface tension, the stability of the suspension and the size of the nanoparticles, which is partially related to an operation performance of the device. [4,9,42]

Ink preparation requires several steps involving optimizing their composition corresponding to the printer's process parameters. The preparation step may lead to complications and requires return to adjustments of the ink composition, necessary for the deposition of the desired pattern quality. Figure 4 shows the generally used components and their requirements relating to inks containing functional materials and layers deposited thereon.

Selection of functional material	Selection on liquid carrier medium	Selection of additives
Fulfills the function of the final layer	Allows the transport of a functional material	Helps to adjust properties for optimal printing process
Meets the technical parameters of the printer	Removable after deposition or does not affect the function of major material	Allows compatibility with used substrate
Compatible with liquid vehicle		

Figure 4 − *Ink components and requirements*
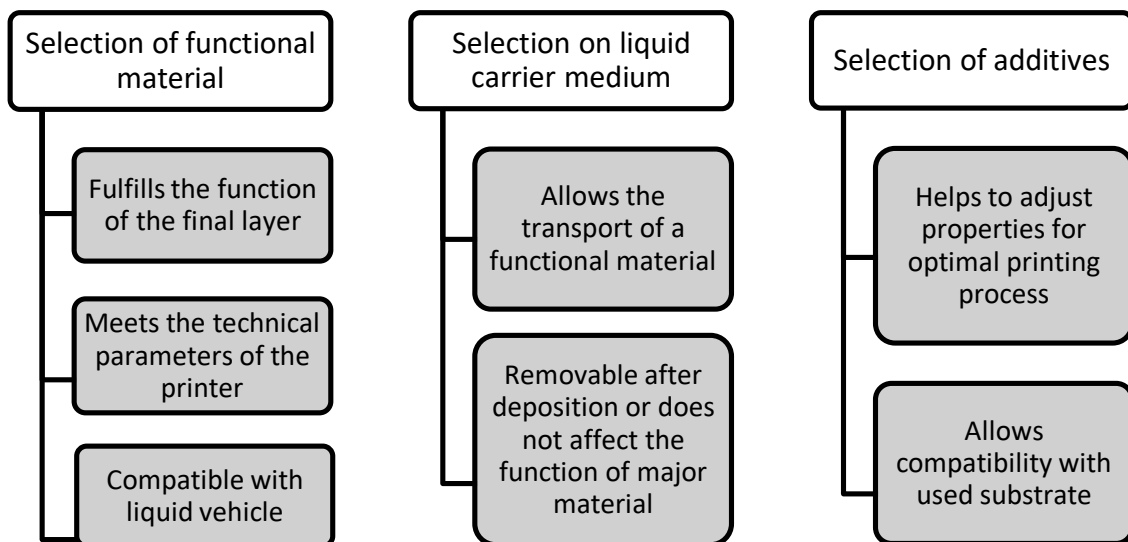
With regard to inks be composed of functional particles, their size must be considered relating to the technical parameters of an ink-jet printer which reach their limitations in terms of particle transport through the print head nozzle and its feeding capillary, but also because of the stabilization in the dispensing medium. Printer specifications enable deposition of particle size smaller than 1/10 of the nozzle diameter as a rule of thumb, which is critical to avoid clogging and therefore, particle size smaller than 1/50 or even 1/100 [36] is preferable. Taking into account the diameter of the nozzles which is in the order of tens of micrometers, then, micro- and nanometer-sized particles are optimal. [6,7,9,10]

3.1 Nanoparticles-based inks

A nanoparticles-based ink, as the name implies, is basically a suspension of functional solid nanoparticles in liquid carrier medium whose nature enables its evaporation readily once the material is deposited and thus, the particle content forms a continuous (homogenous or porous) thin film. Two ways how to prepare NPs-based inks are available, whether direct synthesis of stabilized nanoparticles or their dispersing in liquid medium with assorted components and additives such as co-solvents, stabilizing agents, viscosity modifiers, surfactants and humectants are included. The stability of prepared nanodispersion represents extremely important issue and for their application as inks it is necessary to keep its properties constant over time, at least over the processing time. For more about the properties of the ink, see the chapter 5.1. There are three main types of nanoparticulate systems used for ink-jet printing. Nanodispersions of metallic and semiconductive nanoparticles are most widely used followed by various carbonaceous nanoparticles, among them mainly carbon nanotubes (CNT) and graphene and graphene oxide related materials.

3.1.1 Metal and metal-oxide nanoparticles inks

Plenty of scientific reports describe the preparation of functional inks based on conductive or semi-conductive nanoparticles. The most used material in field of printed and flexible electronics are inks based on silver nanoparticles for printing of conductive patterns. The main advantages of silver nanoparticles are high electrical conductivity and resistance to oxidation as well as dispersibility in water allowing the adjustment of ink parameters by water-soluble additives to achieve optimal printing performance. All mentioned benefits make this material a suitable candidate for patterning of conductive tracks, electrodes etc. Depending

on the particle loading in the ink and the appropriate printing and drying parameters, it is possible to achieve the electrical resistivity values of several $\mu\Omega \cdot cm$. Due to the price and availability of silver; serious attempts to replace it by copper are made. However, the silver inks were not surpassed yet. [43-46]

Another group of materials are metal oxide semiconducting nanoparticles such as indium and tin oxide, zinc oxide, copper oxide etc. which are indispensable materials in fabrication of thin film transistors (TFTs), optoelectronic devices etc. Due to their unique electrical and optical properties especially in thin films, metal oxides are also used in quality environment monitoring devices where play an important role as a gas detecting sensors transducing the interaction with chemicals and vapours into measurable signal based on the property (conductance/resistance) variation.

A very important step is the stabilization of nanoparticles in the liquid vehicle which affects both printing performance and homogeneity of final layer. The most frequently used method of stabilization is a steric stabilization using non-ionic surfactants allowing the adsorption of molecules to the surface of the nanoparticles while maintaining solubility in the dispersing medium. However, any residuals of used additives in printed motifs may adversely affect their functionality. Therefore, it is necessary to remove not only the liquid vehicle but also the surfactants during post-treatment processing steps. For this reason, in addition to a simple drying the films, annealing is performed at high temperatures to achieve degradation and removal of the surfactant and eventual other ink additives, which do not evaporate easily. Alternatively, the additives must be integrated to the material system, if high temperature annealing is not possible. Moreover, the persistence of the polymeric component in the material can be intentional in case of NP/polymer nanocomposite printing. [47]

3.1.2 Carbon nanotubes inks

Carbon nanotubes consisting of single-walled or multi-walled cylinder rolled form of graphitic sheets are a promising material due to their high electrical and thermal conductivity and favourable mechanical properties which makes them an interesting alternative to common metallic conductors applicable in electronics. Depending on diameter, chirality and helicity, single-walled CNTs can exhibit p-type semiconducting (holes as charge carriers) properties usable in sensing devices as a pristine material or as a CNT/polymer composite. However, a highly disadvantaging factor and also a challenging step is the preparation of dispersion in form of printable ink. One of the important factors is the size of nanotubes,

which in the case of SWCNTs reaches hundreds of microns. For this reason, several methods are used to reduce their lengths and to fulfil the process parameters of ink-jet printing. The second crucial factor is the stabilization of CNTs dispersions in both aqueous and non-aqueous environments. Because of the strong van der Waals interaction between the nanotubes, they have tendency to form bundles consisting of several tens of nanotubes in contact with each other which leads to nozzle clogging during the printing. Therefore, various chemical functionalization or stabilization by using surfactants is carried out. [48,49]

3.1.3   Graphene and graphene oxide inks

Graphite is a basic material source for individual molecular sheets consisting of hexagonally arranged carbon atoms for both graphene and graphene oxide (GO). However, they have greatly different fundamental physical and chemical properties because of the corruption of the π-conjugated bonding system due to oxidation in GO. Exfoliated monolayers of graphene or graphene oxide in form of nano-sized flakes/sheets allow heightened overlapping of individual nanoparticles, forming contiguous layers compared to carbon nanotubes, which reach their limits in form of dead-end pathways. Similarly, to carbon nanotubes, the preparation of stable and high-concentrated systems is challenging. In case of graphene, the conventional polymeric binders are used, however their insulating properties degrade the electric performance of graphene; thus, materials based on nanofibrillated cellulose have been investigated to name an unconventional example [50]. On the other hand, chemically modified and delaminated graphite − graphene oxide displays high stability in aqueous environment due to the H-bonding present between the carboxylic and hydroxyl groups attached (on the surface) to the sheets and render the graphene oxide nanosheets hydrophilic. This phenomenon allows the preparation of a stable and water-based printable ink avoiding usage of expensive and often undesirable stabilizers. GO is and electrically insulating material which is caused by introduction of functional groups and disruption of the extended sp^2 hybridized carbon graphene hexagonal structure. However, GO can be chemically, thermally or photo-chemically reduced to graphene called reduced graphene oxide (rGO). Hence, the electrical conductivity of printed GO motifs can be partially restored where needed. Although rGO still contains some impurities in the form of oxygen-containing functional groups, the excellent process-ability of GO and significant recovery of the material's conductivity prevails the drawbacks. To summarize, graphene or graphene oxide appears to be an interesting, inexpensive, large-scale producible

and environmentally friendly material having unique electrical and optical properties applicable in electronics. [51-53]

4. INK-JET PROCESS PARAMETERS

The printing process requires compatibility of parameters of the ink, the printing apparatus and process conditions. Therefore, the ink parameters must be considered prior to the printing process as already mentioned in chapter 3. Individual parameters of the ink, processing velocity and ink-jet tool and their relation are described in this chapter. Interaction between the ink and the substrate surface is also related to the resulting quality and precision of printed shapes.

4.1 Ink parameters

Properties of the inks are the most important factor influencing almost all steps of the entire printing process. Requirements for ink properties, namely viscosity and surface tension are specified by the printer manufacturer. Density and ink stability should meet required specifications also. These advices should be followed for optimal printing performance and high quality of printed motifs. On the other hand, fulfilment of these criteria does not automatically assure good printability of the ink. The overall performance of a printing of an ink is determined by the function of the final thin-film structure. In case the thin-film feature is adversely affected, it is necessary to identify which one of the ink parameter causes these errors and then, tune the ink composition adequately, which actually is the 'trial – error' method. [9]

4.1.1   Stability

First of all, the stability of prepared nanodispersions is required due to storage as well as delivery through the print head nozzle. Sufficient shelf storage life time is a great advantage or at least easy redispersibility must be assured for any practical utilization of inks. The appropriate ratio of the individual components, which enables stabilization, wetting or controlled evaporation of liquid vehicle, must meet the requirements of the printer and must not impede the function of deposited material. In case of solution inks, the stability represents a resistance to phase separation or degradation during storage due to ambient temperature or radiation. In the case of inks containing small solid particles, stability means a resistance to particle agglomeration and rapid settling. In order to avoid particle agglomeration, surfactant binders stabilizing the system by means of steric

stabilization are used. These systems improve sedimentation stability as well. [54,55] Currently, in the case of carbon based nanoparticles, stabilization using nanofibrillated cellulose by means of electrostatic repulsion forces has being considered. [9,24,56]

4.1.2 Density

Definition of density (ρ) of the material is its mass per unit volume (in the SI system the units of kilogram per cubic meter). Density also helps to convert viscosity in case the kinematic viscosity is the default value of measurement. It is necessary to take into account the temperature dependence of the density if the fluid is heated during the printing process. [24]

4.1.3 Surface tension

There are several aspects of the surface tension (σ) in the printing process. Firstly, the surface tension determines capillarity and shape of the meniscus inside the nozzle channel, secondly, plays crucial role in forming the ink drop and is responsible for its spherical shape, and lastly, influences subsequent spreading and coalescing of droplets on the substrate upon contact. In liquid volume, there are asymmetric attractive intermolecular forces at the surface in contact with gas phase forming a tension over the entire liquid/gas interface as Figure 5a displays. When a liquid is deposited on a substrate, its shape depends on the relative strength of attractive forces between liquid phase and solid phase molecules. The surface energy of used solid substrate surface is given by contact angle (θ) of sessile drop measurement and depends on three co-existing interfaces between liquid and vapour phase, solid and vapour phase and solid and liquid phase indexed as *lv*, *sv*, and *sl* respectively. The equilibrium contact angle shown in Figure 5b is given by Young's equation [57]:

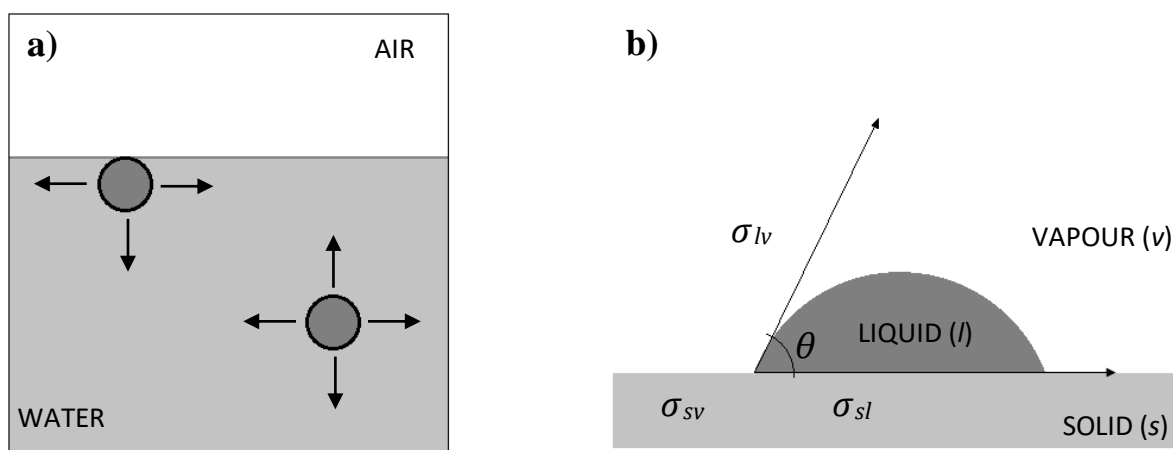$$\sigma_{sv} = cos\theta \cdot \sigma_{lv} + \sigma_{sl} \tag{1}$$

Figure 5 *– Illustration of surface tension; a) formed by intermolecular forces at liquid/air interface, b) and related contact angle of sessile drop on surface. According to [24]*

In case of high surface tension of a liquid vehicle (usually based on water), surfactants and/or co-solvents having low surface tension are used. Organic co-solvents are advantageously used due to good miscibility, relatively low boiling point and therefore simple evaporation without leaving residuals in deposited material. On the other hand, many of these binary solvent mixtures cause the surface tension gradient during evaporation, where volatile alcohols evaporate preferentially and generate a Marangoni flow along the liquid−vapour interface resulting as a *coffee ring effect* determining the thickness of the final pattern from nanoparticles. Therefore, binary or ternary mixtures in ratio close to azeotrope are beneficial. Surfactants or wetting agents are an alternative enabling decrease of the surface tension to the desired level (compatible with the printed substrate surface). The disadvantage is the nature of these substances, which in most cases are macromolecular and their removal requires annealing at high temperatures otherwise the function of the final layer can be affected. In consequence of the high annealing temperature, the use of polymeric substrates is avoided or problematic. [58-61]

4.1.4   Viscosity

Viscosity defined as a resistance to shear deformation is caused by a cohesive intermolecular forces causing friction between adjacent layers of fluid in motion sliding past one another in a velocity gradient increasing towards the applied force/stress. The viscosity (η) is a constant that measures how steeply the linear

dependence of the shear stress (τ) on the shear rate ($\dot{\gamma}$) is slanted for Newtonian flow as defined by Newton's Law:

$$\tau = \eta \cdot \dot{\gamma} \tag{2}$$

The current SI unit for the viscosity is the Pascal-second, often given as mPa·s. [62]

The viscosity is strongly dependent on temperature. At increased temperature, the molecules have higher energy and move away from each other, thus cohesive forces are decreased resulting as a decreased viscosity. Although the interest is confined to temperatures in the interval from ambient temperature up to less than 100 °C for printing aqueous systems, the viscosity decreases exponentially with increase in temperature, approximately according to an Arrhenius equation.

$$\eta = Ae^{\frac{E_a}{RT}} \tag{3}$$

Where the pre-exponential factor A has the dimension of mPa·s, the activation energy is E_a in J·mol^{-1}, T is the thermodynamic temperature in K, and R is the universal gas constant (8.314 J·mol^{-1}·K^{-1}). For instance, the temperature sensitivity of viscosity for water is 3 % per °C at room temperature so keeping a sample of a liquid at a constant value of the viscosity within a ± 1 % range of precision requires the sample temperature to be maintained within ± 0.3 °C. [62]

The dependence of viscosity on pressure is less important in this work, since the key step of printing, i.e. drop formation, occurs at the ambient atmosphere pressure.

In case of non-Newtonian fluids, the viscosity depends on shear rate also. During printing, high shear deformation of hundreds of thousands s^{-1} occurs in the nozzle and therefore the nature of the printed ink needs to be defined. Nanoparticles-based aqueous inks are considered to represent Newtonian behaviour and their viscosity is unchangeable with the suddenly varying shear deformation. While highly diluted solutions of polymers can be considered as Newtonian fluids too, semi-diluted polymer solutions and concentrated particulate systems are weakly viscoelastic. Concentrated polymeric inks exhibit shear deformation−dependent viscosity, which has an ill effect on the drop formation, which is then followed by a tail, formation of satellite droplets or the ink is pulled back into the nozzle and the liquid fails to eject at all, eventually. [24,63]

4.1.5 Viscoelasticity

As outlined above, non-Newtonian behaviour is exhibited by polymeric solution inks at high shear rates primarily during the ejecting phase of printing process and affecting the drop formation. Even though a non-Newtonian fluid behaves as a Newtonian at low shear rates, viscosity of solutions varies after so-called Newtonian plateau at high shear rates in the course of jetting. As a Newtonian inks breakaway shortly from the nozzle, the breakaway of polymeric ink is delayed and the velocity of the drops is reduced. Increased concentration of polymers in the inks can even cause pulling the fluid back to the nozzle, as the elastic forces within the fluid have a significant impact, thus, the drop is never formed. Therefore, concentrations of polymers below the first critical concentration (c^*) are normally used in polymer solution inks while higher concentrations are used for spinning of polymer fibres from solutions. In accord to that, Newtonian-like or only weakly viscoelastic behaviour may be expected for most of used inks. [63-65]

4.2 Tool parameters

The main tool-related parameter playing role in the ink-jet printing process is the nozzle diameter which may be considered as a good approximation of the initial fluid stream diameter, hence its characteristic length. If the geometry of the nozzle's orifice differs from the circular one, the characteristic length A is derived as an equivalent (hydraulic) diameter by a general formula:

$$A \ = \ 4 \cdot \frac{S}{O} \tag{4}$$

where S is the area of the nozzle, and O is its wetted perimeter. In case of a square, A equals to the size of its side. [66]

4.3 Process parameters

There are two main parameters in ink-jet printing which influences the process of drop generation. The temperature may be considered as an external condition, while the fluid flow velocity is a parameter of prime importance which has a direct impact on the process.

As mentioned above, temperature has an impact on viscosity and surface tension of printed liquid vehicle which has to be taken into account during the printing deposition process. Therefore, the temperature needs to be precisely

controlled in experimental work as well as in real applications. A slightly elevated temperature of the printing head is used often to help optimize the process. Moreover, heating the substrate allows quicker drying and film formation of the deposited material and, in case of low surface tension, prevents uncontrolled spreading. With respect to this, it is necessary to characterize the inks at the intended application temperature. [24]

While printing temperature is optimized mainly in order to enhance the process of printed material drying, and the attention is paid to maintaining stable external conditions, the fluid ejection velocity is a parameter which can be varied in a large extent and directly controls the process of ink drop formation and its deposition on the substrate. The piezoelectric element giving momentum to the fluid is driven by the voltage pulse waveform. The waveform is divided into several segments representing a sequence of programmed voltage steps resulting in the sequence of events of the ink fluid ejection from the printing head's nozzle as described in Chapter 2.2.1. The fluid ejection velocity is controlled by the steep increase of voltage deflecting the piezoelectric element which decreases the volume of the nozzle chamber quickly thus generating pressure that expels the fluid out of the chamber. In such way, the drop velocity can be varied from a few $m \cdot s^{-1}$ up to 15 $m \cdot s^{-1}$ for the printer used in this work. A good first guess of velocity to set is about 6 $m \cdot s^{-1}$. [6,7,9,24]

There are many other practical parameters to be set with the Dimatix Materials Printer; however, they are relevant for printing of motifs rather than for material development. These are drop generation rate, printing head movement, resolution, stand-off, etc. [6,7,67]

4.4 Dimensionless correlations of the parameters and drop generation

The drop generation in drop on demand piezoelectric ink-jet printing is a repeated cycle process. The cycle can be described in five steps: (1) ejection and stretching of liquid forming thus a liquid thread – a free surface flow, (2) pinch-off of the liquid thread from the nozzle orifice, (3) contraction of the liquid thread, (4) breakup of the liquid thread into primary drop and satellites, and (5) recombination of primary and satellite drops. In ideal case, no breakup appears and a single spherical drop is formed in the last (fourth) step. Finally, the drop or drops land on the surface of the substrate after traveling through the whole standoff distance. [24,68]

A definition of good printability can be formulated then according to Kim and Baek's conditions of the printing process assuring that a single drop is formed either directly without break up (the second pinch-off) or the satellite drop merges with the main drop within its travel distance forming a single drop safely before hitting the substrate creating thus a single dot [68]. The formation of a single drop either directly without break up or by the merge of the satellite drop with the main drop defines the minimum stand-off distance (MSD) which must be kept in the printing process. A stand-off about 1 mm is widely used in digital ink-jet printing. Moreover, the travel distance of the drop and eventual satellites to the point of their merge must not be longer than twenty times of the characteristic length to achieve acceptable quality of ink-jet printing in term of the dot's placement error with respect to common conditions and processes as defined by Kim and Baek. [68]

A lot of effort has been spent to find suitable correlations between the viscosity, the surface tension, and the density of inks, the characteristic length as the tool parameter, and the fluid velocity as the main variables influencing the success of the ink-jet printing at given conditions. The composition and properties of used inks with used ink-jet printer characteristics and processing parameters can be analysed rationally with the use of dimensionless criteria, namely by the Reynolds (Re), the Weber (We), the Capillary number (Ca), and the Ohnesorge (Oh) number, and the number Z is the reciprocal of the Ohnesorge number. The number Oh^{-2} is known as the Laplace number (La).

$$Re = \frac{v \cdot \rho \cdot A}{\eta} \tag{5}$$

$$We = \frac{v^2 \cdot \rho \cdot A}{\sigma} \tag{6}$$

$$Ca = \frac{We}{Re} = \frac{v \cdot \eta}{\sigma} \tag{7}$$

$$Oh = \frac{\sqrt{We}}{Re} = \frac{\eta}{\sqrt{\sigma \cdot \rho \cdot A}} = Z^{-1} \tag{8}$$

$$La = Oh^{-2} = \frac{Re}{Ca} = \frac{\rho \cdot \sigma \cdot A}{\eta^2} \tag{9}$$

where η, ρ and σ are the dynamic viscosity, the density, and the surface tension of an ink respectively, v is the drop velocity and A is the characteristic length. [67,69,70]

22

According to the literature, the following criteria are the most important. Generally, the printability range used to be determined by a *Z* number, which is the inverse of the Ohnesorge number (*Oh*). The recommendations for the optimum range of the *Z* number vary from $1 - 10$ up to $4 - 14$. However, it was found that the *Z* number (or obviously *Oh* number too) alone is insufficient for describing the droplet formation dynamics because all the terms describing dynamic effects are cancelled in its formula

$$Z = \frac{Re}{\sqrt{We}} = Oh^{-1} \tag{10}$$

and only the material constants and characteristic length remain. [68] Actually, the characteristic length (*A*) is a tool-related property since it is a printing nozzle square shaped orifice characteristic diameter, i.e., the side size of the square (*A* = 21.5 µm). Therefore, other important non-dimensional parameters such as the Reynolds number (*Re*), the Weber number (*We*), and the capillary number (*Ca*) should also be taken into consideration to complete the material-process-tool parameter-related triad. *Re* represents the ratio between the viscous and the inertial forces in moving fluid, *We* is dependent on the ratio between the inertia and the surface tension, *Oh* reflects the physical properties of the liquid (the viscous forces, the inertial and the surface tension forces) and the size scale of the nozzle, but is independent of the driving conditions, and *Ca* is the ratio of the viscous force to the capillary force. [4] A plot of two suitable selected dimensionless numbers should be enough to map the parameter space for Newtonian fluids. A good example may be found in the work of McKinley and Renardy [71] who replotted a diagram originally constructed by Derby [67]. A schematic in Figure 6 adopted from their works shows the operating regime for stable and printable fluids in drop-on-demand ink-jet printing indicating also the adverse effects outside of the good printability area.
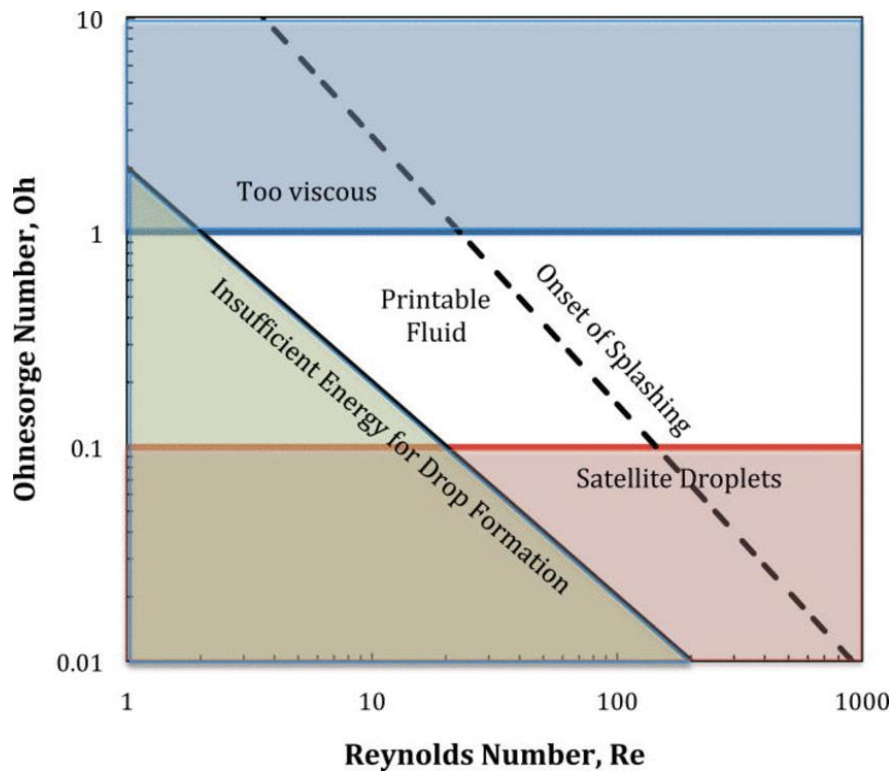
Figure 6 *− Ink suitability using dimensionless criteria, Adopted from [71]*

Another approach with more advanced analysis refining more the modes of drop generation, satellite formation, other instabilities and failures in printing was developed by Kim and Baek. [68] The characteristic length and density are not included in the *Ca* number while the Weber number does not contain viscosity. Hence, they used *Ca* taking into account the drop velocity during printing and demonstrated the printability window based on the Capillary number plotted against the Weber number. The graph is shown in Figure 7. The white polygonal area (regime I) represents the good printability region. The grey polygon marking regime II indicates conditions when one or more satellite drops are generated, but they do not recombine with the main drop. The regime III can be found at larger *Ca* and *We*, where the pinch-off time is relatively long and a thin and long-lasting thread generates a fine satellite drop that does not merge with the main drop. The regime IV at large *Ca* and small *We* is characteristic by domination of the viscosity effects over inertial forces and the fluid fails to be ejected. The regime V is typical by small *Ca* and small *We* when surface tension overbalances both viscous and inertial forces thus the fluid fails to eject. [68]
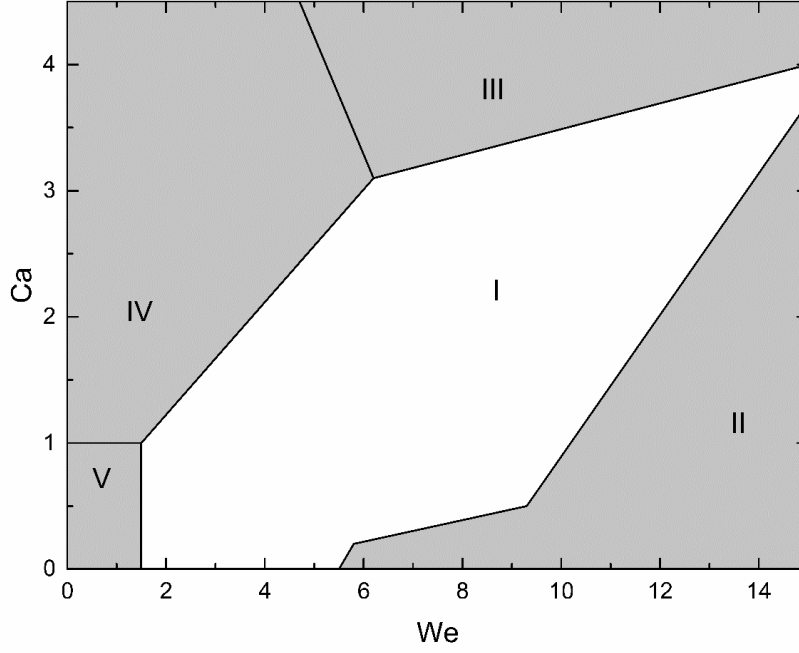
Figure 7 − Regime map of droplet formation dynamics. Adopted from [68] and used with courtesy of Pavol Šulý [63]

On the other hand, the map in Figure 7 does not show inviscid flows as well as the situation of dripping, when the ink leaks from the nozzles. Moreover, the map is too small to include printability window suggested by the producers of the printer used in this study. Indeed, the range of *Ca* and *We* covered by the Kim and Baek plot is quite small in comparison with logarithmic scales used by McKinley and Renardy [71]. Therefore, the attention is turned back to the reinvestigation of the latter approach. Two main reasons for that shall be noted. First, the upper and lower horizontal limits in the graph in Figure 6 suitably represents the *Z* printability range 1-10 which actually means the *Oh* range $1 − 0.1$. Next, the diagonal borders then may be approximated by lines with a slope -1 representing constant values of $We^{1/2}$ since

$$\log Oh = \frac{1}{2}\log We - \log Re \qquad (11)$$

4.5 Substrate

The choice of substrate depends obviously on the intended printing application. It is related to the ink formulation by optimum processing temperature, ink spreading, wetting and adhesion interactions, and the requirement for physical flexibility, if needed. Print substrates include almost any solid material; however,

25

flexible substrates are made almost solely from polymers. The decisive issue is to achieve sufficient matching of the surface tension of the ink to the surface energy of the chosen substrate. Surface energy of a polymer sheet may be modified in many ways; however, this is beyond the scope of this thesis. Let us assume that the substrate can be properly selected and, once the substrate is chosen, the ink and processing conditions are developed to achieve maximum performance. However, use of different substrates will require development of a new different set of inks. Common polymer substrates for flexible electronics are PI (Kapton®), PEN, and PET. The substrates are usually surface modified. [72]

Usual surface energy values of substrates are around 40 mN·m^{-1}, which allows compatibility with various inks. If the surface tension of the ink is too high, there is insufficient wetting (non-wetting or partial non-wetting) of the surface, and the liquid create one large drop instead of desired structure. On the other hand, if the surface tension of the liquid was too low to the surface energy of the substrate, uncontrolled spreading of the ink over the surface occurs. Both of these undesirable cases cause discontinuity and inhomogeneity in the printed layer and deterioration in the quality of the printed structure. [73]

5. ELECTRICAL PROPERTIES OF PRINTED MOTIFS

Essentially, materials are grouped into three categories depending on their electrical behaviour which is based on the ability of the electrons to occupy the conduction and/or valence bands, namely conductors, semiconductors and insulators. Due to the nature of the materials, their electrical properties are characterized on the basis of different methods. As the thesis focuses on printed conductive and semiconductor structures, appropriate methods characterizing required property are described. The material characteristics of conductors and semiconductors are scale independent while the properties of conductors (objects) depend on their size and shape:

Electrical resistance R quantifies how the material reduces flowing electric current and their relationship is determined by the Ohm's law:

$$R = \frac{V}{I} \tag{12}$$

where V is applied voltage and I is measured current. The value of electrical resistance is closely related to the nature of the material as well as its shape. The inverse of the resistance is the electrical conductance, which quantifies the ease with which an electric current passes through an object. Measurement of electrical resistance, and conductance as a reversed value, is also used to characterize response of a sensitive material based on local − mainly surface variations of the charge concentration based on electron donation / acceptance due to absorption / desorption of target gas. [74]

Electrical resistivity ρ ($\Omega\cdot$m or usually $\Omega\cdot$cm) is a characteristic constant describing the electrically resistive nature of the material. It is independent of the sample geometry but strongly dependent on the temperature, especially in case of semiconductor. As already mentioned the relationship between resistance and resistivity is expressed in the following formula:

$$\rho = R\frac{A}{l} = R\frac{h \cdot w}{l} \tag{13}$$

Where R represents electrical resistance, l represents the length of the conductor, h is the thickness of conductor, w stands for the width of conductor and the resulting cross-sectional area is A.
The electrical conductivity is the reciprocal of electrical resistivity, and quantifies ability of a material to conduct an electric current. [74]

Sheet resistance is another important electrical property quantifying the electrical performance of thin conductive films. The value is defined as the resistivity ρ of a material divided by its thickness h:

$$R_{sheet} = \frac{\rho}{h} \tag{14}$$

The units of sheet resistance equation could be resolved as Ω, however, since the value represents the electrical resistance, the units of Ω/sq or Ω/□ are usually used although staying outside of SI. Sheet resistance is related to the thin-film materials which are assumed to carry the charge along the active area of uniform thickness instead of throughout the volume of the material as in the case of conductive wires and interconnects. Sheet resistance is specifically used for electrical characterization of thin-film organic or polymeric light emitting diodes, photovoltaic devices and solar cells. [24,74]

Measurements of electrical characteristics are usually based on two-point or four-point contact probes in the line of equal and known or other specific placing of them as schemed in Figure 8. (for example square layout of electrodes in case of Van der Pauw method) with applied electric current in between. In case of four-point probe measurement the electric current is applied on the two outer probes measuring the voltage between the inner two probes. [74]
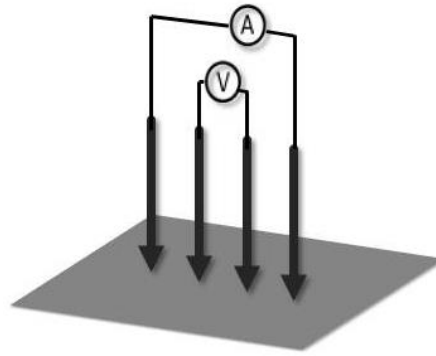

Figure 8 – Linear arrays of four-point probe measurement. Adopted from [24]

6. SELECTED APPLICATIONS

6.1 Conductive interconnects for electric circuits

The deposition of conductive structures in microelectronics is one of a wide range of ink-jet application. Digital ink-jet printing enables integration of components and electronic elements in form of *printed wiring*. In combination with soldering, gluing and mounting allows assembling of circuit boards and other hybrid printed integrated circuits. It is also widely used for deposition of electrode and RFID structures as the basis of antennas and other advanced scanning devices. [43,45,75-77]

6.2 Electronic devices

Ink-jet material printing is also used to fabricate functional elements in the form of thin or thick layers and their overprints. The layers are polymer-based, nanoparticles- or nanostructure-based (or their combinations) as the function comes from their fundamental properties. Except for the above mentioned conductive patterns, active and passive layers are deposited and incorporated in

device construction of desired shapes. The layers are employed due to their capacitive, inductive, emissive, chemo-resistive, magnetic as well as insulating properties and constitute the gist of the device. Recently, research has been focused on the possibilities of preparing diverse sensors, light-emitting diodes, solar cells or energy generators and harvesters and fully ink-jet printed devices have been demonstrated. [78-82]

6.2.1   Gas sensors

In general, a sensor is a device able to response to various nonelectrical stimuli transducing them into an electrical signal. Several transformation steps precede the electric output signal which is generated and converted by a transducing part. The transducer is an electronic device (or its part) converting one form of energy to the other and it can be connected in a series of elements, produces a signal in form of energy which can be finally operated by the direct sensor part of the complex device. Then, the sensing device is able to generate electrical output directly. [49,83,84]

Chemical sensors consist of a recognition element that is sensitive to stimuli produced by various chemical compounds (analyte) and a transduction element that generates a signal whose magnitude is functionally related to the concentration of the analyte [85]. Among chemical sensors, direct sensor can be found as well. In fact, they are in centre of interest of this thesis because of their simplicity both in terms of fabrication and operation. Detection of various gases and vapours of volatile organic compounds and measurement of their concentration is possible due to the change of conductivity of the active sensing material upon their adsorption or desorption to the surface part of the sensor. The change in conductivity is manifested macroscopically as a change of the device's conductance. Hence, the sensor response can be simply monitored as the relative change of its resistance. [47,49]

 A valuable sensory device should be capable to provide information about environmental and chemical composition of ambient conditions in real-time, continuously, repetitively and reversibly. Moreover, a gas sensor should also be able to provide information about the specific amount of various harmful substances selectively. Nevertheless, all of these requirements cannot currently be combined, while maintaining a high level of quality control of the environment at low power consumption. Therefore, it is necessary to choose the appropriate compromise depending on the sensor's working environment, the composition of the ambient atmosphere, the expected occurrence and quantity of substances to be

detected. The performance of the gas sensor can be influenced by several factors. The first which needs to be considered before the fabrication process is its design and construction.

The most used constructions of gas sensor according to the possibilities of preparation by material printing is combination of sensitive material in form of thin or thick film and electrode platform consisting of conductive pads connected to the measuring unit. Electrodes positioning and geometry plays an important role affecting sensor performance and can be designed as follows:

- sensing material placed between two planar parallel electrodes as schemed in Figure 9a,
- sensing material layered with planar interdigital electrodes (IDE) as schemed in Figure 9b.

Contact electrodes can be deposited before or after the deposition of sensing layer on insulating substrate which facilitates technological process of mass fabrication. The choice of one or the other electrode geometry depends on the distance between each conductive pad and the value of resistivity of the specific sensitive material, which together with inter-grain contact resistances determine the overall resistance value of the sensor device. Due to this reason, capacitive planar configuration of conducting electrodes called interdigital electrodes was introduced. IDE design reduces the inter electrode distance (practically reaches millimeter to micrometer pitch size), which reduces voltage while passing a measurable current, increases the relative sensitivity of active layer and enhances a response of the device. In case of semiconducting metal oxides as a sensitive material, interdigital geometry allows to achieve acceptable sensor resistance values for subsequent processing of the measured data within the range of the measuring instrument. Due to this fact, it is possible to set the intensity of output sensor signal simply by changing the electrodes area, number and size of conductive legs, and the spacing between them. [83,86,87] It is also possible to control the sensing performance of the sensor depending on used electrode material which are in many cases noble metals (Ag, Au, Pt, Pd) having specific catalytic properties able to increase activity of sensing material. [42,88-90] Interdigital electrodes design is inexpensive, easy to fabricate and integrate on a chip consisting of sensing element with other processing electronic components.

Among the most commonly used materials with advantageous processing and sensing properties are semiconducting metal oxides, which are discussed in the following chapter.
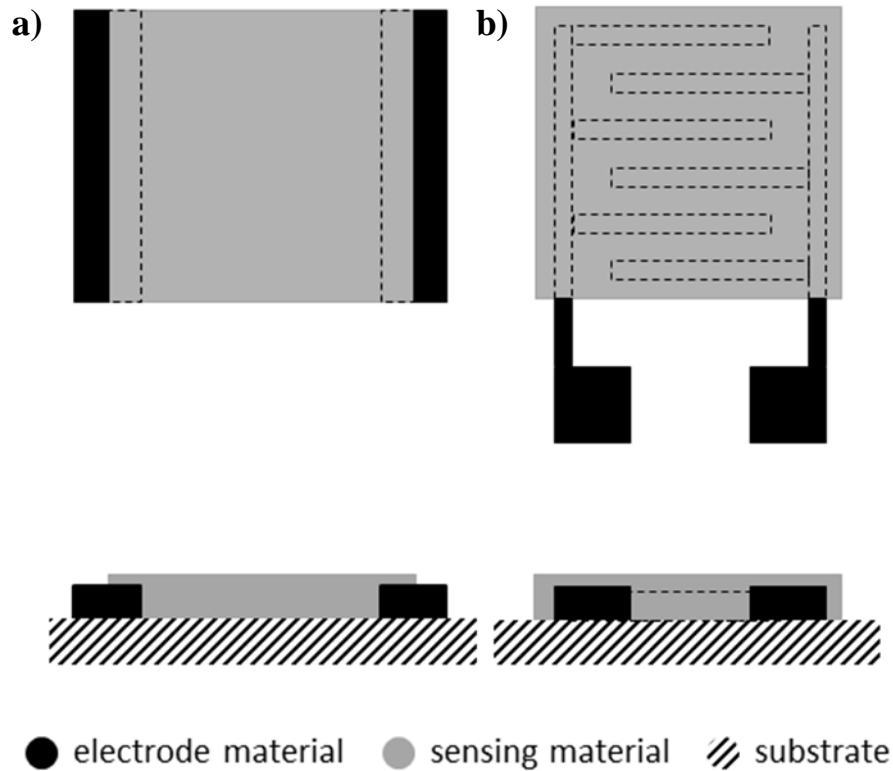
Figure 9 ─ Constructions of gas sensing device with possible designs of measurement contacts (description in the text). Adopted from [87]

6.2.1.1 Metal oxide based gas sensors

Metal oxides due to their unique chemical, optical, electrical and semiconducting properties play the key role in chemical sensor technology offering versatility and detection of a wide range of gases at low as well as high concentration without material consumption for a long service life. The possibilities of preparing these materials at the nanoscale with new morphologies have opened new ways in the application sphere of gas sensors.

The detection mechanism can be performed by measuring the alteration of various physical characteristics of the sensor in the presence of the detected gas; however, the essential is the reaction of gaseous molecules taking place at the metal oxide semiconductor surface changing the density of charge carriers affecting the conductivity of bulk material. Then, the sensor response is categorized as electrical and electrochemical receptor or/and transducer which reacts depending on ambient atmosphere composition by changing of measured specific physical property, for instance electrical conductivity. When a DC

voltage is applied to the device, electric current flows through the sensitive material placed between electrodes and recorded current value is transferred as a signal of the electrical resistance of deposited sensitive film. Measured signal is modulated by the presence of reducing or oxidizing gases depending on the metal oxide nature as a function of the partial pressure of target gas, which is characterized as the sensor's response. Interaction of one type of gas with semiconductors of n-type and p-type have reverse direction of conductivity's change while for n-type materials the conductivity increases, for p-type materials decreases. The response principle is based on the physical nature of the semiconductor which plays a significant role in the manner of the sensor response. [4,47,91,92]

A non-stoichiometry and impurities of crystal structure of metal oxides, which is based on the presence of oxygen vacancies, cation vacancies or other lattice defects, enable the formation of non-bonding electrons having energy of E_D as seen in Figure 10a. For this reason, a low thermal energy at common laboratory temperatures is sufficient to excite the electrons to conducting band; electrons are the major charge carriers and the material exhibits n-type semiconductor behaviour. Contrarily, the electrons can be trapped from the valence band to acceptor energy level E_A (Figure 10b), a hole in the valence band is created and thus, holes are the majority charge carriers. Material exhibits p-type semiconductor behaviour. Typical representatives are listed in the Table 1.
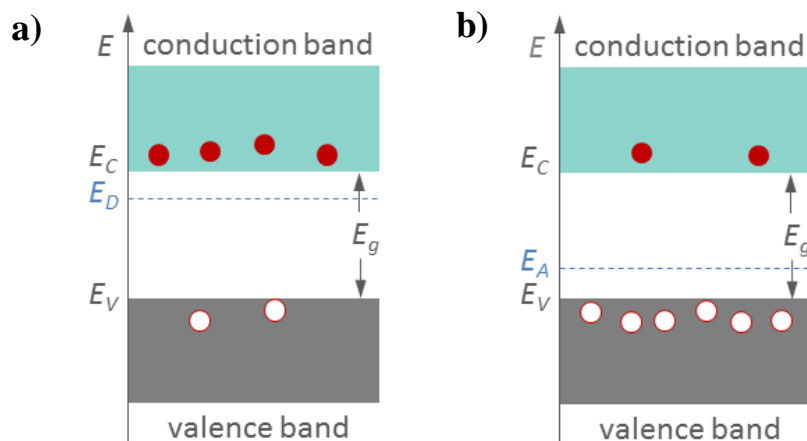

Figure 10 – Schematic band diagram for a) n-type and b) p-type semiconductor at thermal equilibrium

In terms of applicability in sensory devices, n-type metal oxide materials are preferably used due to a necessity of overcoming the energy barriers at the grain boundaries, thereby regulating the overall conductivity of the sensitive layer.

Compared to that, p-type metal oxide materials are generally less used due to poor stability and proportionately weaker responses caused by a hole accumulation layer in the surface region of individual grain and thus, the degree of which molecules of adsorbed gas can affect the resistance, is reduced. However, it is possible to use the combination and the incorporation of both types of materials having increased catalytic activity, depleted layer and p-n junctions. [93]

Table 1 − *Nature of semiconductor materials used in sensory devices*

n-type	ITO, ZnO, SnO$_2$, WO$_3$, TiO$_2$, Fe$_2$O$_3$, In$_2$O$_3$
p-type	CuO, NiO, Co$_3$O$_4$, Cr$_2$O$_3$, Mn$_3$O$_4$

As already mentioned; sensing mechanism is a complex process consisting of gas adsorption, diffusion, chemical reactions and desorption which takes place on the surface of sensing material. Although approaches to the mechanism of gas detection differ, two models are predominant: The ionosorption model considering the space charge modulation of the electrical surface potential of ionosorbed gas molecules and reduction-reoxidation model explaining the effect of changing the amount of the surface oxygen vacancies and their ionization. [30]

Ionosorption model

Despite the lack of spectroscopic studies, the ionosorption mechanism is the most widely accepted and a more attention is paid to it in this chapter. Both detection mechanisms assume a presence of oxygen in surrounding atmosphere, which becomes physically adsorbed (physisorption) by van der Waals interactions on each nanoparticle (grain) of the film surface as:

$$O_{2\,(ambience)} \leftrightarrow O_{2\,(surface)}. \tag{15}$$

Due to highly electronegative nature of oxygen which is adsorbed on the particle surface, the phenomenon causes a donation of electrons e^- from the conduction band of metal oxide, and enables a reaction with ambient oxygen which becomes negatively charged as well as the metal oxide nanoparticle

surface. Negatively charged surface is compensated by decreasing electron density which results as a decrease of conductivity of the thin film. In addition, charge depleted region L_S within the individual metal oxide nanoparticle or nanowire is formed as schemed in Figure 11. Depleted layer corresponds to the Debye-length L_D, which indicates the penetration depth of charge carrier redistribution and it is characteristic for each semiconductor material. The reaction of molecular oxygen takes place at temperature below 100 °C, and it is described as follows:

$$O_{2 \text{ (ambience)}} + e^- \leftrightarrow O_2^-{}_{\text{ (surface)}}, \tag{16}$$
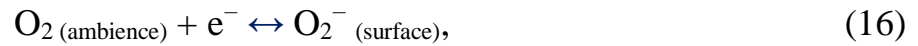
which becomes chemisorbed (involving charge carrier exchange), and continues until equilibrium is reached. At high operating temperatures above 100 °C the process continues by formation of electrostatically charged − ionosorbed atomic oxygen ions O^- and O^{2-} as:
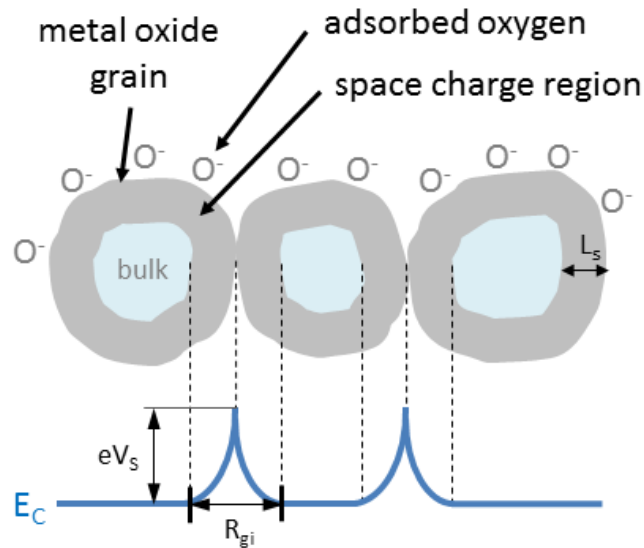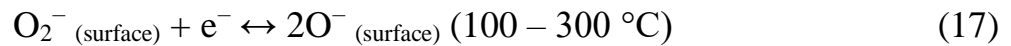
$$O_2^-{}_{\text{ (surface)}} + e^- \leftrightarrow 2O^-{}_{\text{ (surface)}} \ (100 - 300 \text{ °C}) \tag{17}$$

$$O_2^-{}_{\text{ (surface)}} + 2e^- \leftrightarrow 2O^{2-}{}_{\text{ (surface)}} \ (\geq 350 \text{ °C}) \tag{18}$$

Firure 11 *− A schematic diagram of inter-grain contact and corresponding energy bands in the presence of ambient oxygen (for description see text)*

The presence of exposed reducing gas leads to a partial consumption of pre-adsorbed oxygen ions on the surface of the sensitive film presented as [14,16,47]:

$$R + O^-_{\ (surface)} \leftrightarrow RO + e^- \tag{19}$$

This interaction replenishes the concentration of electrons, charge depleted region is reduced by the flow of electrons to the bulk of semiconductor as Figure 12 displays and hence, the response of the sensing layer to the exposure of reducing gas is manifested as an increase of its overall conductance for n-type semiconductor.

Moreover, aforementioned mechanism suggests the existence of grain boundaries consisting of surface potential barriers between the individual grains and Schottky interface in the contact with electrode material (usually noble metal). The height of surface potential of each grain is influenced by bending of electronic band creating barriers eV_S hindering the flow of electrons within the layer which influence comprehensive electrical properties of sensitive layer. The size of barrier depends on the width of charge depleted region L_S, which is directly modified by the amount of adsorbed oxygen. The contact bilayer thickness, R_{gi}, is a double of L_S. Exposed gas reacts with pre-adrosbed oxygen species; release electrons back to the bulk of metal oxide material thereby reducing the width of charge depleted region and decrease the potential barriers at intergrain contacts. [31, 34]
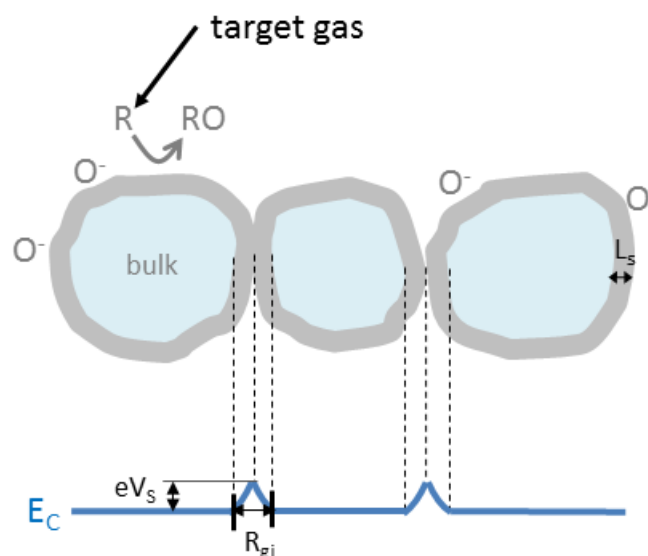

Firure 12 − A schematic diagram of inter-grain contact and corresponding energy bands in the presence of target gas

Nevertheless, there are cases of different ambient gas composition where the mechanism described above fails. Film resistance modulation occurs even in oxygen free conditions, which indicates direct interactions between electrons of sensing material and gas molecules. It was found that electrons in low energy orbitals of sensing material are rather trapped by the tested gas causing increased electrical resistance which is related to the energy of the Lowest Unoccupied Molecular Orbital (LUMO) of volatile organic compounds family such as acetone, ethanol, methanol, benzene, toluene and xylene and thus, molecular orbital theory and orientation of molecule is preferably used for description of these interactions as become important within the surface absorption and its reactivity. [94]

Particle size and film porosity

The ionosorption model offers an explanation of increasing sensing performance depending on the nature of sensing material and its properties such as particle size, film thickness and surface morphology. One of the leading parameters is therefore nanoparticle (crystallite) size. Above described mechanism is directly linked to the surface reactions at the sensing material and ambient gas molecules interface. The sensitivity behaviour is related to surface area and crystallite size, which is crucial in sensing performance.

In case the particle size d is much larger than the eigen charge depleted region L_S, the conductivity and sensitivity are independent of the particle size and are modulated by the bulk conductivity (Figure 13a). In other case of middle-size particles, the sensitivity depends on the particle size and their boundaries, where charge depleted regions create conduction channel within an aggregate (Figure 13b). If the particle diameter is equal or even smaller than twice the charge depleted region, the radius of the particle is exceeding, whole particle is depleted and the energy barriers vanish. Thus, the bulk conductivity becomes imperceptible and sensory response is directly controlled by the conductivity of the space charge region unfolding from the amount of adsorbed species on the surface (Figure 13c). [47,95] This implies, that the particle size has a significant effect on the sensitivity, which can be increased by decreasing particle size. Moreover, nanostructured layers have a large surface to volume ratio, which can be favourably used to overcome high activation energy for surface reactions, especially in the detection of low gas concentrations.
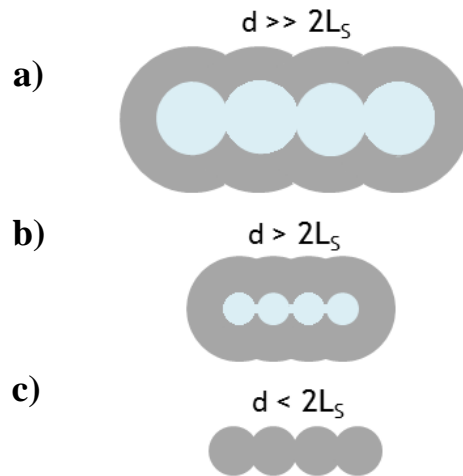
Figure 13 – *Schematic image of particle size influence on sensing mechanism. Adopted from [91]*

Reduction-Reoxidation (Oxygen-Vacancy) model

In terms of oxygen-vacancy model, intrinsic defects such as oxygen vacancies, cation vacancies etc. on the surface of the metal oxide semiconductor act as electron donors and the surface conductivity is therefore controlled by a reduction and reoxidation of gaseous oxygen. The target gas removes oxygen from the surface side of the lattice and produces oxygen vacancies, which introduce electrons into the conduction band and therefore increases the electrical conductivity. In the absence of a target gas, the oxygen vacancies are filled by gaseous oxygen, and captures electrons resulting in a decrease in the electrical conductivity. [4,47]

6.2.1.2 Operating conditions of metal oxide gas sensors Temperature vs. UV irradiation

In general, chemical reactions are influenced and operated by temperature and the same applies to sensor sensing capabilities. Sensor sensitivity can be directly driven by temperature regime controlling the reaction kinetics, electron mobility and overall conductivity. Based on the above described, temperature also strongly influences adsorption and desorption processes and elevated temperature shortens desorption phase decreasing recovery time and device's repeatability. [94] In terms of device construction, the heating element must be in proximity to the active layer which can be directly deposited thereon, or are separated by a

dielectric carrier film as seen in Figure 14. In view of these facts, increased operating temperatures can be dangerous in the case of explosion gas detection and do not allow the use of most polymeric flexible carriers due to their limited thermal stability (except polyimide foils). [91,92,96] Moreover, such sensors consume a considerable amount of supplied power which will in the future be virtually unusable for handheld smart portable devices such as mobile phones, wrist watch etc.
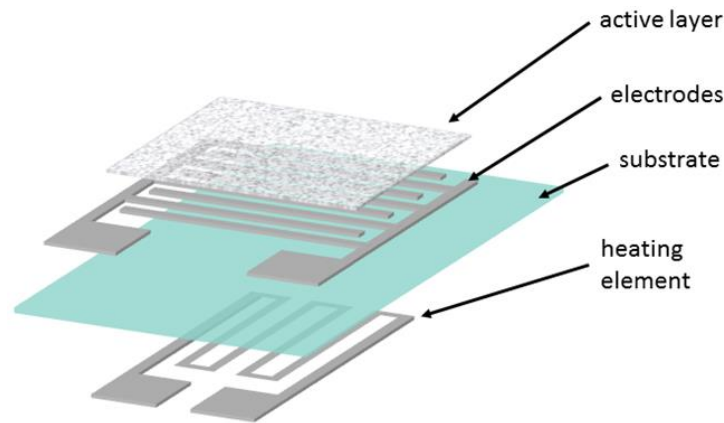

Figure 14 − *A typical example of the most commonly used MOX gas sensor construction including a heating element*

A promising alternative to the thermal activation is the use of UV radiation as excitation energy, which reduces operating temperatures of gas sensors without changing the chemical composition of used semiconductor. Since the sensing device is placed in a dark environment, the maximal wavelength λ_{max} of the UV radiation having the wavelength of energy equal or higher than the band gap of metal oxide and activating the excitation can be calculated as:

$$\lambda_{max} = \frac{h \cdot c}{E_g} \tag{20}$$

where *h* is Planck constant, *c* is the velocity of light and E_g is the band gap of used metal oxide semiconductor.

Photoexcitation increases the density of charge carriers and supply energy to overcome the energetic barriers between metal oxide grains. From the point of view of the model described above, these effects lead to narrow the charge depleted region within the grain which significantly reduces resistance of sensing film. [19,96,97]

Under UV illumination electrons are promptly excited from the valence band to the conduction band generating electron−hole populations mimicking thus the effect of increased temperature.

$$h\nu \rightarrow h^+ + e^-$$ (20)

where ν is photon frequency of UV radiation.

In air atmosphere conditions photo-induced electrons at metal oxide surface interact with oxygen and generate ionosorbed oxygen species which slightly increases resistance of sensing layer:

$$O_2 + e^- \rightarrow O_2{}^-{}_{(surface)}$$ (22)

Nevertheless, oxygen species recombine with generated holes and react with chemisorbed oxygen causing its desorption:

$$O_2{}^- + h^+ \rightarrow O_2$$ (23)

Despite of this fact, electrons of conductive band travelling inside of metal oxide narrow the charge depleted region, lowers the energetic barriers between metal oxide grains which significantly increase conductivity. Instead of a thermodynamic equilibrium, UV irradiation causes a dynamic equilibrium between photogeneration of species contributing to the sensing effectiveness and futile recombination of these species with positively charged holes shifting thus the whole material towards higher efficiency. Moreover, it contributes to eventual photocatalytic decomposition of adsorbed molecules which is a substitute for a desorption process in case of high temperature operated devices. [19,96,97]

6.3 Printing as an auxiliary process

Unlike described in previous chapters (6.1 and 6.2), where material printing was understood as a process employed for preparation of the material substance of fabricated parts or components, the ink-jet printing can be used also as an inter-stage operation, a modification step or an auxiliary process in an entire chain of processes in a product fabrication. It is possible to use material printing for the deposition of precursors, seed layers, or to prepare temporary masks and templates. In addition, it would also be possible to use ink-jet material printing for the deposition of active surface modification agents [98].

6.3.1   Ink-jet printing of nano-seed layers

The seemingly simple technology which precedes several preparatory and testing steps have many challenges and difficulties in preparing stable nanoparticle-based inks. A possibility how to overcome preparation and tuning procedures is a usage of so-called reactive inks, whose principle lies in the deposition of a chemical reactive mixtures. The chemical reaction creating a functional and nanostructured film occurs immediately after deposition or after post-treatment processes. In this way, it is possible to prepare complicated nanostructures, which in other circumstances could not be prepared in a stabilized form of ink, and due to their dimensions it is impossible to deposit through the print head nozzle orifice.

The starting material is mostly in the form of a solution of two or more substances that are involved in the chemical reaction. Assuming that, the carrier medium also participates in the chemical reaction, it is not desirable to modify the ink system to achieve optimal printing conditions.

This approach serves particularly as a depositional and the quality of the printed patterns is not a primary goal. Therefore, slight inaccuracies in formation of satellite droplets or keeping the precise dimensions of the desired motive are negligible. [20-23,99]

7. AIM OF DOCTORAL THESIS

The work aims on original preparation of sensors as representative electronic devices fabricated by using of material ink-jet printing technique from both originally prepared or commercially available nanoparticles-based and solution-based inks. The structure, morphology and properties of deposited materials and prepared devices are investigated with respect to their function.

This aim may be achieved by accomplishment of the following objectives:

- Adoption and mastering of the preparation of conductive interconnects and electrodes by the ink-jet printing using silver nanoparticles-based inks. Particular attention shall be paid to printing on polymer foils applicable in flexible electronics.

- Research and development of an ink based on metal oxide nanoparticles (ITO), its deposition using ink-jet printing technique on suitable substrate and observing and evaluating the response of printed devices to the presence of volatile organic compounds vapours (e.g. toluene). The sensor is intended for low (ambient) temperature operation. Therefore, the sensing mechanism at low temperature shall be elucidated. In order to develop the ink and optimize the printing process in a rational and well-considered manner, printability evaluation approaches based on dimensionless criteria shall be reinterpreted.

- Research and development of advanced sensing devices based on a semiconductor nanowire network prepared using ink-jet printing technique and integrating previous achievements of the work. The device shall be designed in order to unlock further improvement of sensitivity to detect organic vapours and gases at room operating temperatures.

8. EXPERIMENTAL

8.1 Materials and methods

According to previously listed goals:

Preparation of conductive interconnects

Silver nanoparticles-based inks DGP 40LT-15C and DGH 55LT-25C (ANP Co., South Korea) were selected for printing on polymeric foils.

Polyimide (PI) foil Upilex-50S (UBE Industries, Japan) and polyethylene terephthalate (PET) foil Tenolan OA 0006 (Fatra, a.s., Czech Republic) were used as substrates for final model devices. Microscope glass slides (ThermoFisher Scientific) were used as reference substrates for characterization of thickness. The surface energy of foils was estimated by the sessile drop method with the aid of the See System (Advex Instruments, Czech Republic) to 47 mN·m^{-1} for PI and 43.5 mN·m^{-1} for PET.

Water-based Indium Tin Oxide Nanoparticle Ink for Printed Toluene Vapours Sensor Operating at Room Temperature

ITO nanoparticle based aqueous inks were prepared in the form of dispersions. The proper amount (weighed) of indium tin oxide nanopowder < 50 nm particle size (Sigma-Aldrich spol. s r.o., Prague, Czech Republic) was mixed with the optimum ratio of polymeric dispersing agent and silicon surfactant provided by BYK−Chemie, ALTANA (Disperbyk®−190 and Byk®−348). The concentration of both these additives was set to be slightly above their CMCs. Ethylene glycol was chosen for modifying the density and viscosity of the dispersion (Sigma-Aldrich product). Ethylene glycol (EG) also provides a high boiling and humectant component of the solvent system. The dispersions were mixed for several hours in a sealed flask and were sonicated for 30 min by UZ Sonopuls HD 2070 homogenizer and filtered through a 0.22 μm PTFE filter to remove aggregates and agglomerated particles before filling the cartridge (n.b.). The concentrations of the ITO nanoparticles in the prepared inks were set to 10, 15, 20 and 25 wt% to compare the overall performance of each.

The optimum printing conditions were found and used as follows: the driving voltage at the nozzles during the printing process was in the range of 25–27 V with a jetting frequency of 1 kHz, a nozzle temperature of 32 °C and a plate temperature of 50 °C, the spacing of droplets was defined to 30 μm which is equivalent to a resolution of 847 dpi. The films were made by one printing run (one layer).

The printed films were dried in an oven at 60 °C for 30 min and then annealed in a muffle furnace. The annealing temperatures were chosen to clarify the effect of annealing to 400, 500 and 600 °C in an ambient air atmosphere. The sample was always inserted into the cool oven and the temperature program was set to maximum rate increase. The desired temperature was achieved within a few minutes and then the temperature was kept constant for 30 min. The oven was then left to naturally cool down to the laboratory temperature before the samples were taken out. The electrodes were connected to the copper wires by the highly conductive silver paste COATES XZ250 which was dried at 120 °C for 20 min. [4]

Microscope glass slides (ThermoFisher Scientific) were used as substrates. Surface energy of the glass was estimated by the sessile drop method with the aid of the See System (Advex Instruments, Czech Republic) to 42 mN·m^{-1}.

Development of ZnO nanowire-based gas sensor using ink-jet printing

Conductive interdigitated electrodes were printed using silver nanoparticles ink DGH 55LT-25C (ANP Co.) on polyimide foil Upilex-50S (UBE Industries) at following printing conditions: the jetting frequency of 1 kHz, the nozzle temperature of 50 °C and the plate temperature of 60 °C, the spacing of droplets was defined to 70 μm equivalently to a resolution of 363 dpi. The structures were made by one printing run and subsequently cured in oven at 250 °C for 30 minutes.

Zinc acetate dihydrate $Zn(CH_3COO)_2 \cdot (H_2O)_2$ (Penta Chemicals) was dissolved in ethanol for UV spectroscopy grade ≥ 99.8 % (Penta Chemicals) at 50 °C for 1 hour to form a particle-free solution with concentration of 10 mM, filtered through 0.22 μm pore PTFE syringe filter before filling the cartridge and locally printed onto interdigitated electrode structures as a precursor material. Films were formed at 20 μm drop-spacing, which is equivalent to resolution of 1270 dpi to reach equally deposited nanoseeds. Nozzle and plate temperature was kept at laboratory temperature level (i.e. 25 °C). After the deposition, films were thermally decomposed at 250 °C for 10 minutes in a muffle furnace (Nabertherm™, Germany) to form ZnO quantum dots as nanowire seeds. Subsequently, films were subjected to hydrothermal growth in a bath of three different concentrations of a growth-direct agent consisting of polyethylenimine, ethylenediamine branched (Sigma-Aldrich product) at 92 °C for 24 hours. Formed nanostructures were gently rinsed with deionized water, dried at 100 °C for 10

minutes in an oven (Memmert GmbH + Co.KG, Germany) and cured again at 350 °C for 10 minutes in muffle furnace to degrade the residual polymer, which could affect the sensing response and charge transfer within nanowire network.

In the next section, integrated sensing structure were deposited and formed as described above directly onto a commercial SMD UV-LED (Roithner Lasertechnik GmbH, Austria) operating at $\lambda = 365$ nm except that, the printed silver electrodes were dried for 5 minutes on a hot plate as well as the final curing process to keep limitation of mount device. Conductive array of interconnects for stripe connector were printed and cured similarly to interdigitated electrodes using silver nanoparticles ink on polyimide foil. Integrated sensing structure of SMD UV-LED was placed and mounted using highly conductive silver paste COATES XZ250 with copper wires as a vertical interconnect access appropriately and cured on a hot plate at 250 °C for 5 minutes.

8.2 Determination of crucial ink parameters

- **Viscosity** of inks was determined at low-shear rate by rolling ball Microvisco-meter Lovis 2000 ME (1.59 mm capilary) (Anton Paar, Czech Republic)

- **Surface tension** of ITO-based inks was measured by Tensiometer K100MK3 (Krüss, Germany) based on Wilhelmy plate method.

- **Density** was measured by Density meter DMA 5000 M (Anton Paar, Czech Republic).

- **TGA Analysis** was performed with the TA Q500 (TA Instruments, USA) thermal analyser working in TGA mode with programmed constant temperature growth rate 10 °C per minute and nitrogen atmosphere with total flow of 100 sccm.

8.3 Control of printing parameters

All parameters of the printing process including printing preview have been controlled through Dimatix Drop Manager Software with the ability to precisely adjust the cartridge settings, voltage on individual nozzles and the editing of waveform framework. A set of built-in cameras was used to check adjusted printing specifications such as drop generation and initial print position as well as brief printout quality control.

Deposition method

Functional materials in form of inks were deposited using material ink-jet printer FUJIFIM Dimatix DMP-2800 series. Printing nozzle orifice has square shape with the size of its side 21.5 μm which is a fixed characteristic (equivalent diameter) of the used 10 pl nominal drop size printing head cartridge having 16 nozzles. The fluid ejection process and namely drop velocity was controlled by waveform setup individually for each nozzle in the printing head. Volume of the cartridge reservoir is about 2.5 ml.

8.4 Morphology of printed patterns

- **Optical microscopy -** General quality, contiguity and compactness of printed films were preliminary observed by microscope LEICA DVM25000 Digital Camera (Leica Microsystems, Germany).

- **Profilometry -** The thickness of printed films was measured in contact mode by the stylus profiler Dektak XT (Bruker, USA) provided by a diamond stylus (25 μm radius) at 3 mg stylus strain.

- **Atomic force microscopy -** The surface morphology was examined via atomic force microscope Dimension ICON (Bruker, USA) under ambient condition in PeakForce semi-contact mode by ScanAsyst–Air probe whose tip has nominal radius of 2 nm. Scan rate of 0.5 Hz and resolution 512 lines were used in all cases.

- **Scanning electron microscopy -** In case of sensitive nanostructured films the surface morphology was investigated by electron microscope Nova NanoSEM 450 (FEI, Japan).

8.5 Electric properties of printed patterns

Resistance measurements

Resistance was measured generally throughout this work using multimeter UNI-T HC-UT71D with interface software that records observed resistance and multimeter Keithley 2010. It must be noted, that these simple multi- or Ohm-meters use two-point measurement method. It means that a known electric current is passed through the measured device specimen and the voltage is measured on the multimeter's terminals. Resistance is then estimated from the Ohm's law and displayed or recorded by the multimeter. In other words, this measurement setup

does not use one single defined operating point on the sensor device's I-V characteristic curve. Hence, any change in resistance of the measured device (in fact this pertains sensors) results into a change of the applied voltage used for the resistance measurement which will result into eventual non-linear resistance behaviour observation if the device is not purely ohmic.

Resistivity measurement

The electrical properties of semiconductor patterns were characterized by mean of resistivity measurements of printed films using four-point probe setup based on Van der Pauw method.

In case of ink-jet deposited silver conductive interconnects, electrical resistivity characterization based on two-point resistance measurement with corresponding conductor cross-section geometry was determined. For this purpose, gold coated spring test probes with round shape head avoiding scratching the surface were used to contact each side of printed line. Testing probes were connected through wiring to multimeter terminals.

8.6 Sensor performance characterization

Response of sensors consisting of indium tin oxide layer was measured using multimeter UNI-T HC-UT71D with interface software that records observed resistance. Changes between "On" and "Off" sensor states upon exposure to vapours of toluene and removal from the vapours were measured. Experiments were carried out at the ambient atmosphere in the laboratory and in nitrogen atmosphere (less than 1 ppm of O_2 and H_2O) in the glove box GP Campus (Jacomex).

Response of sensors consisting of ZnO nanostructures grown on pre-printed interdigitated electrodes were measured using customized gas sensing measurement setup as schemed in Figure 15. The amount of carrier gas was accurately controlled by arrange of mass flow controllers EL-FLOW Prestige (Bronkhorst High-Tech BV, Netherland). Precise dosing of targeted organic substance represented by ethanol was carried out manually by microliter syringe (Hamilton, USA) and transferred through the evaporating unit into a gas chamber. Sensor devices were plugged in 4-pin stripe connector placed inside the gas chamber for easy and fast sample installation and without the need for soldering. Two terminals of stripe connector were used for logging the resistance and remaining two terminals supplied a UV–LED element. Resistance changes of the sensor devices were measured and logged using multimeter UNI-T HC-UT71D

with interface software. The temperature inside the gas chamber was monitored using platinum temperature sensor PT100.
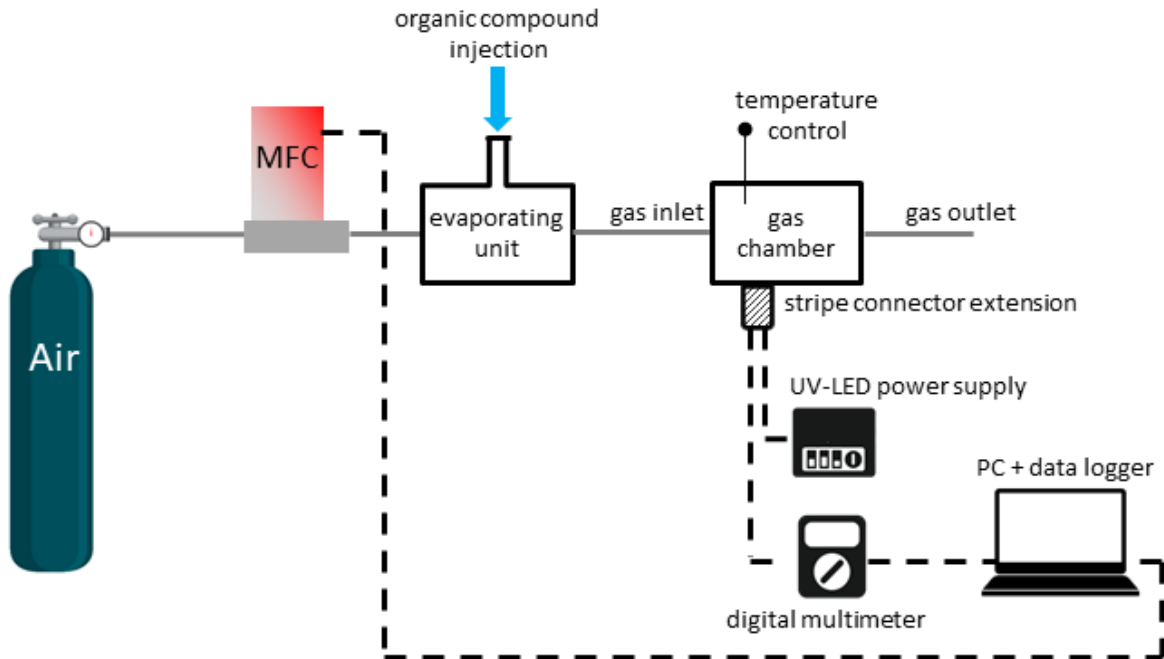

Figure 15 – Scheme of gas sensing measurement setup

The measured electrical resistance is calculated as a sensor response ratio S_R expressed as a percentage as defined [16]:

$$S_R(\%) = \left(\frac{R_{gas}}{R_{air}} - 1 \right) \cdot 100\% \tag{21}$$

where R_{air} represents the sensor resistance in air free of vapours atmosphere conditions and R_{gas} resistance upon exposure of ambience or carrier gas with targeted vapours. [4]

9. RESULTS AND DISCUSSION

Results corresponding to objectives defined in the aim of the doctoral thesis include the preparation and characterization of functional materials in the form of inks for the material ink-jet deposition of simple conductive interconnects, structures with sensing properties and nanostructured thin films, their characterization and applicability in gas sensor devices.

9.1 Research and development of conductive interconnects

Preparation and printing setup

Printing of conductive structures with commercial inks includes preparatory steps such as re-dispersing contained particles settled by storage using magnetic stirrer or ultrasonic bath and followed by filtration before filling the cartridge.

Subsequent steps include setting the printing process parameters to achieve desired dimensions and shapes of deposited structures:

- Adjusting the waveforms for optimal shape of the drop as far as possible without forming of satellite droplets.
- Adjusting the voltage on the individual nozzles to set the velocity of jetted drops.

Deposition of continuous layers

The size of the deposited drops determines and limits the dimensions of the formed structures. Depending on the size of individual deposited drops, the *drop spacing* is selected indicating the distance between the centres of individual drops deposited in a row behind. Due to overlapping and coalescing of drops after the deposition, a continuous layer is formed, which is necessary for the formation of conductive interconnects as can be seen in Figure 16. The process is exemplified on a line with one drop width. Part (**a**) of the figure shows the deposition at drop spacing 60 μm where the individual drops are separated. Decreased drop spacing to 50 μm (**b**) causes initial overlapping and coalescing of drops including random gaps between contiguous groups of drops. When the drop spacing is downsized to 30 μm (**c**) a continuous line (layer) is formed.
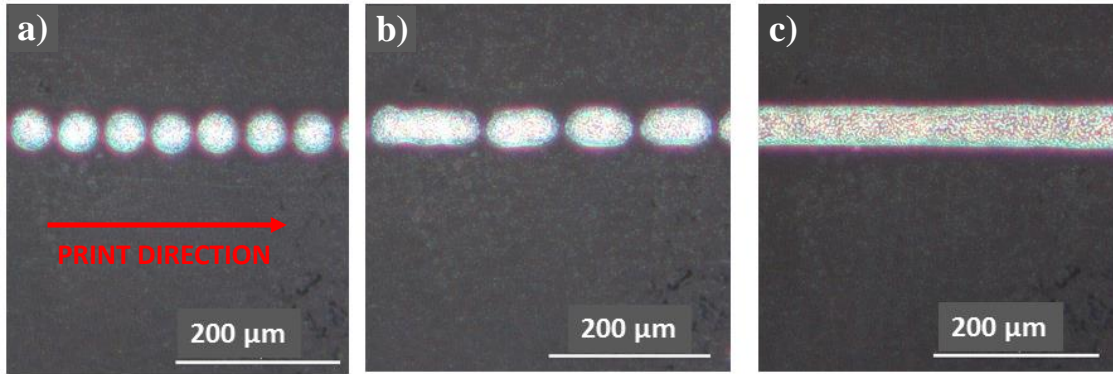
Figure 16 – Development of continuous line structure

Characterization of electric properties

Resistivity characterization of silver conductive interconnects took place on the basis of two-point resistance measurement of the pixelated lines array (see Figure 17) printed on microscope glass slide as a reference substrate. The ink DGP 40LT-15C, which is intended for printing on the PET foil, was cured at 150 °C and the ink DGH 55LT-25C, which is intended for printing on the PI foil, was cured at 250 °C both in air ambient for 30 minutes after the printing process. Exact geometry of each line was determined using stylus profiler at several places along the line. The correlation between measured lines resistance and the corresponding geometry enable to obtain a characteristic resistivity from linear regression of plotted values as seen in Figure 18 and Figure 19, respectively. For the calculation, an equation describing the relationship between resistivity and resistance was used:

$$R = \rho\frac{l}{A} + R_0 = \left(\rho\frac{l}{h}\right)\frac{1}{w} + R_0 \tag{22}$$

where R_0 represents residual resistance.

Figure 17 – Ink-jet printed silver lines array on microscopic glass slide. Width of lines is pixelated as 1, 3, 5, 10, 20 and 40 pixels. Length of 71 mm was kept constant.

Table 2 – *Properties of pixelated lines array printed of DGP 40LT-15C ink*

Line width (pix)	Line width (μm)	Thickness (nm)	R (Ω)
1	120 ± 2	94 ± 8	3860 ± 170
3	201 ± 9	168 ± 5	1040 ± 90
5	271 ± 18	197 ± 15	500 ± 100
10	471 ± 16	190 ± 30	224 ± 43
20	860 ± 20	154 ± 12	95 ± 20
40	1676 ± 17	170 ± 60	46 ± 13
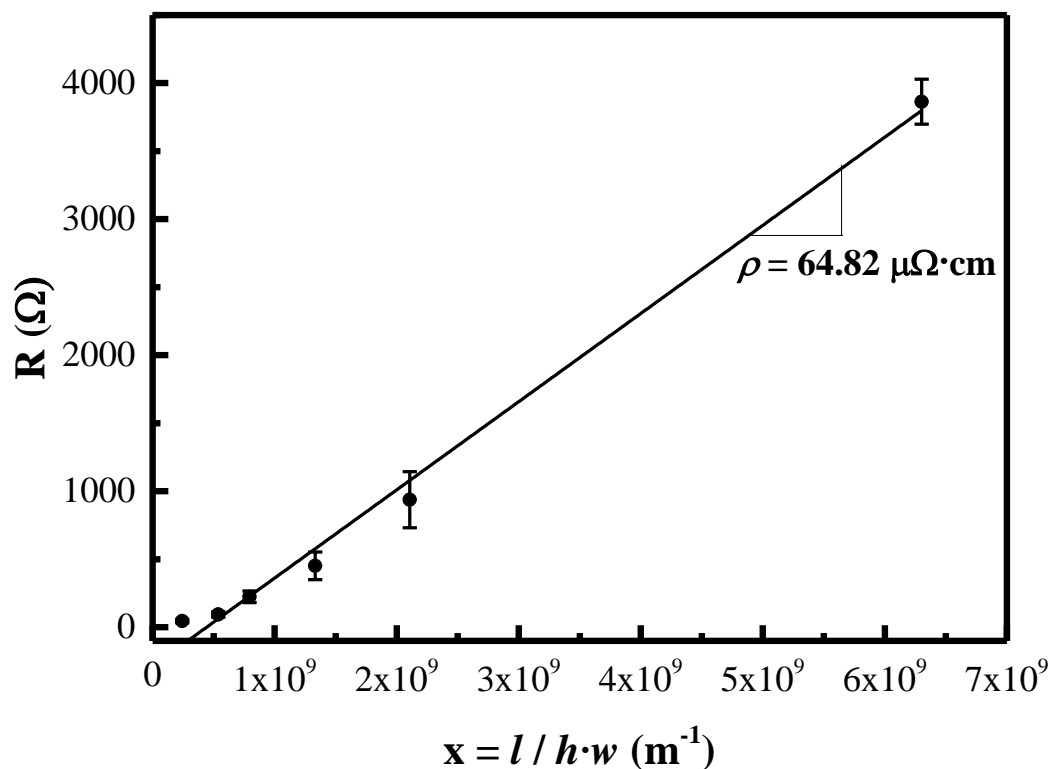
Figure 18 − *Linearized dependence of dimensions of pixelated lines on their resistance printed of DGP 40LT-15C ink. Electrical resistivity is extracted from the regression formula*

Table 3 – *Properties of pixelated lines array printed of DGH 55LT-25C ink*

Line width (pix)	Line width (μm)	Thickness (nm)	R (Ω)
1	129 ± 12	156 ± 14	230 ± 20
3	200 ± 30	320 ± 20	82 ± 10
5	267 ± 18	360 ± 40	57 ± 7
10	484 ± 12	420 ± 40	37 ± 4
20	880 ± 11	478 ± 14	23 ± 3
40	1730 ± 60	520 ± 30	13 ± 2
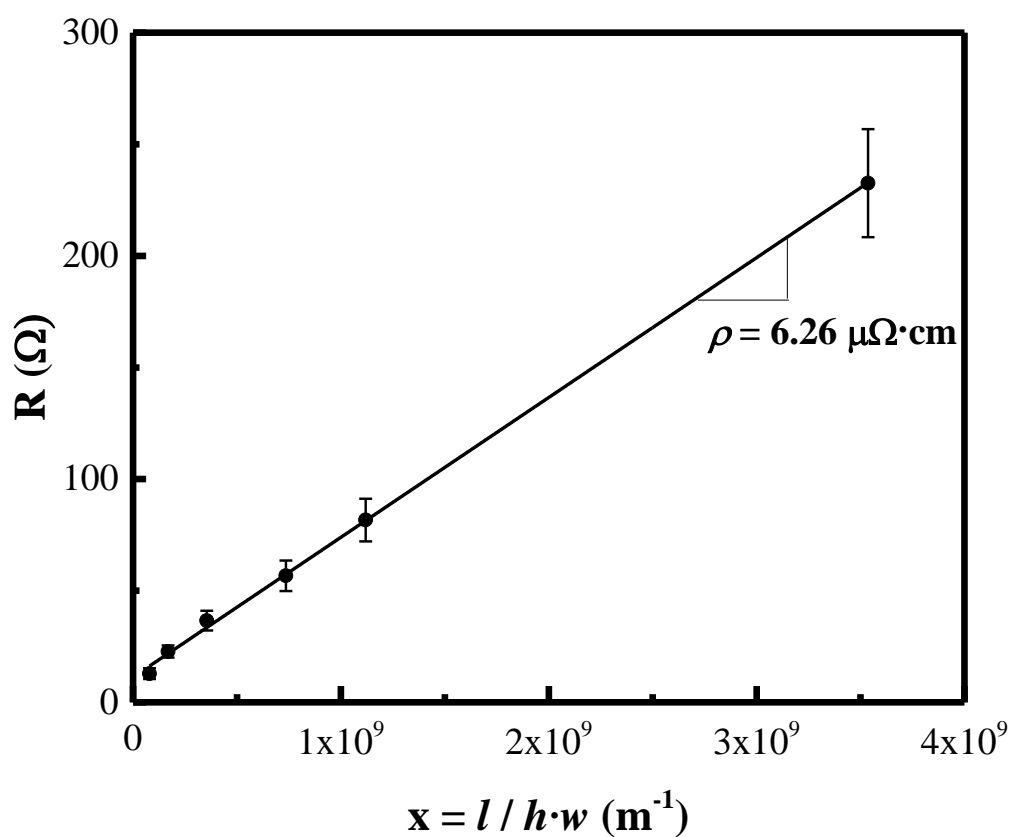
Figure 19 − *Linearized dependence of dimensions of pixelated lines on their resistance printed of DGH 55LT-25C ink. Electrical resistivity is extracted from the regression formula*

Development of printed conductive structures for electronic devices

Figure 20 illustrates developing process of hybrid electronic element containing printed conductive structure of interconnects and indicating green SMD LEDs. Step **1.** involves designing of required structure in an appropriate scale. Subsequently, image is transferred to the printer pattern creator software, where the resolution parameters are defined. In the next step **2.**, the structure is printed and its quality is characterized. In the last step **3.**, the functional components are implemented in the element and connected to a power supply.
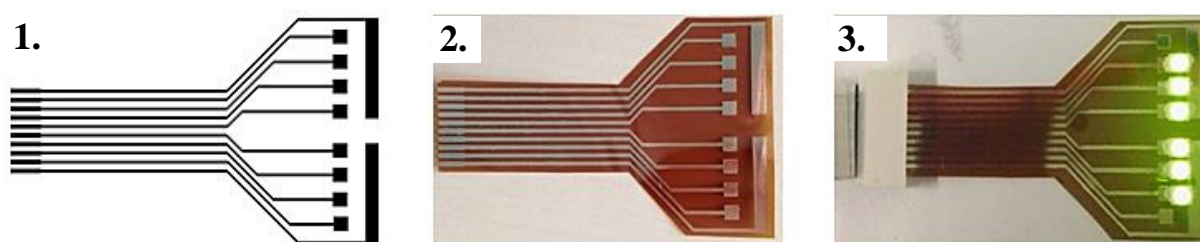
Figure 20 – Development of ink-jet printed device

9.2 Development of metal oxide nanoparticles-based ink, deposition of sensing layers by ink-jet printing and observing its response to toluene vapours

Ink composition development

The key properties determining good processability by the used ink-jet printer Dimatix DMP-2800 Series are listed by the producer for disposable cartridges with printing heads as follows. The ink fluid viscosity shall be kept in a range of 10–12 mPa·s and its surface tension in a range of 28–42 mN·m^{-1}. Furthermore, it is suggested to use a drop velocity in a range of 7–9 m·s^{-1} as the first guess [26], however, according to literature and experience in this study, a fluid ejection velocity of about 6 m·s^{-1} is commonly used. It is also recommended to filter all fluids to 0.2 μm, because particles bigger than 1/100 of the nozzle diameter may cause nozzle clogging. The first two parameters may be substantially changed by the ink composition and the size of the nanoparticles must be chosen to be smaller than the critical level. The processing parameters, namely the fluid ejection velocity and the droplet formation, are controlled by using waveform; however, they can be only slightly varied in comparison with the relatively free choice of

the ink viscosity and the surface energy. According to the producer, the viscosity range may be extended from 1 mPa·s for water-like fluids up to 30 mPa·s which is declared as the highest viable for the printer. Similarly, a surface tension of about 70 mN·m^{-1} represents the upper limit for printing with a given machine while the lower limit is 20 mN·m^{-1}.

The original ink composition was experimentally developed within this space of parameters by the trial-error method of changing and alternating always only one variable until a satisfactory performance of the process was achieved. The properties of developed inks with variable nanoparticle loading are listed in Table 4. The surface tension of the used ink compositions is compatible with the surface characteristics of the chosen substrate. The viscosity and the surface tension under given dynamic conditions did not result in the optimum formation of single droplets only, but the system worked in the regime of the one satellite droplet formation that merges with the main droplet during its flight before hitting the surface. Although this is a suboptimum process, it yielded good printing quality while other parameters were relatively easily kept at sufficient levels too. [4]

Table 4 − *Main material properties of ITO inks, [4]*

Nanoparticles loading / wt%	10	15	20	25
Surface tension / mN·m^{-1}	21.6±0.1	21.6±0.1	21.6±0.1	21.7±0.1
Density / kg·m^{-3}	1127.6	1186.7	1241.9	1306.6
Viscosity / mPa·s	3.078	3.518	4.128	4.703

Due to the above-mentioned requirements the optimal amount and ratio of the two additives was determined based on the critical micelle concentration in an aqueous medium. The surface tension was controlled by using a wetting agent which produces a significant decrease in the surface tension of the aqueous system and therefore particularly improves substrate wetting and levelling. The achieved stability of the ink compositions guaranteed their safe use within the timescale of several days and is displayed in the example in Figure 21. [4]
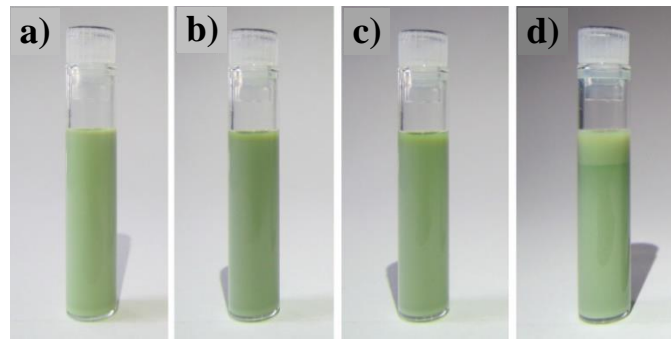
Figure 21− Demonstrating of the achieved stability and the sedimentation progress of the ink composition (25 wt% loading) over time (a) t = 0 h, (b) t = 24 h, (c) t = 72 h, (d) t = 10 days. [4]

According to the literature as described in introductory chapter 4.4, Table 5 summarises the calculated dimensionless criteria of the prepared inks with the use of ink ejection fluid velocity finally estimated with the help of analysis discussed below. The influence of gravity is considered as being of very low relevance on the investigated range of parameters (including the stand-off being 1 mm) and therefore is not considered in this analysis. The formulas of used criteria are given in Eq. 5 – 8 for dimensionless criteria. [4]

Table 5 − Calculated dimensionless criteria of prepared inks[4]

Nanoparticles loading / wt%	10	15	20	25
Re	47.26	43.51	38.81	35.84
We	40.44	42.50	44.42	46.60
Oh	0.13	0.15	0.17	0.19
Z	7.43	6.67	5.82	5.25
Ca	0.86	0.98	1.14	1.30

The prepared suspensions were intentionally theoretically treated as Newtonian fluids only, neglecting the eventual weak viscoelasticity. Such an approach simplifies the problem radically; however, it can be applied until it produces predictions comparable with experiment. According to an analysis of ink-jet

printing regimes by E. Kim and J. Baek [68], all prepared inks fall into the "regime II" which is characterized by relatively small Ca and large We numbers. These conditions are manifested by a satellite formation and the merging of the satellite with the main droplet during its flight, thus fulfilling the definition of good printability when "a single drop is formed either directly without a second pinch-off or the satellite drop merges with the main drop within its travel distance less than 20 times A forming thus a single drop".

Referring back to literature sources, a simpler and earlier solution involving all material-tool-process characteristics may be found in the work of McKinley and Renardy [71], who redrew the schematic diagram originally constructed by Derby [67] to show the field of parameters for stable operations of drop on demand inkjet printing by using logarithmic coordinate system defined by plotting Ohnesorge against Reynolds number. The graph constructed with the help of their definition of printability boundaries is presented in Figure 22. The quadrangle ABCD defines a region, in which the particular fluids are printable and single drop formation may be achieved or merging with the satellite can be expected. The diagram does not resolve between regime I and II as defined later by E. Kim and J. Baek.
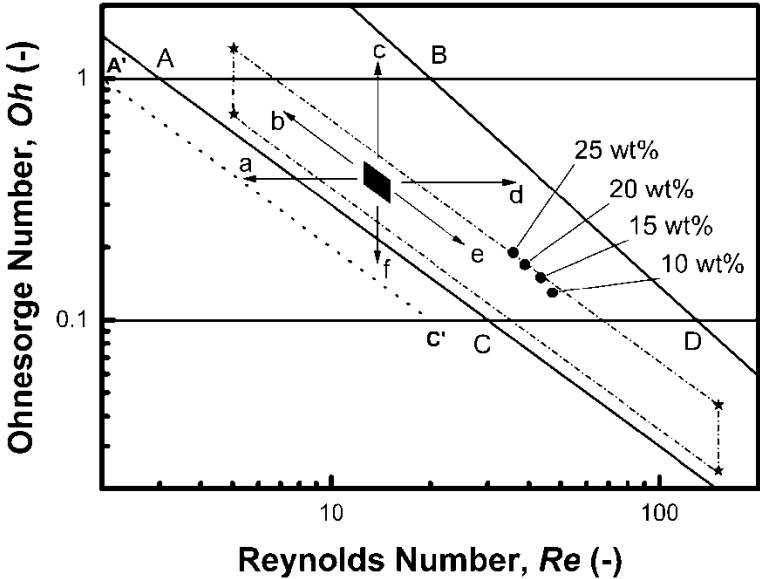
Figure 22 − *Map of Oh and Re dimensionless correlations space for a printing process with the printability area ABCD replotted according to McKinley and Renardy [71]. For a detailed description please see text. [4]*

The purpose of printing process optimization is an achievement of the good printability conditions which is an absolute prerequisite for obtaining good-quality thin film layer including its precise location, resolution and functionality. We found it to be useful to discuss the printing parameters according to the suggestions of the printer producer and compare them with our experimental procedure. The small black full quadrangle in the center of the ABCD area in Figure 22 represents the optimum printability space for the Dimatix printer (i.e., viscosity 10–12 mPa·s and the surface tension in the range of 28–42 mN·m^{-1}) while the typical value of the density of our suspensions varies slightly between 1.1 g·ml^{-1} and 1.3 g·ml^{-1}, therefore 1.2 g·ml^{-1} was chosen for the model. The droplet velocity can be varied by the waveform process control; nonetheless our typical final optimum value 6 m·s^{-1} is taken into account in this analysis. Finally, the characteristic length A is strictly given by the nozzle geometry in the used printing heads and cannot be changed at all. The changes of the variables involved in the dimensionless criteria result in typical shifts or extensions of this parameter space in the directions indicated by the six arrows marked from **a** to **f**. Decreasing the fluid velocity corresponds to the direction a while the use of higher velocity shifts the area in the direction **d**. Increasing the surface tension shifts the parameter space border downwards in direction **f** while decreasing the surface tension results in the shift upwards in direction **c**. Increasing the fluid viscosity results in the shift along the arrow **b** and decreasing the viscosity extends the area in the direction of the arrow **e**. Changes in the characteristic length or the density will result in a diagonal shift too, however, the slope will be −1/2. The full extension of the printability span according to the extreme viscosities and the surface tensions declared by the printer producer is indicated by the quadrangle with asterisks in its corners and the short dash dot sides. The position of the prepared inks is marked by the four full circle data points labelled by ITO concentrations. It must be noted that the points are aligned along a virtual line, which has slope −1 and represents a line with a constant value of $We^{1/2}$ of about 6.6 which corresponds to the average We number value from Table 5 of about 43.5. Although a good printability was finally achieved for all compositions by varying the parameters, the point closest to the centre of the printability area corresponds to the ink composition with 25 wt% of ITO.

Actually, the graph in Figure 22 can be parametrised by a set of $We^{1/2}$ isolines based on the formula in Equation (11). These hyperbolic isolines are represented as straight lines using logarithmic axes. The similarity of these lines with the diagonal borders of the ABCD area invokes somewhat the old idea of the

importance of a single dimensionless number again, *We* number this case. The line AC corresponds exactly to the *We* value 9 (means $We^{1/2} = 3$). The importance of the *We* criterion was raised by Derby himself again in [100], where a corrected version of his original printability graph is published. However, *We* value 4 is used by Derby according to Duineveld et al. [101] as a minimum Weber number for a drop generation thus delineating the border to overcome the surface tension at the exposed nozzle. This value corresponds to the dotted line A'C' with $We^{1/2} = 2$ in the graph in Figure 22, predicting a larger printability area. On the other hand, the splashing threshold line BD is not characterized by one value of the Weber number only. Actually, $We^{1/2}$ linearly varies from 20 for the point B to 13 for the point D. To generalize this lesson, we believe that the exclusiveness of *We* among all the other dimensionless numbers used for describing the printability of inks it is due to the prime importance of the surface tension among all the discussed ink-jet material characteristics. The absolute condition *sine qua non* of printing is the formation of the ink droplets and there is only one physical variable that is the source of the forces forming the droplet spherical shape, and it is the surface tension. It shall be mentioned that if the fluid is viscoelastic, the elasticity will contribute to the drop formation also. Moreover, the Weber number also contains the tool (*A*) and the process (*v*) characteristics in contrast to the *Z* number which is based on the material characteristics only. In our specific case, we experienced the good printability when decreasing the *We* value below 47. [4]

Annealing Temperature Optimization

Optimizing the annealing temperature is the key step in post-printing treatment of the manufactured device. Indeed, this important factor (i) influences grain size, densification or porosity of metal oxide film, which is closely related to the sensing efficiency [2,87,102] furthermore it (ii) determines the resistance of the film and (iii) allows the removal of additives, which could cause interactions with the gas being sensed and thus influence the response of the sensory layer. Finally, the annealing temperature influences (iv) the choice of an appropriate substrate for the final device. Therefore, a thermogravimetric analysis of the prepared ink compositions has been accomplished to observe the temperature ranges corresponding to the evaporation of solvents and the vaporization of surface active polymer additives. A decomposition of the ink proceeded as shown in Figure 23. In the first two steps low-molecular substances (water and ethylene glycol) were volatilized. Their complete evaporation was achieved below a temperature of 200 °C. The complete decomposition step of the present surfactant and the

dispersant agents was observed in a range of 300 °C to 400 °C hence the lowest annealing temperature for printed films was set to 400 °C, and other samples were made at 500 °C and 600 °C for comparison too. [4]
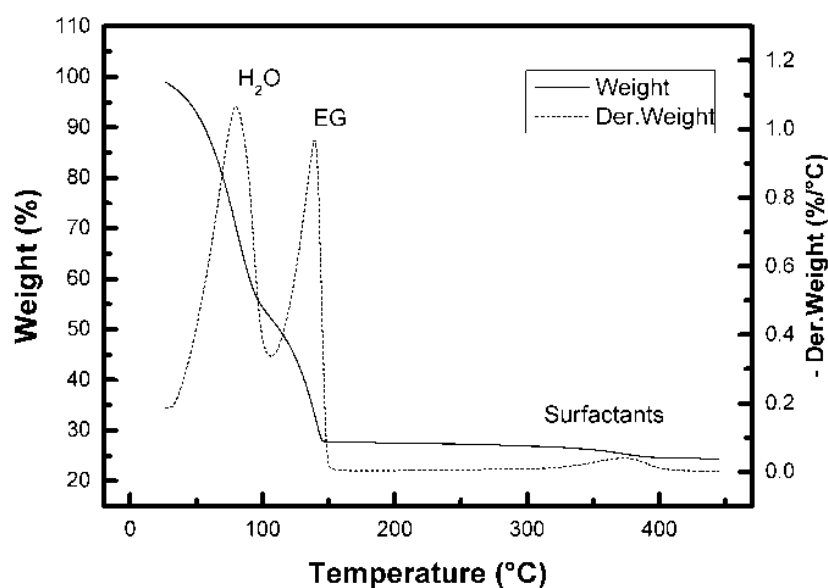

Figure 23 − The thermogravimetric curve and its derivative recorded for the ink composition with ITO particle loading 25 wt%, [4]

The morphology of original ITO particles as well as annealed films is shown in Figure 24a in the figure depicts the ITO nanopowder as received. Presence of a wide size distribution can be observed. The biggest tetragonal bipyramids are of size below 100 nm but the vast majority of particles is significantly smaller and the powder materials generally corresponds to the specification provided by the supplier (<50 nm particle size). Treating deposited layers at temperatures of 400 °C, 500 °C and 600 °C leads to the formation of separated grains, which are in physical contact, see Figure 24b,c,d respectively. Formation of short necks between individual grains was not confirmed and could be expected for higher temperatures. Thus, the sensing mechanism can be described using the "grains" or "grain boundary" model, where the Schottky interface between the grains, the height of potential barrier and therefore the dimension of the depletion region variation depends on the ambient atmosphere composition. The conductivity of this treated type of nanocrystalline metal oxide operates by grain boundary space charge (band bending) on inter-grain contact interfaces.
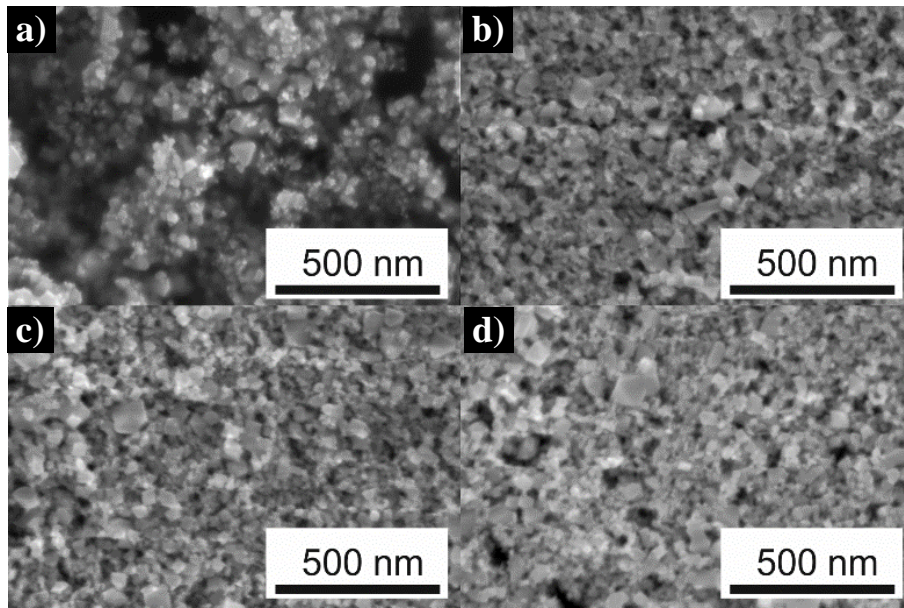
Figure 24 − *SEM images of ITO particles as received (a) and films made from the ink with ITO particle loading 25 wt% annealed to 400 °C (b), 500 °C (c) and 600 °C (d). [4]*

Higher annealing temperatures increase the contact between the grains and can lead to the sintering of the grains in the agglomerates (>500 °C) [103], which contributes to electric transport and increases conductivity. On the other hand, lower annealing temperatures allow for forming a more porous structure and the volume of the layer is more accessible to the detected gas, thus, the active surface is kept. As can be seen in Figure 25, the formation of a granular and porous structure is evident. A higher concentration of the charge due to the densification of the structure at a higher annealing temperature of 600 °C, and on the contrary a more porous structure in depth containing less neck connected grains at a lower annealing temperature of 400 °C was observed using scanning tunnelling microscopy combined with surface morphology and scanning electron microscopy of printed and heated films. [4]
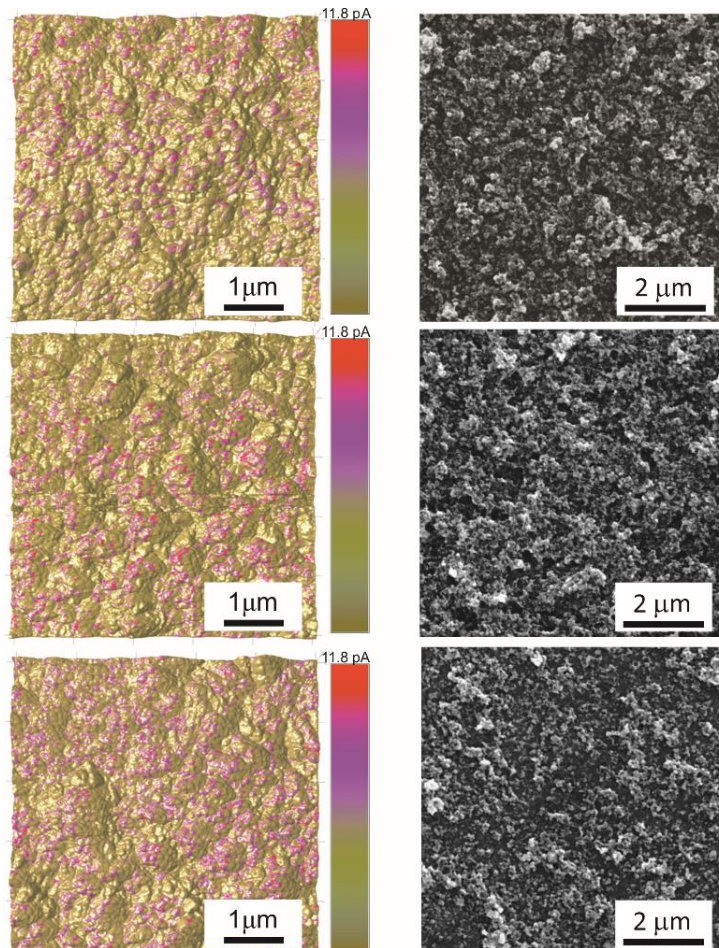
Figure 25 − *The current mapping (left side) and the SEM images (right side) on the surface of the printed and annealed films at 400 °C (top), 500 °C (middle) and 600 °C (bottom). [4]*

Ink-jet deposited films characteristics

In general, in comparison to vapour deposition methods, ink-jet material printing does not allow for preparing highly homogenous and flat surfaces (depending on the nature and composition of the ink), which may not be a disadvantage for sensing films, due to the formation of a porous structure. For sensing devices fabricated by an ink-jet printing method it is necessary to achieve high-quality and compact layers which are conductive throughout their volume. A set of representative optical micrographs of printed films is shown in Figure 26. Magnified images of edges of printed rectangular motifs were used to overall quality assessment of the printing. Best contours of the motif were obtained with the 25 wt% ITO ink; hence it performed best among tested dispersions. Therefore, this ink was chosen for printing test specimens and further research. Moreover, Figure 26 documents the high compactness of the printed

layer achieved by optimal selection of the ink composition, tuning of the printing process and appropriately selected drop-spacing. An increased amount of nanoparticles in the ink composition increases the thickness of the deposited layers linearly. This finding could lead to the setting of the required thickness through the concentration or loading of particles in the ink. From the obtained values of surface roughness, which decreases with the amount of particles in the ink, it can be concluded that higher loading and a constant annealing temperature leads to the densification of the deposited layer due to easier access and the formation of the grains during the annealing process, which is confirmed by the decrease in bulk resistivity. The densification of the layer and therefore a reduction in porosity may not always be desirable for sensor layers. The data in Table 6 shows that the resistivity of the prepared ITO layers decreases with increasing density of the ink due to an increased concentration of ITO nanoparticles. [4]
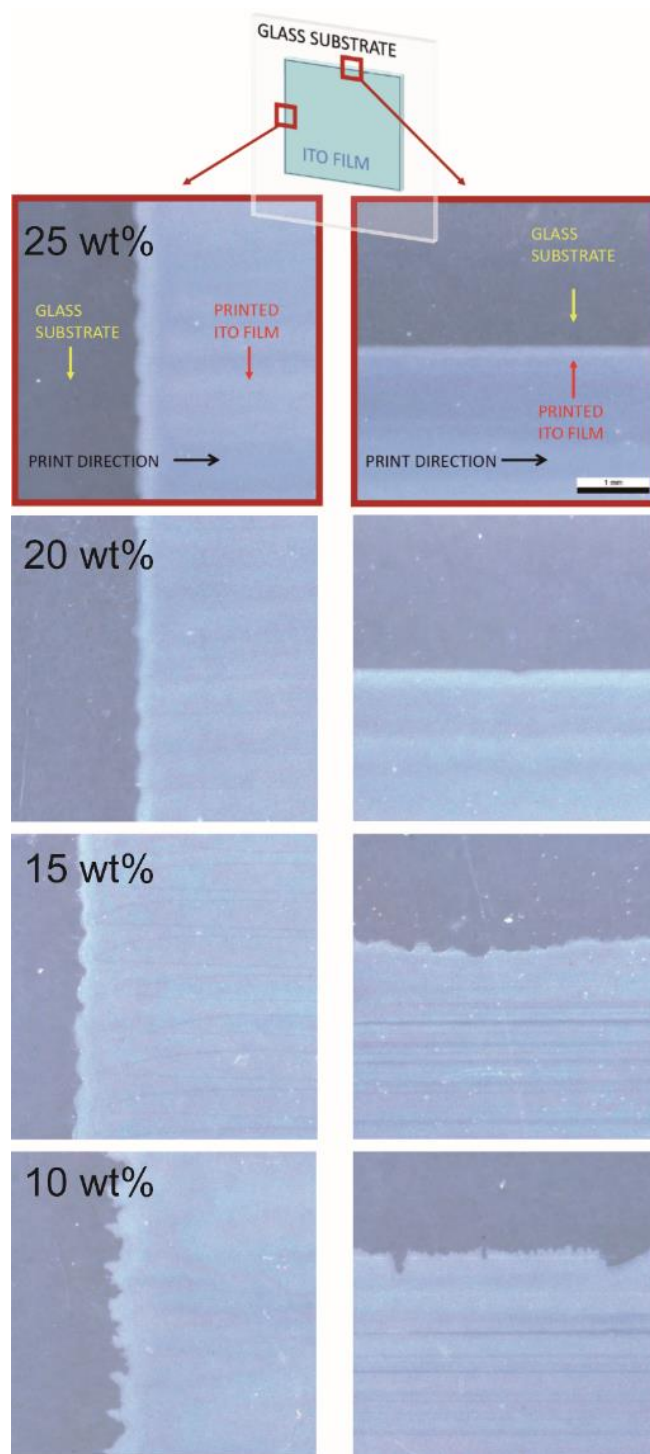
Figure 26 − *Optical micrographs of one printed layer ITO rectangular motifs. Pairs of magnified edges of squares printed by different ITO concentration inks are presented. The side edge is always in the left image and the top edge is always in the right image. The locations of imaged areas on the specimen, substrate and film material identification, and printing direction are indicated by arrows in the first row of images and this orientation pattern applies for all other rows also. [4]*

Table 6 − Thickness, resistivity and surface roughness of one-run printed layers of different ITO inks loading after annealing process at 400 °C, [4]

Nanoparticles loading / wt%	10	15	20	25
Film thickness / nm	550±30	780±30	1140±30	1510±40
Resistivity / $\Omega \cdot cm$	51.88±0.02	45.76±0.03	40.37±0.02	14.21±0.01
Roughness $_{RMS}$ / nm	41±3	31±1	31±2	34±1

Gas sensing test

Prepared sensing devices consisting of ink-jet deposited ITO films were arranged as schematically shown in Figure 27.
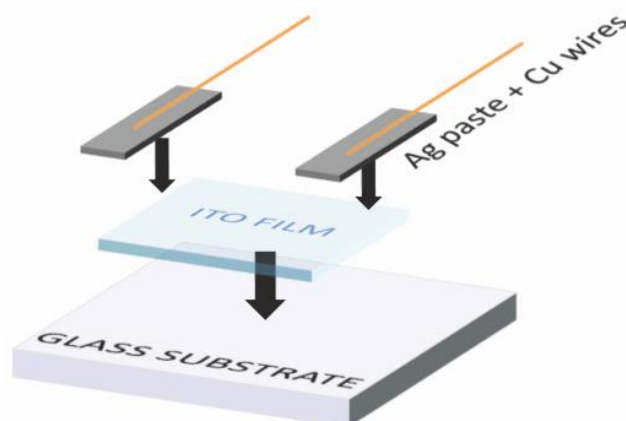
Figure 27 − Schematic design of sensing device, [4]

The mechanism responsible for the changes in the conductivity/resistivity of the layer observed in the presence of vapours can be attributed to predominating models: oxygen ionosorption and oxygen-vacancy model (reduction-reoxidation mechanism). The ionosorption mechanism of the metal oxide sensor response to the gases assumes a reaction of exposure gases with directly pre adsorbed O_2 species, from ambient oxygen, on the film surface. Oxygen molecules capture free

excess electrons from the valence band of the oxide lattice structure and changed as O_2^-. This process continues by formation of O^- and leads to decreasing the carrier concentration and causes a slight increase in the resistance of the thin film. [4]

In accordance with the described mechanisms in Chapter "Metal oxide based sensors", we noticed a variation in the electrical resistance of the printed sensors (with a sensing layer prepared from ITO 25 wt% loading ink) upon exposure to saturated vapours of toluene in ambient air (toluene/air) at 25 °C as shown in Figure 28 (upper graph window), which corresponds with the n-type semiconductor behaviour as described by Vaishnav [14]. The response of the sensor operated in air can be explained by both the above-discussed mechanisms. However, the equilibrium in the reactions (17) and namely (18) is shifted to the left side at low temperatures (25 − 150 °C). The species O^- is believed to be dominant at an operating temperature of 300 − 450 °C while molecular forms should be favourable at low temperatures [104,105]. Therefore, we consider the oxygen vacancy model more plausible for operating the ITO sensor in air atmospheres. Baseline drift can be attributed to the presence of coexisting gases in an uncontrolled ambient laboratory atmosphere since we experienced it regardless to the pre-equlibration of the sensor. Because of the porous nature of the layer as well as a low operating temperature, the sensor requires a longer recovery time needed for desorption and diffusion of vapour molecules from the porous film. We also observed that resistance increases when the sensor is exposed to saturated toluene vapours in an oxygen-free atmosphere as shown in Figure 28 (lower graph window). This conductivity behaviour inversion can be attributed to a change to the sensing mechanism after placing the sensor into an N_2 atmosphere similarly as in [47,106-108]. However, none of the above-discussed models can apply for this case. It can be reasonably expected that oxygen adsorbates likely desorb from the surface in inert atmosphere, leaving behind electrons to the bulk of the semiconductor. On the other hand, the adsorption of electron accepting gas molecules causes a charge carrier transfer resulting in band bending and the formation of a charge depleted region, which is manifested as an increase in resistance. It is noteworthy that in a controlled inert atmosphere no baseline drift is experienced. The overall sensitivity of the prepared devices is in order of several % in both types of atmospheres (slightly higher in N_2) as measured at room temperature which can be explained by a high intrinsic conductivity of the ITO material and a suboptimal thickness of the sensing layer. The charge carrier density of ITO is reasonably high and the shape

of the conduction band at the Fermi level faithfully retains the intrinsic parabolic character due to the contribution of Sn 5s electrons. This unique material property makes ITO a highly degenerate n-type semiconductor or, alternatively, a low-carrier-concentration metal [109]. The Debye length of ITO is very small and therefore also the depletion layer on the particle surface is extremely thin hence the main contribution to the sensing layer conductivity is due to the grain volumes which is not affected by the stimulating gas adsorption/desorption [105]. On the other hand, a fast response and recovery of the sensor resistance was experienced, and the performance (sensitivity) of the prepared device can be assessed as very promising if room temperature is considered as the operating temperature. [4]
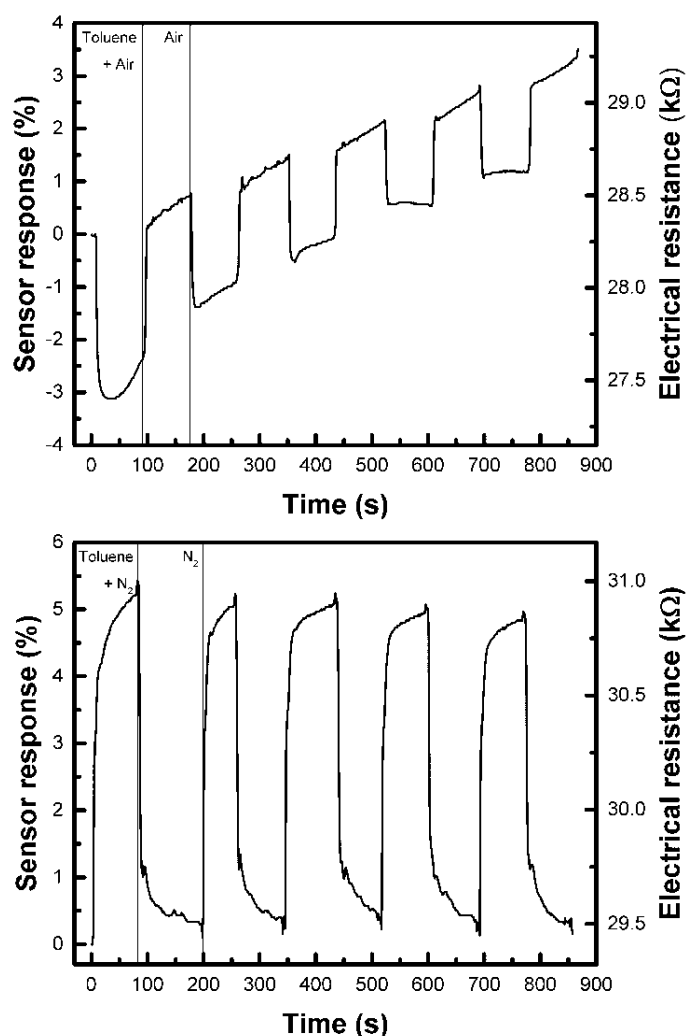
Figure 28 − *The sensor's response magnitude to the exposure of Toluene/Air and the saturated vapours of Toluene in an N₂ ambient atmosphere at 25 °C. The film was prepared from ITO 25 wt% loading ink composition. [4]*

9.3 Research and development of ZnO nanostructure network by ink-jet printing for volatile organic compounds sensor

The last part of the thesis deals with the preparation of nanostructured zinc oxide networks by ink-jet printing and their integration in a sensing device in order to increase the sensitivity to detect volatile organic compound at low operating temperatures.

The intention of depositing semiconductor nanostructures is to increase surface-to-volume ratio thereby increasing the concentration of active centres and the adsorption capacity on the metal oxide surface comparing to polycrystalline thin metal oxide film. Moreover, individual nanowires having the length in micrometre scale provide a resistance-free pathway and the overall resistance of the network is given by energetic barriers at the boundaries of nanowires percolation. At appropriate thickness of nanowires, the sensing response can be directly driven by a depth of charge depleted region corresponding to a concentration of detected gas or vapours. From this point of view, nanowire networks seem very advantageous and are a very promising material for a new generation of gas sensors. [110]

However, due to the process parameters of ink-jet printing described above, and the proportions of nanowires whose length reaches micrometre orders, the preparation of stabilized dispersions and incidental clogging of the nozzles during printing process could cause many complications in localized deposition of the homogenous structure. This can be avoided by depositing a precursor solution followed by nanoparticle synthesis and subsequent crystals growth.

Nanoseed precursor was ink-jet deposited onto pre-printed interdigitated silver electrode structures from prepared solution which was subsequently subjected to hydrothermal growth for 24 hours at 92 °C at three different concentrations of a growth-direct agent resulting in different thickness, shape and growth direction of nanostructures as seen in Figure 29. To note, further increase of PEI concentration did not yield any defined structure. Grown ZnO nanostructures were subsequently dried and observed by electron microscopy. The sensing responses of prepared devices were tested for the presence of ethanol at room temperature and the responses of the variously formed nanostructures were compared. Furthermore, the structure with the most favourable response was selected and incorporated into a novel integrated UV-assisted low temperature gas sensing device. Measurement was performed in the dark environment of the gas chamber as well as with UV activation upon exposure of ethanol vapours pulses repeatedly.
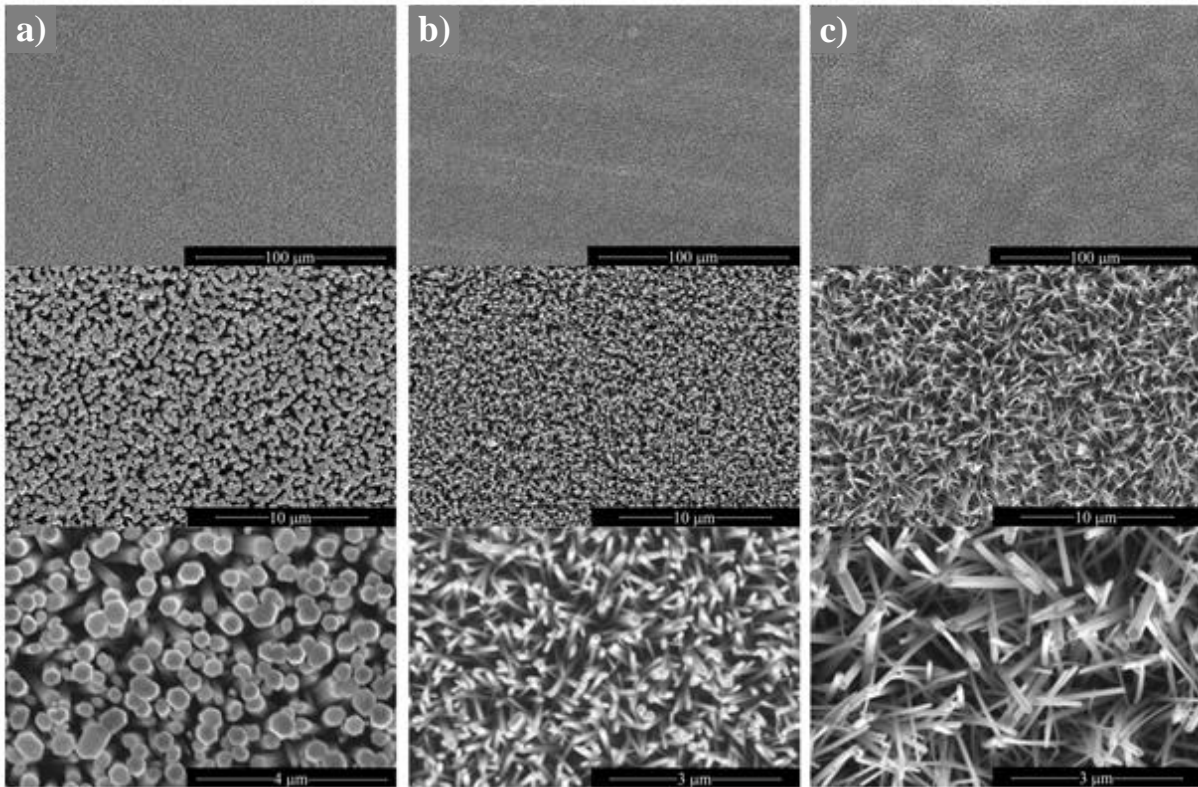
Figure 29 – SEM pictures display homogeneity of nanostructures as well as detailed shapes of nanowires at different magnitudes. Nanostructures in column a) were grown in bath without addition of growth-direct agent, bath in column b) contained 0.008 M and column c) 0.016 M solution of growth-direct agent.

9.3.1 Development of flexible gas sensor of ZnO nanostructures

In order to increase the effect of sensitive layer, improve repeatability and response stability, the placement and the arrangement of electrodes carrying the active layer is the first important step in sensor fabrication. While in the chapter 9.2 of this thesis, parallel conductive pads were employed as contact electrodes of resistive layer, capacitive planar geometry of conducting electrodes called interdigitated electrodes (IDE) was designed and tested in this section. This electrode configuration is the most commonly utilized design allowing the detection of resistance or capacitance of sensitive layer generating output signal associated with the exposed gas. Thus, the conductivity of the sensitive material and the distance of the electrodes in between the material is placed, determine the initial signal value which must be chosen within the range of the measuring instrument. A proprietary design of the device is schemed in Figure 30. A challenging minimization of electrode width and gap size was applied.
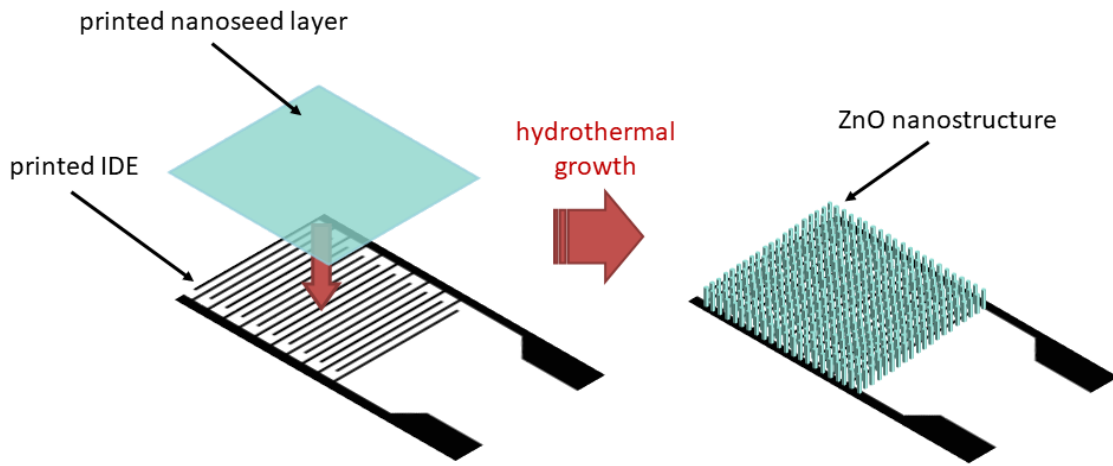
Figure 30 – Schematic illustration of fabrication process of flexible sensing device

The configuration of the lowest possible distance between each leg (digit) of IDE having single-pixel line deposited on the substrate surface by means of the coalescing of deposited droplets and three-pixel gap in between the lines was set as a minimal possible area to maintain the necessary space for sensitive material intended to overprint. Designing a smaller gap size could cause overlapping of drops belonging opposite electrode and hence undesirable conductive interconnects (short-circuits). Even though the arrangement is very convenient, it reaches the limits of ink-jet printing such as minimal linewidth and relatively high incidence of errors, hence the dimensions may vary considerably depending on surface tension of the used ink, the interaction with different substrates and selected drop spacing.

In order to increase the reproducibility and repeatability of ink-jet printed IDE platform, two-pixel conductive lines in between four-pixel gaps were arranged. Deploying two-pixel lines significantly reduces the error rate within the leg arrangement and four-pixel gap is sufficient to avoid accidental short-circuiting overlaps caused by accidental generation of satellite droplets or by a random change the trajectory of jetting drop. The resulting dimensions of the deposited lines and the gaps between them are listed in the Table 7.

Table 7 − Dimensions of printed IDE configuration

Pattern of 30 legs		Pattern of 20 legs	
Leg width	**Gap size**	**Leg width**	**Gap size**
1 pix	3 pix	2 pix	4 pix
(182 ± 15) μm	(94 ± 12) μm	(239 ± 16) μm	(174 ± 16) μm

The design and preparation steps of the flexible ZnO nanowire based device is presented in Figure 31. The real printing motif is magnified to the same size as the images of the IDE intermediate and the final device captured by optical microscopy. A well resolved structure of 2-pixel width electrodes (the 20 legs pattern design according to Table 7) was prepared, successfully overprinted by the seed layer and hydrothermally covered by the ZnO nanowire forest.
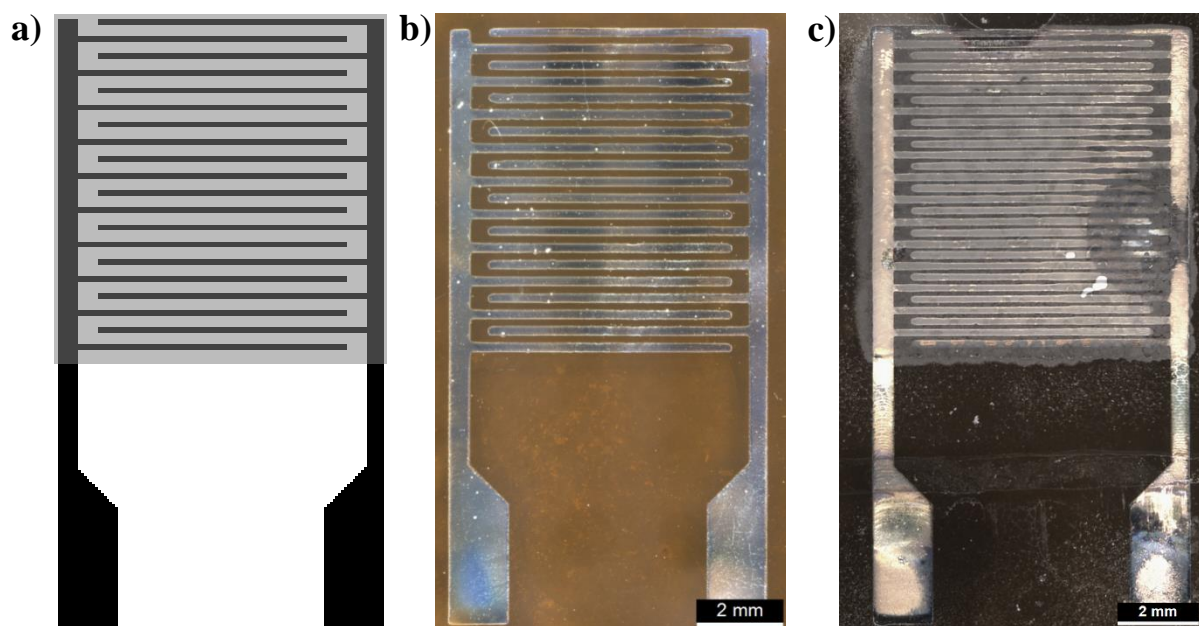
Figure 31 – Development of flexible gas sensing device from a) designing, b) printing of IDE to c) printing and forming of active layer

Three different methods of hydrothermal ZnO nanowire growth were applied, thus three sets of flexible specimens were obtained and tested in the apparatus described in chapter 8.6 at the room temperature. The three types of response curves to the pulses of the analyte in dry air flow (200 sccm, dose of 1 µl of ethanol injected and instantaneously vaporised every 5 minutes, performed in dark) are plotted in the graph in Figure 32. The first type of nanostructured ZnO which consists of thick well-ordered vertically aligned nanorods does not exhibit any response to the pulses at all. Moreover, continuous and non-monotonous drift of the baseline was observed although the conditions of the carrier gas were under perfect control by using synthetic gas of high purity from a gas cylinder. Thus no repeatability can be expected for this type of device (material) and it was excluded from further considerations. Application of the PEI growth modifying agent allowed to prepare thinner nanowires in form of a forest. Use of 0.008 M

concentration of PEI in the growing bath solution resulted into an ordered but vertically slightly misaligned structure while doubling the concentration of PEI (16 mM) resulted into even more misaligned nanowire structure with longer but thicker wires having apparently more connections than in previous case. Influence of such morphology is manifested in the response curves for these devices which are plotted in Figure 32 as well. The 8 mM sample has bigger response to each pulse than the 16 mM sample which can be correlated with the thickness of the nanowires. The thinner the nanowires the bigger sensitivity can be expected. On the other hand, the stability of the baseline and background signal (i.e. off state) was much better for the last type on nanostructure, possibly due to better development of nanowire percolation. On the base of these findings, the last type of material was selected for further development of a novel integrated UV-assisted low temperature gas sensing device. It must be noted, that this IDE designed sensor is actually a partial result and can be considered as an independent proof of concept as well. It is actually an intermediate result associated with the accomplishment of the third goal of the dissertation.
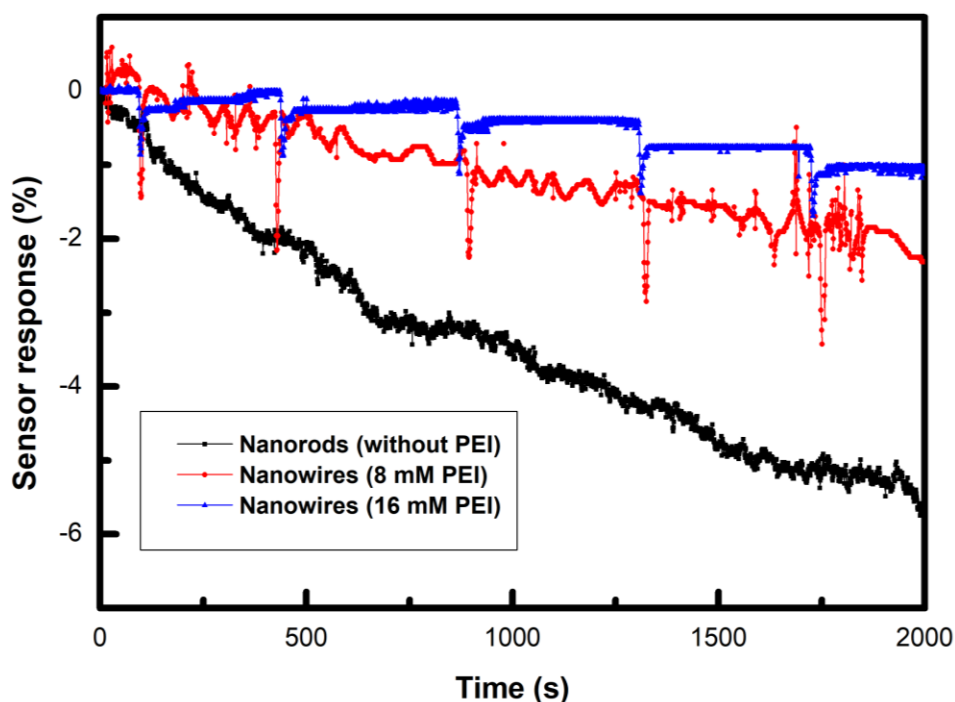
Figure 32 − The response magnitudes of sensing devices consisting of ZnO nanostructures formed at various concentrations of growth-direct agent to the exposure of pulses of Ethanol in dried Air at 25 °C

9.3.2 Development of UV-assisted gas sensor of ZnO nanowire network

Unlike previous attempts of UV application discussed in chapter 6.2.1.2 'Operating conditions of metal oxide gas sensors Temperature vs. UV irradiation' and references therein, here it is intended to integrate the sensing layer directly on top of the UV irradiation source (quartz window of the LED emitting at $\lambda = 365$ nm) while in the previous literature, the sensor was always irradiated from the top by an external UV light source. The closest contact between the semiconducting ZnO sensing material and the source window is achieved by utilization of this design, however, such geometry imposes strong requirements on the active layer thickness (fineness of the structure) and fabrication process development. Figure 33 depicts the sequence of the three fabrication steps including (i) printing of all the miniature motifs on the UV LED window followed by (ii) hydrothermal growth requiring protection of the LED substrate against corrosion by the chemical growth bath solution and accomplished by (iii) assembly of the SMD to the printed conductive platform for operation of the whole device.
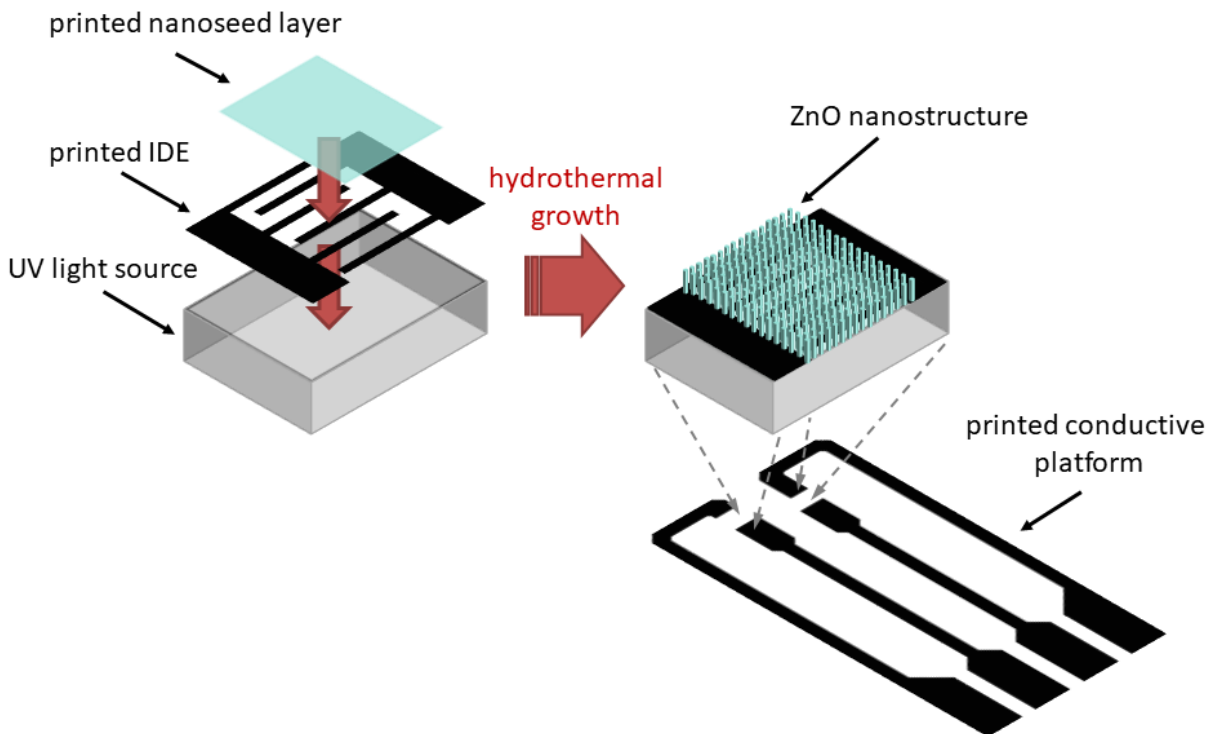
Figure 33 *− Schematic illustration of fabrication process of integrated sensing element assembled on printed circuit board*

The starting LED structure and the results of the first two fabrication steps are documented by micrographs in Figure 34 while the preparation of the flexible conductive platform by inkjet printing and the final device with a stripe connector as a result of the assembly mounting step is documented in Figure 35.
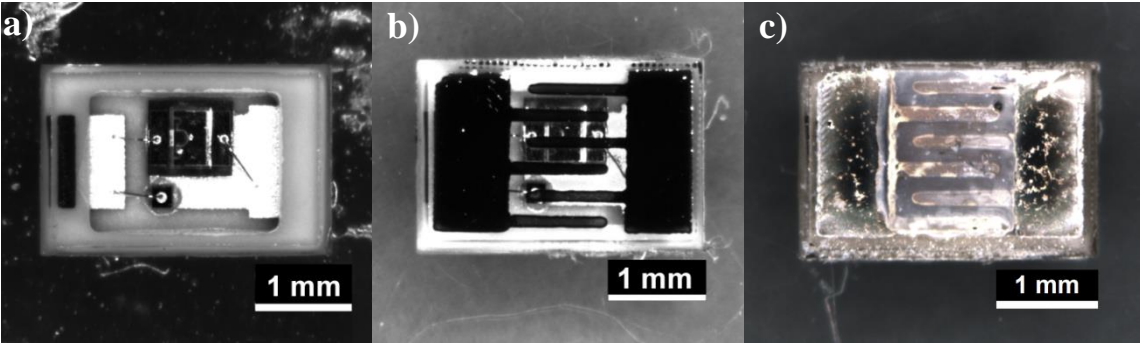
Figure 34 − a) SMD UV-LED b) printed silver IDE on top of the LED window c) printed and formed layer of ZnO nanowire network as obtained from the hydrothermal growth step
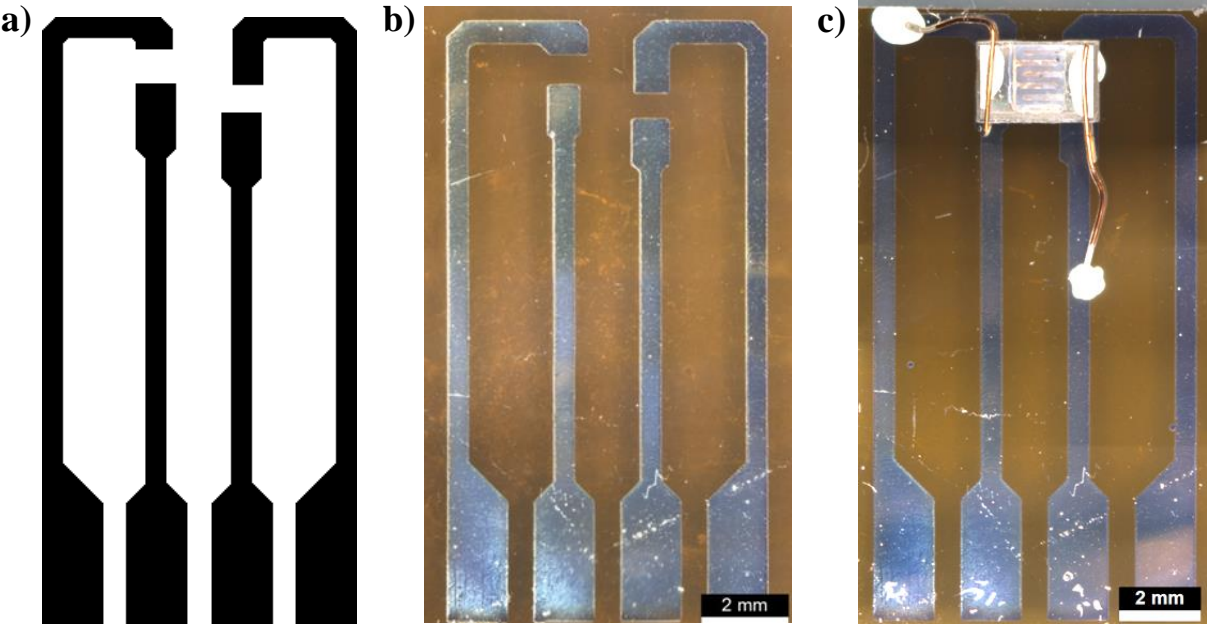
Figure 35 − Development of flexible circuit board for stripe connector from a) designing the pattern, b) printing of interconnects and c) assembling with integrated gas sensing element

Prepared sensing device was tested in the same apparatus as the flexible IDE devices at the room temperature, however the flow rate of the carrier gas (synthetic air) was 200 sccm and amount of 1 µl of ethanol was injected and instantaneously vaporised every 2 minutes. Response curves to these analyte pulses were recorded with and without UV activation. The results are plotted in Figure 36. Forward voltage for the used LED was 3.6 V, which is the optimum performance as suggested by the producer of the diode. It can be clearly seen in the graph that the application of UV enhances the response of the sensing element and increases apparently the recovery time. Since the initial resistance value reaches order of kΩ, a sharp decrease of about one order of magnitude after UV activation was experienced. Therefore, two plausible explanations can be considered that it is due to the sensitivity increase and saturation of the system at the peak (pulse) arrival time or due to modified dynamics of the recovery process. Nevertheless, the baseline (background in off-state) stability and reproducibility seem to be sufficient for both regimes of the device operation. With the full awareness of the need of other characterizations remaining to be performed in future work, it can be concluded that the main achievement of the proof of concept device and demonstration of the original device functionality was accomplished.
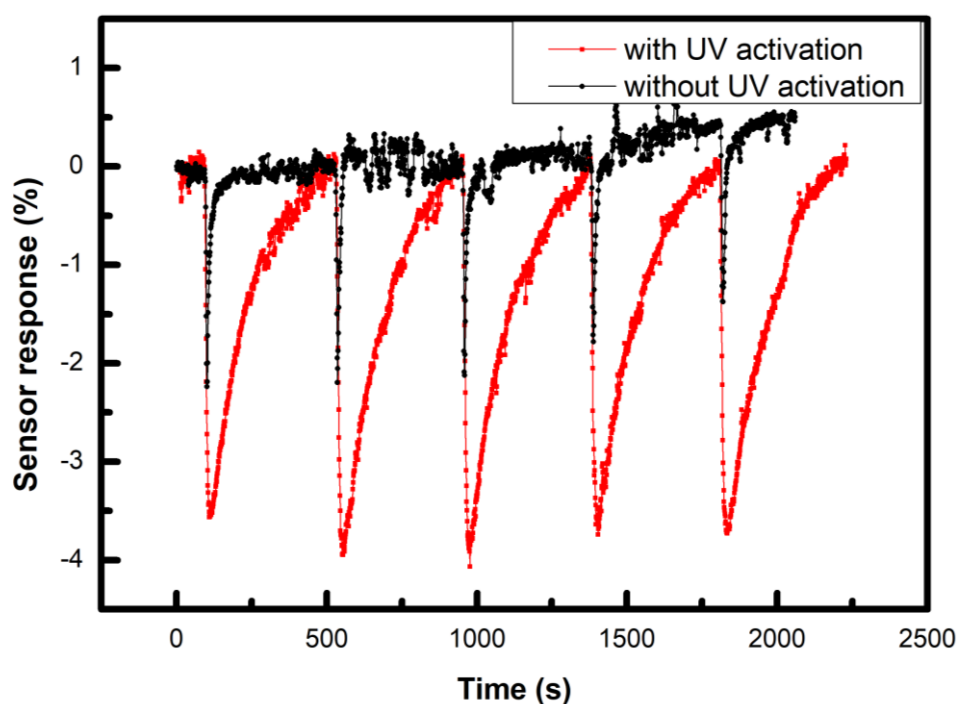
Figure 36 − The response magnitudes of integrated sensing device consisting of ZnO nanowire network to the exposure of pulses of Ethanol in dried Air at 25 °C in dark gas chamber and with activated UV-LED

10. CONCLUDING SUMMARY

Conductive structures of interconnects were deposited by ink-jet printing technology from two commercially available silver nanoparticles-based inks on polyethylene terephthalate and polyimide foils. Reference samples printed on glass substrate were characterized and resistivity of each material was extracted from linear regression of pixelated lines array measured by using two-point probe method. The resistivity value of ink DGP 40LT-15C, intended to print on polyethylene terephthalate foil limited by curing temperature of 150 °C, was determined to 64.8 μΩ·cm. In case of ink DGH 55LT-25C, intended to print on polyimide foil, the resistivity value was determined to 6.26 μΩ·cm. For comparison, the tabulated resistivity value of pure silver is 1.59 μΩ·cm (at 20 °C) [111]. At appropriately set conditions, the latter ink exhibits excellent jetting performance and conductivity of printed interconnects. The descent of resistivity values of silver inks is given by the solid content and the size of particles. Evaporation of the carrier medium while curing leads to densification and compaction of the structure with diminishing particle size having appropriate bulk density and corresponding residual pore space. While aggregation of particles and formation of conductive channels between them contribute to conductivity, porous space can be assumed to increase the overall resistivity compared to the pure bulk silver. In order to demonstrate the functionality of printed circuitries, indicating SMD LEDs were assembled with printed interconnects and plugged in as a functional flexible circuit. The photograph of a fabricated model sample is seen in Figure 20.

A successful development of stabilized indium tin oxide (ITO) nanoparticles-based ink in an aqueous medium was demonstrated. The ink was characterized and optimized for ink-jet printing technology. Dimensionless correlations were used for the analysis of the material-tool-process parameter space. Among the single criterion approaches, the importance of the Weber number was re-discussed and raised again. On the other hand, the description of the processing window requires at least a two dimensional map. We refrained from incorporating the viscoelasticity into our models in favour of reemploying older yet still valuable models limited for Newtonian fluids only. The presented approach enables fast advances in ink formulations and process development with the used DOD printer and a simple experimental instrumentation. The prepared ink is applicable for the deposition of conductive and transparent thin (about 500 nm) or thick (micrometres) films depending on the nanoparticles loading. Only one printing

run assured a sufficient final quality of films. On the ink-jet printed ITO sensor demonstration specimens, we observed fast response and recovery times to toluene vapours at laboratory temperature although with relatively small overall sensitivity. The type of ITO sensor response depends on the kind of atmosphere under which the sensor is operated in. In air atmospheres, even the low temperature sensing mechanism can be explained by well-established models for n-type semiconductors, among them the oxygen vacancy model seems to be the most favourable. To explain the sensing response inversion observed for the sensor operated in an oxygen-free atmosphere, the charge transfer mechanism between the adsorbent and adsorbate gas molecules was proposed. The overall sensitivity of the device was slightly larger and the sensor response was more stable over the tested number of cycles in pure nitrogen than in an open air ambient. No baseline drift was experienced in a protective atmosphere unlike in air.

Nanoseed ZnO precursor was ink-jet deposited on interdigitated sensor platform and subsequently subjected to hydrothermal growth. Different concentration of growth-direct agent in hydrothermal bath allows the formation of ZnO nanostructures in form of nanorods and nanowires having different thickness and sizes which affect the resulting sensing properties. A new design of built-in sensing structure was prepared in combination with SMD ultraviolet light emitting diode assemble a sensing element mounted on printed flexible circuit board patterned for stripe connector of power supply and measuring unit. The sensing structure performed a detection of ethanol vapours pulses repeatedly in the dark. A significant improvement of sensitivity with UV light irradiation keeping the low operating temperatures was confirmed. The proposed arrangement must be tuned according to inceptive resistance of sensing structure, which will decrease rapidly after activation of the UV radiation. Since the initial resistance value reaches $k\Omega$, a sharp decrease of about one order of magnitude after UV activation was experienced. This can be avoided by appropriate setting the resistance of nanowire network by suitable distance of interdigitated electrodes and shedding the nanowire network nascent from nanoseeds printed at given concentration of precursor ink. Despite these shortcomings and with the full awareness of the need of many other characterizations remaining to be performed in future work, a novel approach of integrated sensing structure with UV-activating system was presented which will facilitate an applicability in smart portable electronic devices and can replace gas sensors working at high operating temperatures in the future.

11. SUMMARY OF CONTRIBUTIONS TO SCIENCE AND PRAXIS

An original method of preparation of sensors for toluene and ethanol as representative volatile organic compounds were developed by using of material ink-jet printing technique from both originally prepared and commercially available nanoparticles-based and solution-based inks. These sensor devices were prepared by a low temperature process enabling use of polymer components and successfully demonstrated their function when operated at the room temperature. Towards these ends, structure, morphology and properties of deposited materials and prepared devices were investigated with respect to their function. It was revealed, that the sensing mechanism of the n-type semiconductors is still remained in action although its effectivity is quite low at the room temperature. Moisture and other components of ambient atmosphere interfere the sensor function of the device by non-specific stimulation of its response resulting thus into inevitable shifts of the measurement baseline (off-state background) of the device. This disadvantage is normally overcome by the operation of the sensor at high temperature, but addressing this issue at the room temperature was one of the goals of this theses. Indeed, a miniature device prepared directly on the quartz window of a UV LED was developed and successfully fabricated to demonstrate the viability of the use of UV cold activation of the semiconducting active sensor layer instead of the utilization of high temperature.

The research work presented in this thesis can be considered an original contribution to unlocking the future improvement of sensitivity of metal oxide based sensors to detect organic vapours and gases at room operating temperatures. To summarize the contribution of the results corresponding to objectives defined in the aim of the doctoral thesis, following practical points as well as theoretical contributions can be emphasized:

- Optimization of the preparation of conductive interconnects and electrodes by the ink-jet printing using silver nanoparticles-based inks on polymer foils applicable in flexible electronics.

- Development of an ink based on ITO nanoparticles and its deposition by the ink-jet printing technique on suitable substrate. A framework using dimensionless criteria was developed for ink formulation and printing process optimization. Fabrication of a toluene sensing device which can be operated at the room temperature was demonstrated.

- The sensing mechanism of the ITO sensor at low temperature was elucidated as the typical response for an n-type semiconductor. The low efficiency and inevitable interference of the ambient atmosphere stimulated the next research on ZnO based sensors, where the cold UV activation instead high temperature operation was expected plausible.

- A combination of printing and hydrothermal growth resulted into preparation of an IDE designed sensor fabricated on a polymer substrate which allowed to find a suitable morphology of ZnO nanowire forest and method of its preparation which was successfully used in fabrication of a novel integrated UV-assisted low temperature operated gas sensing device.

REFERENCES

[1] J.B. Fortin, A. Zribi, Functional Thin Films and Nanostructures for Sensors: Synthesis, Physics and Applications, Springer, New York; London, 2009.

[2] A. Gurlo, M. Ivanovskaya, N. Bârsan, M. Schweizer-Berberich, U. Weimar, W. Göpel, A. Diéguez, Grain size control in nanocrystalline In2O3 semiconductor gas sensors, Sensors Actuators B: Chem. 44 (1997) 327-333.

[3] K. Sahner, H.L. Tuller, Novel deposition techniques for metal oxide: Prospects for gas sensing, Journal of Electroceramics. 24 (2010) 177-199.

[4] J. Maslik, I. Kuritka, P. Urbanek, P. Krcmar, P. Suly, M. Masar, M. Machovsky, Water-Based Indium Tin Oxide Nanoparticle Ink for Printed Toluene Vapours Sensor Operating at Room Temperature, Sensors. 18 (2018).

[5] H. Kipphan, Handbook of Print Media: Technologies and Production Methods, (2001) 1207.

[6] Hutchings, Ian M.,Martin, Graham, Inkjet technology for digital fabrication, (2012) 390.

[7] Anonymous, FUJIFILM Dimatix Materials Printer DMP-2800 Series User Manual, User Manual ed. U.S.A.: FUJIFILM Dimatix, Inc. (2010).

[8] J. Jeong, J. Lee, H. Kim, H. Kim, S. Na, Ink-jet printed transparent electrode using nano-size indium tin oxide particles for organic photovoltaics, Solar Energy Mater. Solar Cells. 94 (2010) 1840-1844.

[9] S. Magdassi, The Chemistry of Inkjet Inks, First ed., World Scientific Publishing Co. Pte. Ltd., Singapore, 2010.

[10] R.H. Leach, The Printing Ink Manual, Kluwer, Dordrecht, 1999.

[11] A. Facchetti, T.J. Marks, Transparent Electronics: From Synthesis to Applications, in: Anonymous Transparent Electronics: From Synthesis to Applications, , 2010.

[12] H. Mbarek, M. Saadoun, B. Bessaïs, Screen-printed Tin-doped indium oxide (ITO) films for NH3 gas sensing, Materials Science and Engineering: C. 26 (2006) 500-504.

[13] B. Bessais, N. Mliki, R. Bennaceur, Technological, structural and morphological aspects of screen-printed ITO used in ITO/Si type structure, Semiconductor Science and Technology. 8 (1993) 116-121.

[14] V.S. Vaishnav, S.G. Patel, J.N. Panchal, Development of indium tin oxide thin film toluene sensor, Sensors Actuators B: Chem. 210 (2015) 165-172.

[15] M. Afshar, E.M. Preiß, T. Sauerwald, M. Rodner, D. Feili, M. Straub, K. König, A. Schütze, H. Seidel, Indium-tin-oxide single-nanowire gas sensor fabricated via laser writing and subsequent etching, Sensors Actuators B: Chem. 215 (2015) 525-535.

[16] C. Lin, H. Chen, T. Chen, C. Huang, C. Hsu, R. Liu, W. Liu, On an indium–tin-oxide thin film based ammonia gas sensor, Sensors Actuators B: Chem. 160 (2011) 1481-1484.

[17] J. Koo, S. Lee, S. Cho, J. Chang, Effect of additives on the properties of printed ITO sensors, J. Korean Phys. Soc. 71 (2017) 335-339.

[18] J. Koo, S. Park, W. Lee, Y. Cho, H. Lee, S. Lee, J. Chang, Room temperature operation of ITO nano-crystal gas sensor, Phys. Status Solidi C. 10 (2013) 873-876.

[19] L. Zhu, W. Zeng, Room-temperature gas sensing of ZnO-based gas sensor: A review, Sensors and Actuators A: Physical. 267 (2017) 242-261.

[20] R. Kitsomboonloha, S. Baruah, M.T.Z. Myint, V. Subramanian, J. Dutta, Selective growth of zinc oxide nanorods on inkjet printed seed patterns, Journal of Crystal Growth. 311 (2009) 2352-2358.

[21] S.H. Ko, D. Lee, N. Hotz, J. Yeo, S. Hong, K.H. Nam, C.P. Grigoropoulos, Digital Selective Growth of ZnO Nanowire Arrays from Inkjet-Printed Nanoparticle Seeds on a Flexible Substrate, Langmuir. 28 (2012) 4787-4792.

[22] V. Tran, Y. Wei, H. Yang, Z. Zhan, H. Du, All-inkjet-printed flexible ZnO micro photodetector for a wearable UV monitoring device, Nanotechnology. 28 (2017) 095204.

[23] C.P. Tsangarides, H. Ma, A. Nathan, ZnO nanowire array growth on precisely controlled patterns of inkjet-printed zinc acetate at low-temperatures, Nanoscale. 8 (2016) 11760-11765.

[24] S.D. Hoat, Fundamentals of inkjet printing : the science of inkjet and droplets, (2016) 449.

[25] J. Korvink G., P. Smith J., D. Shin, Inkjet-based micromanufacturing, (2012) 371.

[26] I. Burgues-Ceballos, M. Stella, P. Lacharmoise, E. Martinez-Ferrero, Towards industrialization of polymer solar cells: material processing for upscaling, J. Mater. Chem. A. (2014) 17711-17722.

[27] O.A. Basaran, H. Gao, P.P. Bhat, Nonstandard Inkjets, Annu. Rev. Fluid Mech. 45 (2013) 85-113.

[28] J.R. Castrejon-Pita, W.R.S. Baxter, J. Morgan, S. Temple, G.D. Martin, I.M. Hutchings, Future, opportunities and challanges of inkjet technologies, Atomization and Sprays. 23 (2013) 541-565.

[29] O.A. Basaran, Small-scale free surface flows with breakup: Drop formation and emerging applications, AIChE J. 48 (2004) 1842-1848.

[30] J. Heinzl, C.H. Hertz, Ink-Jet Printing, Advances in Electronics and Electron Physics. 65 (1985) 91-171.

[31] E.P. Furlani, B.G. Price, G. Hawkins, A.G. Lopez, Thermally induced Marangoni instability of liquid micro-jets with application to continuous inkjet printing, (2006) 534-537.

[32] E.P. Furlani, Numerical analysis of nonlinear deformation and breakup of slender microjets with application to continuous inkjet printing, (2007) 444-446.

[33] E.P. Furlani, Temporal instability of viscous liquid microjets with spatially varying surface tension, Journal of Physics A: Mathematical and General. 38 (2005) 263.

[34] E. Furlani, Thermal modulation and instability of Newtonian liquid microjets, (2005) 668-671.

[35] E.P. Furlani, M.S. Hanchak, Nonlinear analysis of the deformation and breakup of viscous microjets using the method of lines, Int. J. Numer. Meth. Fluids. 65 (2011) 563-577.

[36] G. Cummins, Marc P.Y. Desmulliez, Inkjet printing of conductive materials: a review, Circuit World. 38 (2012) 193-213.

[37] H. Wijshoff, The dynamics of the piezo inkjet printhead operation, Physics Reports. 491 (2010) 77-177.

[38] H. Wu, W. Hwang, H. Lin, Development of a three-dimensional simulation system for micro-inkjet and its experimental verification, Materials Science & Engineering A. 373 (2004) 268-278.

[39] T.W. Shield, D.B. Bogy, F.E. Talke, Drop formation by DOD ink-jet nozzles: A comparison of experiment and numerical simulation, IBM Journal of Research and Development. 31 (1987) 96-110.

[40] F. Tseng, C. Kim, C. Ho, A high-resolution high-frequency monolithic top-shooting microinjector free of satellite drops - Part II: Fabrication, implementation, and characterization, 11 (2002) 437.

[41] T. Lindemann, D. Sassano, A. Bellone, R. Zengerle, P. Koltay, I. Olvetti, Three-dimensional CFD-simulation of a thermal bubble jet printhead, (2004) 227-230.

[42] N. Yamazoe, G. Sakai, K. Shimanoe, Oxide semiconductor gas sensors, Catalysis Surveys from Asia. 7 (2003) 63-75.

[43] T. Joubert, P.H. Bezuidenhout, H. Chen, S. Smith, K.J. Land, Inkjet-printed Silver Tracks on Different Paper Substrates, Materials Today: Proceedings. 2 (2015) 3891-3900.

[44] S. Magdassi, A. Bassa, Y. Vinetsky, A. Kamyshny, Silver Nanoparticles as Pigments for Water-Based Ink-Jet Inks, Chem. Mater. 15 (2003) 2208-2217.

[45] W. Shen, X. Zhang, Q. Huang, Q. Xu, W. Song, Preparation of solid silver nanoparticles for inkjet printed flexible electronics with high conductivity, Nanoscale. 6 (2014) 1622-1628.

[46] S. Das, D. Cormier, S. Williams, Potential for Multi-functional Additive Manufacturing Using Pulsed Photonic Sintering, Procedia Manufacturing. 1 (2015) 366-377.

[47] M.A. Carpenter, S. Mathur, A. Kolmakov, Metal Oxide Nanomaterials for Chemical Sensors, Springer, New York Hiedelberg Dordrecht London, 2013.

[48] S. Kholghi Eshkalak, A. Chinnappan, W.A.D.M. Jayathilaka, M. Khatibzadeh, E. Kowsari, S. Ramakrishna, A review on inkjet printing of CNT composites for smart applications, Applied Materials Today. 9 (2017) 372-386.

[49] J. Fraden, Handbook of Modern Sensors: Physics, Designs, and Applications, Springer-Verlag, New York, 2010.

[50] A.B. Fall, S.B. Lindström, O. Sundman, L. Ödberg, L. Wågberg, Colloidal Stability of Aqueous Nanofibrillated Cellulose Dispersions, Langmuir. 27 (2011) 11332-11338.

[51] M. Michel, C. Biswas, A.B. Kaul, High-performance ink-jet printed graphene resistors formed with environmentally-friendly surfactant-free inks for extreme thermal environments, Applied Materials Today. 6 (2017) 16-21.

[52] D.R. Dreyer, S. Park, C.W. Bielawski, R.S. Ruoff, The chemistry of graphene oxide, Chem. Soc. Rev. (2010) 228.

[53] S. Kashyap, S. Mishra, S.K. Behera, Aqueous Colloidal Stability of Graphene Oxide and Chemically Converted Graphene, Journal of Nanoparticles. 2014 (2014) 6.

[54] F. Gambinossi, S.E. Mylon, J.K. Ferri, Aggregation kinetics and colloidal stability of functionalized nanoparticles, Advances in Colloid and Interface Science. 222 (2015) 332-349.

[55] Y. Cho, H. Kim, J. Hong, G. Yi, S.H. Jang, S. Yang, Dispersion stabilization of conductive transparent oxide nanoparticles, Colloids Surf. Physicochem. Eng. Aspects. 336 (2009) 88-98.

[56] A. Hajian, S.B. Lindström, T. Pettersson, M.M. Hamedi, L. Wågberg, Understanding the Dispersive Action of Nanocellulose for Carbon Nanomaterials, Nano Letters. 17 (2017) 1439-1447.

[57] D. Ronan, Surface Characterization, in: Anonymous Fundamentals of Inkjet Printing, Wiley-Blackwell, 2015, pp. 365-396.

[58] Y. HAMAMOTO, J.R.E. CHRISTY, K. SEFIANE, The Flow Characteristics of an Evaporating Ethanol Water Mixture Droplet on a Glass Substrate, Journal of Thermal Science and Technology. 7 (2012) 425-436.

[59] H. Hu, R.G. Larson, Analysis of the Effects of Marangoni Stresses on the Microflow in an Evaporating Sessile Droplet, Langmuir. 21 (2005) 3972-3980.

[60] K. Sefiane, L. Tadrist, M. Douglas, Experimental study of evaporating water–ethanol mixture sessile drop: influence of concentration, International Journal of Heat and Mass Transfer. 46 (2003) 4527-4534.

[61] T. Still, P.J. Yunker, A.G. Yodh, Surfactant-Induced Marangoni Eddies Alter the Coffee-Rings of Evaporating Colloidal Drops, Langmuir. 28 (2012) 4984-4988.

[62] H.A. Barnes, J.F. Hutton, K. Walters, An Introduction to Rheology, Elsevier Science, 1989.

[63] P. Šuly, Study of Poly(Vinyl alcohol) Solution for Inkjet Printing, (2017).

[64] T. Sochi, Non-Newtonian flow in porous media, Polymer. 51 (2010) 5007-5023.

[65] N.F. Morrison, O.G. Harlen, Viscoelasticity in inkjet printing, Rheologica Acta. 49 (2010) 619-632.

[66] J.A. Roberson, J.J. Cassidy, H.M. Chaudhry, Hydraulic Engineering, Wiley, 1998.

[67] B. Derby, Inkjet Printing of Functional and Structural Materials: Fluid Property Requirements, Feature Stability, and Resolution, Annu. Rev. Mater. Res. 40 (2010) 395-414.

[68] E. Kim, J. Baek, Numerical study on the effects of non-dimensional parameters on drop-on-demand droplet formation dynamics and printability range in the up-scaled model, Phys. Fluids. 24 (2012) 082103.

[69] D. Jang, D. Kim, J. Moon, Influence of Fluid Physical Properties on Ink-Jet Printability, Langmuir. 25 (2009) 2629-2635.

[70] J. Kunes, Dimensionless Physical Quantities in Science and Engineering, Elsevier, London, 2012.

[71] G.H. McKinley, M. Renardy, Wolfgang von Ohnesorge, Phys. Fluids. 23 (2011) 127101.

[72] J. Izdebska, S. Thomas, Printing on Polymers: Fundamentals and Applications, Elsevier, 2015.

[73] Anonymous, Critical Surface Tension, Surface Free Energy, Contact Angles with Water, and Hansen Solubility Parameters for Various Polymers, (©2018).

[74] L. Eckertová, Physics of Thin Films, Plenum Publishing Corporation, New York, 1986.

[75] H.A. Andersson, A. Manuilskiy, S. Haller, M. Hummelgård, J. Sidén, C. Hummelgård, H. Olin, H. Nilsson, Assembling surface mounted components on ink-jet printed double sided paper circuit board, Nanotechnology. 25 (2014) 094002.

[76] T. Ohlund, A. Schuppert, B. Andres, H. Andersson, S. Forsberg, W. Schmidt, H. Nilsson, M. Andersson, R. Zhang, H. Olin, Assisted sintering of silver nanoparticle inkjet ink on paper with active coatings, RSC Adv. 5 (2015) 64841-64849.

[77] J. Matyas, P. Slobodian, L. Munster, R. Olejnik, P. Urbanek, Microstrip antenna from silver nanoparticles printed on a flexible polymer substrate, Materials Today: Proceedings. 4 (2017) 5030-5038.

[78] L. Mu, Z. Hu, Z. Zhong, C. Jiang, J. Wang, J. Peng, Y. Cao, Inkjet-printing line film with varied droplet-spacing, Organic Electronics. 51 (2017) 308-313.

[79] T. Chu, Z. Zhang, A. Dadvand, C. Py, S. Lang, Y. Tao, Direct writing of inkjet-printed short channel organic thin film transistors, Organic Electronics. 51 (2017) 485-489.

[80] M. Rieu, M. Camara, G. Tournier, J. Viricelle, C. Pijolat, N.F. de Rooij, D. Briand, Fully inkjet printed SnO2 gas sensor on plastic substrate, Sensors and Actuators B: Chemical. 236 (2016) 1091-1097.

[81] C. Bali, A. Brandlmaier, A. Ganster, O. Raab, J. Zapf, A. Hübler, Fully Inkjet-Printed Flexible Temperature Sensors Based on Carbon and PEDOT:PSS, Materials Today: Proceedings. 3 (2016) 739-745.

[82] M. Bissannagari, J. Kim, Inkjet printing of NiZn-ferrite films and their magnetic properties, Ceramics International. 41 (2015) 8023-8027.

[83] K. Kalantar-zadeh, Sensors: An Introductory Course, Springer US, New York, 2013.

[84] J.S. Wilson, Sensor Technology Handbook, Newnes, Burlington, 2005.

[85] J. Janata, Principles of Chemical Sensors, Springer US, New York, 2009.

[86] A. V. Mamishev, K. Sundara-Rajan, Fumin Yang, Yanqing Du, M. Zahn, Interdigital sensors and transducers, Proceedings of the IEEE. 92 (2004) 808-845.

[87] G. Korotcenkov, The role of morphology and crystallographic structure of metal oxides in response of conductometric-type gas sensors, Materials Science and Engineering: R: Reports. 61 (2008) 1-39.

[88] N. Yamazoe, Y. Kurokawa, T. Seiyama, Effects of additives on semiconductor gas sensors, Sensors and Actuators. 4 (1983) 283-289.

[89] D. Kohl, The role of noble metals in the chemistry of solid-state gas sensors, Sensors and Actuators B: Chemical. 1 (1990) 158-165.

[90] V. Brinzari, G. Korotcenkov, J. Schwank, Y. Boris, Chemisorptional approach to kinetic analysis of SnO2:Pd-based thin film gas sensors, J. Optoelectron. Adv. Mat. 4 (2002) 147-150.

[91] G. Korotcenkov, Handbook of Gas Sensor Materials: Properties, Advantages and Shortcomings for Applications Volume 1: Conventional Approaches, 1st ed., Springer-Verlag New York, 2013.

[92] G. Korotcenkov, Handbook of Gas Sensor Materials: Properties, Advantages and Shortcomings for Applications Volume 2: New Trends and Technologies, 1st ed., Springer-Verlag New York, 2014.

[93] M. Hübner, C.E. Simion, A. Tomescu-Stănoiu, S. Pokhrel, N. Bârsan, U. Weimar, Influence of humidity on CO sensing with p-type CuO thick film gas sensors, Sensors Actuators B: Chem. 153 (2011) 347.

[94] J.M. Walker, S.A. Akbar, P.A. Morris, Synergistic effects in gas sensing semiconducting oxide nano-heterostructures: A review, Sensors and Actuators B: Chemical. 286 (2019) 624-640.

[95] W. Göpel, T.A. Jones, M. Kleitz, I. Lundström, T. Seiyama, J. Hesse, J.N. Zemel, Sensors, A Comprehensive Survey: Chemical and Biochemical Sensors Part 1, Volume 2 ed., Wiley, 2008.

[96] S. kimiagar, V. Najafi, B. Witkowski, R. Pietruszka, M. Godlewski, High performance and low temperature coal mine gas sensor activated by UV-irradiation, Scientific Reports. 8 (2018) 16298.

[97] E. Comini, G. Faglia, G. Sberveglieri, UV light activation of tin oxide thin films for NO2 sensing at low temperatures, Sensors and Actuators B: Chemical. 78 (2001) 73-77.

[98] K.Y. Mitra, C. Sternkiker, C. Martínez-Domingo, E. Sowade, E. Ramon, J. Carrabina, H.L. Gomes, R.R. Baumann, Inkjet printed metal insulator semiconductor (MIS) diodes for organic and flexible electronic application, Flexible and Printed Electronics. 2 (2017) 015003.

[99] S.B. Walker, J.A. Lewis, Reactive Silver Inks for Patterning High-Conductivity Features at Mild Temperatures, J. Am. Chem. Soc. 134 (2012) 1419-1421.

[100] B. Derby, Additive Manufacture of Ceramics Components by Inkjet Printing, Engineering. 1 (2015) 113-123.

[101] P. Duineveld, M. de Kok, M. Buechel, A. Sempel, K. A. H. Mutsaers, P. van de Weijer, I. G. J. Camps, T. van de Biggelaar, J. J. M. Rubingh, E. Haskal, Ink-jet printing of polymer light-emitting devices, 4464 (2002).

[102] I. Bernacka-Wojcik, P.J. Wojcik, H. Aguas, E. Fortunato, R. Martins, Inkjet printed highly porous TiO2 films for improved electrical properties of photoanode, J. Colloid Interface Sci. 465 (2016) 208-214.

[103] G. Korotcenkov, V. Brinzari, M. Ivanov, A. Cerneavschi, J. Rodriguez, A. Cirera, A. Cornet, J. Morante, Structural stability of indium oxide films deposited by spray pyrolysis during thermal annealing, Thin Solid Films. 479 (2005) 38-51.

[104] N. Barsan, M. Schweizer-Berberich, W. Göpel , Fundamental and practical aspects in the design of nanoscaled SnO2 gas sensors: a status report, Fresenius J. Anal. Chem. 365 (1999) 287-304.

[105] C. Wang, L. Yin, L. Zhang, D. Xiang, R. Gao, Metal Oxide Gas Sensors: Sensitivity and Influencing Factors, Sensors (Basel, Switzerland). 10 (2010) 2088-2106.

[106] D. Smyth, The Role of Impurities in Insulating Transition-Metal Oxides, Progress in Solid State Chemistry. 15 (1984) 145-171.

[107] D. Williams, P. Moseley, Dopant Effects on the Response of Gas-Sensitive Resistors Utilizing Semiconducting Oxides, Journal of Materials Chemistry. 1 (1991) 809-814.

[108] A. Gurlo, N. Barsan, A. Oprea, M. Sahm, T. Sahm, U. Weimar, An n- to p-type conductivity transition induced by oxygen adsorption on alpha-Fe2O3, Appl. Phys. Lett. 85 (2004) 2280-2282.

[109] J. Lin, Z. Li, Electronic conduction properties of indium tin oxide: single-particle and many-body transport, Journal of Physics: Condensed Matter. 26 (2014) 343201.

[110] N. Ramgir, N. Datta, M. Kaur, S. Kailasaganapathi, A.K. Debnath, D.K. Aswal, S.K. Gupta, Metal oxide nanowires for chemiresistive gas sensors: Issues, challenges and prospects, Colloids and Surfaces A: Physicochemical and Engineering Aspects. 439 (2013) 101-116.

[111] Smithsonian Institution., W.E. Forsythe, Smithsonian Physical Tables, 9th edition ed., The Institution, Washington, D.C., 1954.

LIST OF FIGURES

LIST OF TABLES

LIST OF ABBREVIATIONS

Alphabetically ordered

AFM	Atomic force microscopy
CIJ	Continuous ink-jet
CMC	Critical micelle concentration
CNT	Carbon nanotube
CVD	Chemical vapour deposition
DC	Direct current
DOD	Drop-on-demand
EG	Ethylene glycol
GO	Graphene oxide
IDE	Interdigital electrodes
ITO	Indium tin oxide
LED	Light-emitting diode
LUMO	Lowest unoccupied molecular orbital
MSD	Minimum stand-off distance
PEI	Polyethyleneimine
PEN	Polyethylene naphthalate
PET	Polyethylene terephthalate
PI	Polyimide
PTFE	Polytetrafluoroethylene
PVD	Physical vapour deposition
PZT	Lead zirconium titanate
RFID	Radio frequency identification
rGO	Reduced graphene oxide
RMS	Root mean square
SMD	Surface-mount device
SWCNT	Single-walled carbon nanotube
TFT	Thin film transistors
UV	Ultraviolet
VOC	Volatile organic compounds

LIST OF SYMBOLS

Alphabetically ordered

A	Pre-exponential factor (in equation 3)
A	Characteristic length (in equation 4, 5, 6, 8 and 9)
A	Conductor cross-sectional area (in equation 13)
c	Velocity of light
c^*	Critical concentration
d	Particle diameter
e^-	Electron
eV_S	Surface potential barrier
E_A	Acceptor energy level
E_a	Activation energy
E_D	Donor energy level
E_g	Band gap
$\dot{\gamma}$	Shear rate
h	Conductor thickness (in equation 14)
h	Planck constant (in equation 20)
η	Dynamic viscosity
I	Electrical current
L_D	Debye length
L_S	Charge depleted region
l	Conductor length
λ_{max}	Maximal wavelength
O	Wetted perimeter
R	Electrical resistance (in equation 12, 13 and 22)
R	Universal gas constant (in equation 3)
R_0	Residual resistance
R_{air}	Sensor resistance in air atmosphere
R_{gas}	Sensor resistance upon vapours ambience
R_{sheet}	Sheet resistance

ρ	Density (in equation 5, 6, 8 and 9)
ρ	Electrical resistivity (in equation 13, 14 and 22)
S	Area
S_R	Sensor response ratio
τ	Shear stress
σ	Surface tension
σ_{lv}	Surface tension of liquid in equilibrium with its saturated vapours
σ_{sl}	Surface tension between solid and liquid phase
σ_{sv}	Surface tension of the solid in equilibrium with the saturated vapours of the liquid
V	Electrical voltage
w	Conductor width

LIST OF DIMENSIONLESS NUMBERS

Alphabetically ordered

Ca	Capillary number
La	Laplace number
Oh	Ohnesorge number
Re	Reynolds number
We	Weber number
Z	Z number, Reciprocal Ohnesorge number

LIST OF UNITS
Alphabetically ordered

°C	Degree Celsius
dpi	Dot per inch
eV	Electronvolt
$g \cdot ml^{-1}$	Gram per millilitre
Hz	Hertz
$J \cdot mol^{-1} \cdot K^{-1}$	Joule per mole times Kelvin
K	Kelvin
$kg \cdot m^{-3}$	Kilogram per cubic meter
m^{-1}	Reciprocal meter
mg	Miligram
min	Minute
mM	Milimole
mm	Milimeter
$mN \cdot m^{-1}$	Millinewtons per meter
$mPa \cdot s$	Millipascal-second
$m \cdot s^{-1}$	Meter per second
nm	Nanometer
pix	Pixel
pl	Pikoliter
ppm	Parts per million
s^{-1}	Reciprocal second, Sheer deformation units
sccm	Standard cubic centimeters per minute
wt%	Weight percent
μm	Micrometer
Ω	Ohm
Ω·cm, μΩ·cm	Ohm-centimeter, microohm-centimeter
Ω/sq, Ω/□	Ohms per square, ohms square

CURRICULUM VITAE

Personal information

Name:	Jan Mašlík
Date of birth:	15th October 1987
Place of birth:	Zlín, Czech Republic
Permanent address:	1. máje 1019, 763 02 Zlín 4, Czech Republic
Affiliation:	Polymer Centre, Faculty of Technology, Tomas Bata University in Zlin, Namesti T.G. Masaryka 275, 76272 Zlin, Czech Republic
E-mail:	maslik@utb.cz; jan.maslik@angstrom.uu.se

Education

2013 – to date

Tomas Bata University in Zlin, Faculty of Technology, Ph.D. studies in Chemistry and Materials Technology, Specialization: Technology of Macromolecular Compounds

2011 – 2013

Tomas Bata University in Zlin, Faculty of Technology, Master's degree in Chemistry and Materials Technology, Specialization: Material Engineering

2008 – 2011

Tomas Bata University in Zlin, Faculty of Technology, Bachelor's degree in Chemistry and Materials Technology, Specialization: Material Engineering

2004 – 2008

Technical High School Otrokovice

Work experience

2019/02 – to date

Department of Engineering Sciences, Division of Microsystems Technology, Ångström Laboratory, Uppsala University, Lägerhyddsvägen 1, 752 37 Uppsala, Sweden
Research assistant

2015 – 2019

Centre of Polymer Systems, Tomas Bata University in Zlin, Trida Tomase Bati 5678, 760 01 Zlín, Czech Republic
Project researcher

Stays abroad

2017/09 – 2017/11

ERASMUS+ Traineeship at Department of Electronics Design, Mid Sweden University, Holmgatan 10, 85170 Sundsvall, Sweden

2015/10 – 2016/01

ERASMUS+ Study Stay at Laboratoire Charles Coulomb, Université de Montpellier, Batiment 13, 34095 Montpellier, France

Projects

Internal funding

IGA/FT/2012/025 − Modified polymer materials for thin films – member of the research team

IGA/FT/2013/025 − Material printing of polymer and inorganic inks for advanced applications – member of the research team

IGA/FT/2014/006 − Modification of polymer substrates and new materials for inkjet printing of sensors – project investigator (head of research team)

IGA/CPS/2015/006 − Preparation of functional inks for material inkjet printing and their applications in printed electronics and sensors – project investigator (head of the research team)

IGA/CPS/2016/007 – Preparation and characterization of functional polymer materials for thin films applicable in printed electronics and sensor technology – member of the research team

IGA/CPS/2017/008 − Preparation and characterization of nanocomposite thin films for polymer electronics – member of the research team

External funding

FR-TI3/424 Electroluminescent films for security interior lighting (2011-2014) – project researcher

NPU I LO1504 – Centre of Polymer Systems plus (2015-2020) – project researcher

CZ.01.1.02/0.0/0.0/15_019/0005090 – Stenopeic aperture for presbyopy correction (2016-2019) – project researcher

LIST OF PUBLICATIONS

RAFAJOVÁ, M.; MINAŘÍK, A.; SMOLKA, P.; MRÁČEK, A.; MAŠLÍK, J.; MACHOVSKÝ, M. Factors determining hydrophobicity silicon-based materials. *Chemicke Listy*. 2014, **108**(1), 35-39. ISSN: 1213-7103

ŠULY, P.; KRČMÁŘ, MAŠLÍK, J.; URBÁNEK, P.; KUŘITKA, I. Poly(vinyl alcohol): formulation of a polymer ink for the patterning of substrates with a drop-on-demand inkjet printer. *Materiali in tehnologije*. 2017, **51**(1), 41-48. ISSN: 1580-2949. doi: 10.17222/mit.2015.180

TORRES-CANAS, F.; BLANC, CH.; MAŠLÍK, J.; TAHIR, S.; IZARD, N.; KARASAHIN, S.; CASTELLANI, M.; DAMMASCH, M.; ZAMORA-LEDEZMA, C.; ANGLARET, E. Morphology and anisotropy of thin conductive inkjet printed lines of single-walled carbon nanotubes. *Materials Research Express*. 2017, **4**(3). ISSN: 2053-1591

KRČMÁŘ, P.; KUŘITKA, I.; MAŠLÍK, J.; URBÁNEK, P.; BAŽANT, P.; MACHOVSKÝ, M.; ŠULY, P.; MĚRKA, P. The preparation and characterization of CuO inkjet inks for fully printed alcohol vapours and humidity sensors on flexible polymer substrate. *Sensors*. 2018 – Submitted

MASLIK, J.; KURITKA, I.; URBANEK, P.; KRCMAR, P.; SULY, P.; MASAR, M. and MACHOVSKY, M. Water-Based Indium Tin Oxide Nanoparticle Ink for Printed Toluene Vapours Sensor Operating at Room Temperature. *Sensors*. 2018, **18**(10)

ANDERSSON, H.; ŠULY, P.; THUNGSTRÖM, G.; ENGHOLM, M.; ZHANG, R.; MAŠLÍK, J.; OLIN, H. PEDOT: PSS Thermoelectric Generators Printed on Paper Substrates. *J. Low Power Electron. Appl.* 2019, **9**(14)

OVERVIEW OF OTHER ACTIVITIES

Utility models and patent

1. MINAŘÍK, A.; SMOLKA, P.; MRÁČEK, A.; NOVÁK, L.; MINAŘÍK, M.; MAŠLÍK, J. Variable multiposition injection pump. ID 22866 – Utility model

2. MINAŘÍK, A.; SMOLKA, P.; NOVÁK, L.; MINAŘÍK, M.; MAŠLÍK, J. Experimental device for modification of polymorphic morphology in non-stationary temperature fields. ID 23263 – Utility model

3. KUŘITKA, I.; URBÁNEK, P.; KRČMÁŘ, P.; MAŠLÍK, J. Polymeric Ink for Material Printing. ID 26729 – Utility model

4. KUŘITKA, I.; URBÁNEK, P.; KRČMÁŘ, P.; MAŠLÍK, J.; ŠULY, P. Inorganic ink based on nanoparticles, intended especially for material printing. ID 307435 – Patent

Conference contributions

1. KRČMÁŘ, P.; URBÁNEK, P.; KUŘITKA, I.; MAŠLÍK, J.; BARTOŠ J. The Effect of the Exalite on Photoluminescence of Poly(methylphenylsilane) in Thin Films, In *NANOCON Conference proceedings*. 2012, Brno, Czech Republic. ISBN 978-80-87294-32-1

2. URBÁNEK, P.; KUŘITKA, I.; KRČMÁŘ, P.; MAŠLÍK, J.; BARTOŠ J. Polysilanes Thin Films Doped by Coumarin, In *NANOCON Conference proceedings*. 2012, Brno, Czech Republic. ISBN 978-80-87294-32-1

3. MAŠLÍK, J.; URBÁNEK, P.; KUŘITKA, I.; KRČMÁŘ, P. Paper No P20: Surface Modification of ITO-Coated PET Foil for Material Printing. In: SID Symposium Digest of Technical Papers, 70-71. *EuroDisplay 2013*, London, United Kingdom. doi: 10.1002/sdtp.33

4. URBÁNEK, P.; KUŘITKA, I.; KRČMÁŘ, P.; MAŠLÍK, J. Paper No P31: Optoelectronic Properties of MEH-PPV Thin Films Influenced by their Thickness. In: SID Symposium Digest of Technical Papers, 105–107. *EuroDisplay 2013*, London, United Kingdom. doi: 10.1002/sdtp.32

5. URBÁNEK, P.; ŠEVČÍK, J.; MAŠLÍK, J.; KRČMÁŘ, P.; KUŘITKA, I.; ŠULY, P.; HANULÍKOVÁ, B. The influence of ZnO nanoparticles content on the luminescence of the MEH-PPV in OLED devices. In: *Plastko 2014 Conference Proceedings*, Zlín, Czech Republic. ISBN 978-80-7454-335-7

6. ŠULY, P.; KRČMÁŘ, P.; MAŠLÍK, J.; URBÁNEK, P.; KUŘITKA, I. Polyvinyl Alcohol: Preparation of a Polymer Ink for Patterning of Substrates by Piezoelectric Drop-on-demand Inkjet Printer. In: *23rd ICMT Conference*. 2015, Portorož, Slovenia

7. MAŠLÍK, J.; KUŘITKA, I.; URBÁNEK, P.; KRČMÁŘ, P.; ŠULY, P.; MUNSTER, L. Water-based Indium Tin Oxide Nanoparticles Ink for Printed Ammonia Gas Sensor. In *Sustainable Science Materials and Technology*. 2015, Paris, France

8. ŠEVČÍK, J.; URBÁNEK, P.; ŠULY, P.; URBÁNEK, M.; MAŠLÍK, J.; ANTOŠ, J.; KUŘITKA, I. Enhanced electrical and optical properties of organic light emitting devices. In: *Plastko 2016 Conference Proceedings*, Zlín, Czech Republic. ISBN 978-80-7454-590-0

9. FORSBERG, V.; MAŠLÍK, J.; ANDERSSON, H.; HUMMELGÅRD, M.; TOIVAKKA, M.; KOPPOLU, R.; DAHLSTRÖM, Ch.; OLIN, H.; NORGREN, M. Printability of functional inkjet inks onto commercial inkjet substrates and a taylor-made pigment-coated paper. Presented at the *E-MRS, European Materials Research Society Spring Meeting 2018*, 2018, Strasbourg, France

10. MAŠLÍK, J.; ANDERSSON, H.; FORSBERG, V.; ENGHOLM, M.; ZHANG, R.; OLIN, H. Temperature sensor based on PEDOT: PSS ink-jet printed on paper substrate. Presented at the *20th International Workshop on Radiation Imaging Detectors*, 2018, Sundsvall, Sweden

Pedagogic activities

Participated on teaching in laboratory classes of "Preparation and Characterization Methods" and "Nanomaterials and Nanotechnology"

Trainings

Scanning probe microscopy course, Czech Metrology Institute (Brno, Czech Republic)

Jan Mašlík

Preparation of Conductive and Semiconductive Patterns by Digital Printing of Nanodispersions for Sensing Devices of Organic Compound Vapours

Příprava vodivých a polovodivých vzorů digitálním tiskem nanodisperzí pro senzory par organických látek

Doctoral Thesis